

The Electrostatic Wind Energy Converter

electrical performance of a high voltage prototype

The Electrostatic Wind Energy Converter

electrical performance of a high voltage prototype

Proefschrift

ter verkrijging van de graad van doctor
aan de Technische Universiteit Delft
op gezag van de Rector Magnificus prof.dr.ir. J.T. Fokkema
voorzitter van het College voor Promoties,
in het openbaar te verdedigen,
op woensdag 10 december 2008 om 10:00 uur
door

Dhiradj DJAIRAM

natuurkundig ingenieur
geboren te Groningen

Dit proefschrift is goedgekeurd door de promotor:
Prof.dr. J.J. Smit

Samenstelling promotiecommissie:

Rector Magnificus	Voorzitter
Prof.dr. J.J. Smit	Technische Universiteit Delft, promotor
Prof.dr.eng. J.A. Ferreira	Technische Universiteit Delft
Prof.dr. G.J.W. van Bussel	Technische Universiteit Delft
Prof.dr.ir. G.P.A Bot	Wageningen Universiteit en Researchcentrum
Prof.dr. W. Balachandran	Brunel University, West London, United Kingdom
Dr.ir. P.H.F. Morshuis	Technische Universiteit Delft
Dr.ir. J.C.M. Marijnissen	Technische Universiteit Delft / University of Florida

This research project has been supported with a grant from the Dutch Programme EET (Economy, Ecology and Technology, EETK02005)

ISBN: 978-90-8559-482-6

Copyright © 2008 by D.Djairam

Cover: An artist's impression of an EWICON system at sea.
Design: Tomas Pasma

Calvin: "I've been thinking, Hobbes..."

Hobbes: "On a weekend?"

Calvin: "Well, it wasn't on purpose...."

- Calvin and Hobbes

*Aan mijn ouders
mijn broertje
en mijn zusje*

Summary

The Electrostatic Wind Energy Converter electrical performance of a high voltage prototype

The increasing global demand for energy has rekindled the interest for various forms of renewable energy production, including wind energy. In addition to the conventional wind turbines, research efforts have been directed to other more experimental methods of extracting energy from the wind. One of these methods is the electrostatic wind energy converter (EWICON) in which wind energy is converted to electrical energy by letting the wind move charged particles against the direction of an electric field.

In chapter 1, the current global energy situation and the wind energy situation in particular are described. Conventional and experimental forms of wind energy extracting methods are described together with their respective advantages and disadvantages. Subsequently, the concept of the EWICON principle is explained and two possible implementations are discussed of which one is chosen. Finally, a comparison is made between wind turbines and the EWICON system, which indicates that there are significant advantages of a fully operational EWICON system over wind turbines.

In chapter 2, the theoretical framework that governs the operation of the EWICON system is laid out. The influence of the charge and particle size together with the electric field strength and the wind speed on the output power of the EWICON system is discussed. Issues such as life times of charged particles are also addressed. An analytical model that describes the trajectories of the charged particles is used to calculate the output power. Finally, the EWICON Performance Index (EPI) is defined in order to rank the efficiency of different versions of the EWICON system.

In chapter 3, a number of spraying methods to create charged particles are discussed. All these discussed methods require liquids to create charged droplets. Based on a number of requirements which the ideal method should adhere to, two methods are chosen for further investigation. These methods are electrohydrodynamic atomisation (EHDA) and high pressure monodisperse spraying (HPMS). The spraying liquids are demineralised (saline) water, ethanol and mixtures of water and ethanol. Using single nozzle versions of both spraying

methods, droplets can be sprayed and charged and, therefore, both methods will be used in the final versions of the EWICON system.

In chapter 4, the design of an EWICON test system is discussed, which include insulation issues, the design and placement of electrodes and the liquid supply system. Scaled up multi-nozzle versions of the two spraying methods are constructed and tested with a generator that provides laminar air flow. These experiments confirm that the wind can move the charged droplets against the electric field while the EWICON system is still connected to earth without electrical load. These experiments also show that currents associated with the production of charged droplets are not always proportional to the number of nozzles.

In chapter 5, various versions of the EWICON system are tested while allowing the charged droplets to charge the system up to a certain potential. These experiments were either conducted with or without an electrical load. Parameters such as wind speed, spraying liquid and spraying nozzles have been varied. The experimental results are statistically analysed and used in circuit equivalent models to verify the operation of the EWICON system. In most cases, the maximum output power was higher than the required operating power. Compared to the maximum convertible power available in the wind, the net output power is in the order of a few percent.

Based on these results, some considerations are given to a scaled up version, 100 kW, of the EWICON system.

In chapter 6, this thesis concludes for both spraying methods that while a net gain has been achieved in terms of output power, significant research must be undertaken to make the EWICON concept commercially viable.

A number of recommendations are given to increase the output power of the EWICON. First of all, the maximum current output of a single nozzle needs to be increased significantly. Secondly, the proportionality between the current and the number of spraying nozzles needs to be improved. Thirdly, spraying with the individual nozzles needs to be optimised such that sea and tap water can be used. Lastly, the design of the spraying systems should be such that the nozzles can be packed more closely together.

Samenvatting

The Electrostatic Wind Energy Converter electrical performance of a high voltage prototype

Door de wereldwijde toenemende vraag naar energie is het onderzoek naar verschillende vormen van duurzame energie weer in de volle belangstelling gekomen, waaronder windenergie. Naast de verbetering van bestaande windturbines vindt er ook onderzoek plaats naar nieuwe methoden voor het benutten van windenergie. Eén van deze methoden wordt toegepast in een elektrostatische windenergie converter (EWICON), waarin energie uit wind gewonnen wordt door de wind elektrisch geladen deeltjes tegen de richting van een elektrisch veld te laten bewegen.

In hoofdstuk 1 wordt de huidige mondiale energiesituatie uiteengezet waarin met name aandacht wordt besteed aan windenergie. De voor- en nadelen van de huidige windturbines alsmede die van andere experimentele windenergietechnieken worden besproken. Vervolgens wordt het concept van de EWICON uitgelegd waarbij twee mogelijke implementaties worden behandeld en waaruit er één gekozen wordt. Uiteindelijk wordt er een vergelijking gemaakt tussen de conventionele windturbines en de EWICON-methode, waaruit volgt dat er significante voordelen ten opzichte van windturbines kunnen zijn indien een volledig operationeel EWICON-systeem gerealiseerd kan worden.

In hoofdstuk 2 wordt het theoretisch fundament van de werking van het EWICON-systeem gelegd. Het effect op het uitgangsvermogen van de EWICON als functie van de elektrische lading en de afmetingen van de deeltjes in samenhang met de windsnelheid en de grootte van het elektrische veld wordt behandeld. Hierbij worden zaken zoals o.a. de levensduur van deeltjes ook in acht genomen. Een analytisch model wordt opgesteld waarmee de afgelegde weg van de geladen deeltjes en het uitgangsvermogen van de EWICON kunnen worden bepaald. Als laatste wordt de EWICON Performance Index gedefinieerd, waarmee verschillende varianten van het EWICON-systeem met elkaar vergeleken kunnen worden.

In hoofdstuk 3 wordt een aantal verschillende methoden behandeld waarmee geladen deeltjes gecreëerd kunnen worden. Al deze methoden zijn gebaseerd op het versproeien van vloeistof. Aan de hand van een lijst van eisen zijn

twee methoden gekozen waar nader onderzoek aan verricht wordt. Deze methoden zijn electrohydrodynamic atomisation (EHDA) en high pressure monodisperse spraying (HPMS). De gebruikte sproeivloeistoffen zijn gedemineraliseerd (evt. licht zout) water, ethanol en mengsels van beide vloeistoffen. Met beide sproeimethoden blijken geladen druppels gecreëerd te kunnen worden in testopstellingen waarbij gebruikt wordt gemaakt van één enkel vernevelaarsysteem. Daarom zullen beide sproeimethoden gebruikt worden in de uiteindelijke versies van het EWICON-systeem.

In hoofdstuk 4 wordt het ontwerp van het algehele EWICON-testsysteem besproken, waarbij zaken als de isolatie, het ontwerp en de plaatsing van elektrodes en vloeistoftoevoersysteem aan de orde komen. Systemen met meerdere vernevelaars zijn getest in een omgeving met een laminaire windstroming. Deze experimenten, die uitgevoerd zijn met een geaard EWICON systeem zonder elektrische belasting, laten zien dat de wind in staat is de geladen druppels mee te bewegen tegen de richting van het elektrische veld. Deze experimenten laten ook zien dat de elektrische stroom, die gepaard gaat met de creatie van geladen druppels, niet altijd evenredig is met het aantal vernevelaars

In hoofdstuk 5 worden verschillen versies van het EWICON-systeem getest, waarbij nu het systeem elektrisch zwevend is en dus opgeladen kan worden tot een bepaalde eindspanning door de geladen druppels. Deze eindspanning is o.a. afhankelijk van de windsnelheid, de opgewekte stroom en de isolatie van de het systeem. Deze experimenten zijn uitgevoerd met en zonder elektrische belasting. Parameters zoals de windsnelheid, de sproeivloeistof en het aantal vernevelaars zijn hierbij gevarieerd. De experimentele resultaten zijn statistisch geanalyseerd en verwerkt in een circuit equivalent model om de werking van het EWICON-systeem te verifiëren. In meeste gevallen was het opgewerkte vermogen groter dan het benodigd vermogen. Vergeleken met het beschikbare vermogen in de wind, ligt het netto uitgangsvermogen van het EWICON-systeem in de orde van enkele procenten.

Op basis van de extrapolatie van de resultaten is er nog gekeken naar de aspecten die een rol zouden spelen bij een opgeschaald 100 kW EWICON-systeem.

In hoofdstuk 6 wordt dit proefschrift afgesloten met de conclusie dat, hoewel er in veel gevallen netto vermogen wordt opgewekt, er nog een veel onderzoek uitgevoerd moet worden alvorens een EWICON commercieel haalbaar zal zijn. Dit geldt voor beide sproeimethoden.

Om dit te bewerkstelligen wordt er een aantal aanbevelingen gedaan om het uitgangsvermogen van het EWICON-systeem te verhogen. Als eerste moet de opbrengst per vernevelaar verhoogd worden. Ten tweede moet de evenredigheid tussen het aantal vernevelaars en de geproduceerde elektrische stroom verbeterd worden. Ten derde moeten de vernevelaars zodanig aangepast worden dat het

succesvol sproeien van kraan- en zoutwater mogelijk is. Als laatste moeten het ontwerp van de sproeisystemen zodanig verbeterd worden dat een hoge concentratie van vernevelaars per oppervlakte mogelijk is.

Table of Contents

Summary	vii
Samenvatting	ix
1. Introduction	1
1.1 Energy production in general	1
1.2 Alternative energy sources	3
1.3 Wind energy in general	4
1.3.1 Conventional methods	6
1.3.2 Drawbacks of wind turbines	7
1.3.3 Alternative wind energy methods	8
1.3.4 Use of wind energy	8
1.4 A new concept, a system with very little mechanical movement	8
1.4.1 Principle: work on charge carriers	9
1.4.2 Implementation of the EWICON method	10
1.4.3 Expected advantages and disadvantages	14
1.4.4 Goals EWICON research project	16
1.4.5 Contents and approach	16
1.5 Acknowledgment	17
2. Theoretical basis and modelling	19
2.1 Energy and power contained in the wind	20
2.2 EWICON model	21
2.2.1 Rayleigh limit and droplet parameters	21
2.2.2 Analytical model for simple configuration	27
2.2.3 Constraints on size and charge, electrical mobility	31
2.2.4 Computation & numerical values	37
2.3 Performance Index of the EWICON system	40
2.4 Conclusions	41
3. Charged droplet creation methods	43
3.1 EWICON requirements on droplet creation	44
3.1.1 Low energy consumption with respect to the energy in the wind	44
3.1.2 Controllable charge, high current output	45
3.1.3 Monodispersity	45

3.1.4	Operable under windy condition	47
3.1.5	Environmentally friendly spraying liquid	47
3.2	Previously considered creation and charging methods	48
3.2.1	Droplet creation - Ultrasonic atomisation	48
3.2.2	Droplet creation - Centrifugal or rotating disk atomisation	48
3.2.3	Droplet charging - Corona charging.....	49
3.3	Electrohydrodynamic atomisation	50
3.3.1	EHDA principle.....	50
3.3.2	Analytical model: EHDA	52
3.3.3	EHDA implementation and experiments.....	55
3.3.4	Conclusions on EHDA based spraying systems.....	66
3.4	High pressure monodisperse spraying	66
3.4.1	HPMS principle.....	67
3.4.2	Analytical model: HPMS	68
3.4.3	HPMS implementation and experiments.....	70
3.4.4	Conclusions on HPMS based spraying systems	72
3.5	Suitable charging method for the EWICON	72
3.5.1	Summarising conclusions.....	72
3.5.2	Decision.....	73
4.	EWICON system design.....	75
4.1	General design.....	76
4.1.1	Platform and isolation	77
4.1.2	Liquid supply system.....	80
4.1.3	Electrical system.....	81
4.2	Charged droplet transportation.....	81
4.2.1	Wind generator	82
4.2.2	EHDA.....	83
4.2.3	HPMS.....	85
4.2.4	Conclusions: charged droplet transportation of both methods	85
4.3	Increased charged droplet production	86
4.3.1	EHDA: Multi-needle systems.....	86
4.3.2	EHDA: Self-adjusting nozzles wire spraying system.....	93
4.3.3	HPMS: Multi-device systems.....	97
4.4	Lowering required wind speed by field grading	97
4.4.1	Analysis of droplet trajectories.....	97
4.4.2	Steering electrode(s).....	101
4.4.3	Conclusions on field grading.....	103
4.5	Rising EWICON potential and droplet movement	104
4.6	Overall conclusions and final experimental set-up	105
4.6.1	Conclusions	105
4.6.2	Final experimental test set-up.....	106

5. Testing of the complete EWICON system	109
5.1 Experimental method	110
5.2 EWICON with single nozzle EHDA spraying systems	111
5.2.1 Single ring electrode.....	111
5.2.2 Single cylindrical electrode.....	113
5.3 EWICON with multiple nozzle EHDA spraying systems	114
5.3.1 Multiple needles with rod or rounded ring electrodes.....	114
5.3.2 Multiple needle with cylindrical electrode configurations.....	117
5.3.3 Self-adjusting nozzles configuration.....	119
5.4 EWICON with HPMS system.....	120
5.4.1 Single spraying device.....	120
5.4.2 Multiple spraying devices	121
5.5 Analysis of the experimental results	121
5.5.1 EWICON circuit equivalent	122
5.5.2 Charging of the EWICON, output power.....	124
5.5.3 Analysis of the charging current.....	126
5.5.4 Analysis of the output power.....	126
5.5.5 The output power vs. the wind speed	127
5.5.6 Efficiencies of the spraying systems, EPI	129
5.6 Conclusions.....	131
5.7 Scaling up the EWICON.....	131
5.7.1 General considerations	131
5.7.2 Extrapolation based on the conducted experiments	132
6. Conclusions and recommendations	133
6.1 Conclusions.....	133
6.1.1 Conclusions per chapter	133
6.1.2 Overall conclusions on the EWICON concept.....	135
6.2 Recommendations.....	136
Appendix A. Betz' law	139
Appendix B. Evaporation and relaxation times of droplets.....	143
Appendix C. Numerical modelling in MATLAB.....	147
Appendix D. Statistical analysis in MATLAB	157
D.1 Rounded ring electrode – single nozzle	157
D.2 Rounded ring electrodes – six nozzles	158
D.3 Output power vs. wind speed	159
Appendix E. LORENTZ	161

The Electrostatic Wind Energy Converter

List of symbols and abbreviations	163
List of references	165
Acknowledgments	169
Curriculum Vitae	173

1

Introduction

“The answer, my friend, is blowin’ in the wind.”

– Bob Dylan

Wind energy has had a profound impact on the way our world has taken form, from the first sailing ships that discovered new worlds to the wind mills that were used to create dry lands in the Netherlands. With every new era, an inventive way was found to make use of the energy contained in wind. In this thesis, we will introduce an alternative method of extracting this energy.

While wind energy is often viewed as an energy source on its own, technically speaking, wind energy is mainly a form of solar energy, because air flow is generated due to the uneven heating of the Earth’s surface by the sun. About 1% of the solar energy reaching the earth is transformed into wind energy. Due to the uneven heating of the Earth’s surface, there are some locations that are more suitable for the exploitation of wind energy, like at sea or oceans, on wide open plains or along coastal lines.

In this chapter, firstly, we will start with a general outline of the energy production in the world. After a quick review of the conventional methods that are currently employed to utilise wind power, the theoretical concepts of the new method will be explained and, finally, we will conclude by stating the goals of this PhD research project.

1.1 Energy production in general

Worldwide energy consumption is growing and as countries like China and India are rapidly industrialising towards western standards, the demand for energy will become even higher. Currently, as we can see in Figure 1.1, the world primary energy demand at this moment is roughly 150000 TWh and according to the International Energy Agency, this demand will increase to almost 200000 TWh in 2030, see [1].

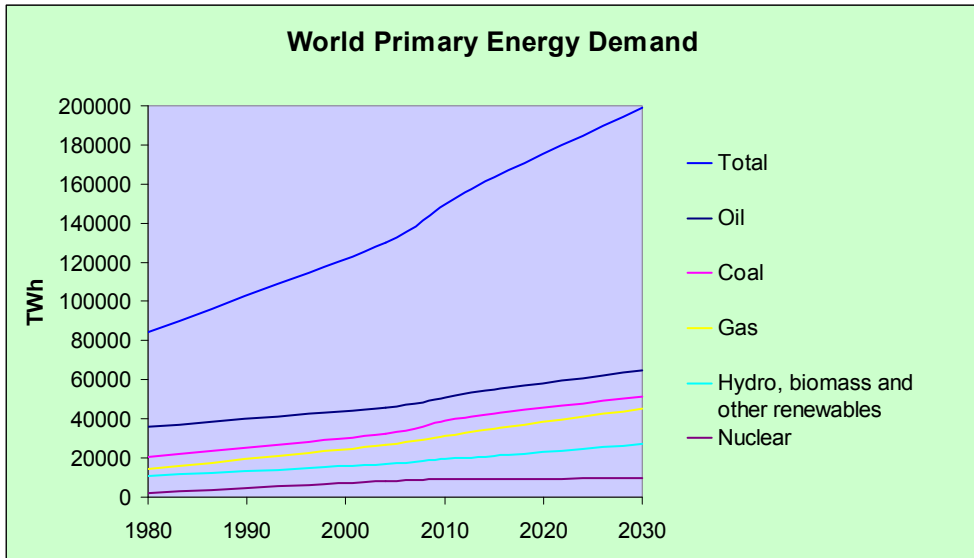


Figure 1.1. World primary energy demand of the last decades and the forecast until 2030 according to the International Energy Agency, see [1].

Of the current global energy production 86 percent is delivered using fossil based energy sources, i.e. oil, coal and gas. Another major form of energy production is nuclear energy which, at this point in time, is of the fission variety, which currently contributes 6 percent of the global energy production.

Both forms of energy production have their own drawbacks considered from various points of view, which are not always technical or environmental viewpoints. For example, with regards to fossil based energy sources, the main issue is the finiteness of the supply of oil, gas and (to a lesser degree) coal reserves. The most pessimistic estimation according to the International Energy Agency is that there will be enough to sustain this consumption rate approximately 164 years for coal, 64 for natural gas and 42 for crude oil, see [2]. Since oil and gas also serve other purposes than the production of electricity, such as the manufacturing of plastics, alternative means of energy production would mean a reduction of the pressure on these fossil reserves.

Furthermore, with the burning of fossil fuels CO_2 is produced. While the full effects of CO_2 production on the climatologic changes have yet to be understood, it is internationally acknowledged that the reduction of the release of CO_2 into the atmosphere is necessary.

Similar considerations can be made concerning fission based nuclear energy. Firstly, just like with the fossil based energy sources, there is a limit to the supply of uranium and plutonium, a limit we might see most pessimistically around 2030, see [3]. Furthermore, even though many countries, like e.g. France and the USA, utilise nuclear energy, public perception is still negative, mostly because of the operating risks and the problems surrounding the disposal of the nuclear waste. In general, whenever new plans for building a nuclear reactor are disclosed, popular resistance to these plans can be expected. In addition, certain governments, like that of Germany, have decided to shut down all nuclear reactors by 2020, see [4].

Nuclear energy from fusion has a more positive image than its fission counterpart, but it is still in an experimental phase and it is generally thought that it will take at least a few decades before this technology is commercially available, see [5].

1.2 Alternative energy sources

Considering the issues with the aforementioned sources of energy, alternative means of energy production have been investigated. About 17% of the global electricity production is generated through the use of alternative energy sources, see [6]. Some examples of methods employing renewable energy sources are:

- hydrogen/ethanol fuel cells,
- biomass energy
- photovoltaic solar cells
- hydro energy
- tidal energy

of which their share in the total world renewable energy usage, according to the Renewable Energy Network Policy Network [7], can be seen in Figure 1.2.

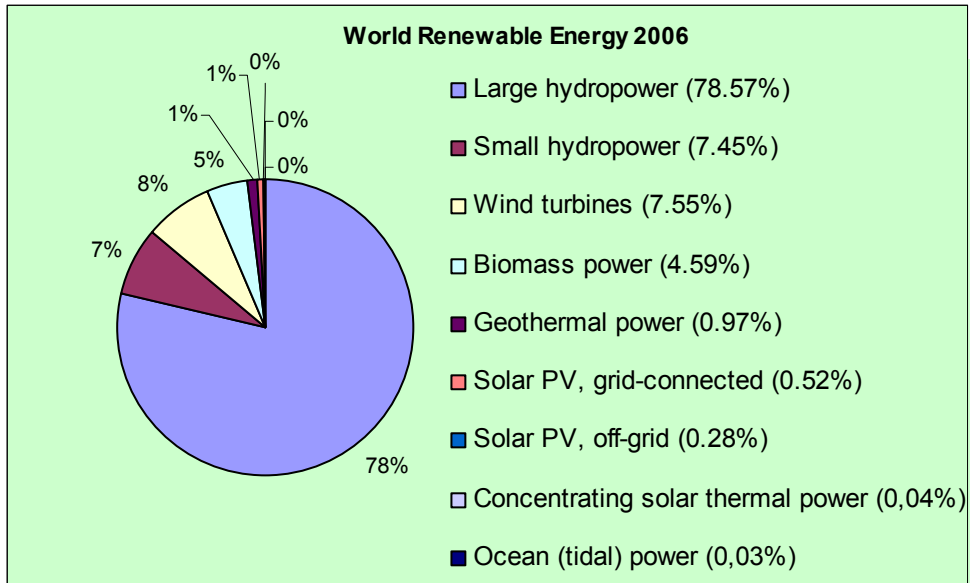


Figure 1.2. The world renewable energy sources broken down in categories for 2006, according the REN21, see [7].

Most of these alternative methods of energy production are still only used on a small scale basis. The independent economic viability of these alternative renewable energy sources is low to non-existent and, therefore, most of these methods need to be promoted through the use of subsidies and tax incentives. Slowly, energy companies are trying to adopt a “greener” image and have started to offer electricity generated through sustainable means. The rates for this “green” electricity are usually equivalent to the rates for electricity generated through conventional means, again promoted by tax breaks.

1.3 Wind energy in general

Firstly, we will briefly mention the current status of the use of wind energy, its current capabilities, its drawbacks and what can be expected of wind energy. Then, we will introduce a different concept of converting wind energy to electrical energy in order to address some of the drawbacks currently associated with wind energy production.

Usually, when it comes to alternative means of generating energy, several terms are used to label these alternative means using adjectives like “sustainable” or “renewable” and sometimes these adjectives are used indiscriminately.

Therefore, for the sake of clarity, the following definitions, which are commonly accepted, will be used throughout this thesis:

Sustainable energy: A form of energy generation which can be maintained economically without depleting or damaging the resources.

Renewable energy: A form of energy generation in which the required resources are normally replenished through natural processes.

Usually, this means that forms of renewable energy are also sustainable if they can also be maintained economically.

Of all the various forms of sustainable energy generation, wind energy is one of the most utilised forms, together with hydro energy. It is a growing source of sustainable energy which has the potential to ease the pressure on fossil based energy sources. The fact that there is virtually no CO₂ emission when generating wind energy also means that this form of power generation could play an important role in global energy supply especially considering the issue of global warming.

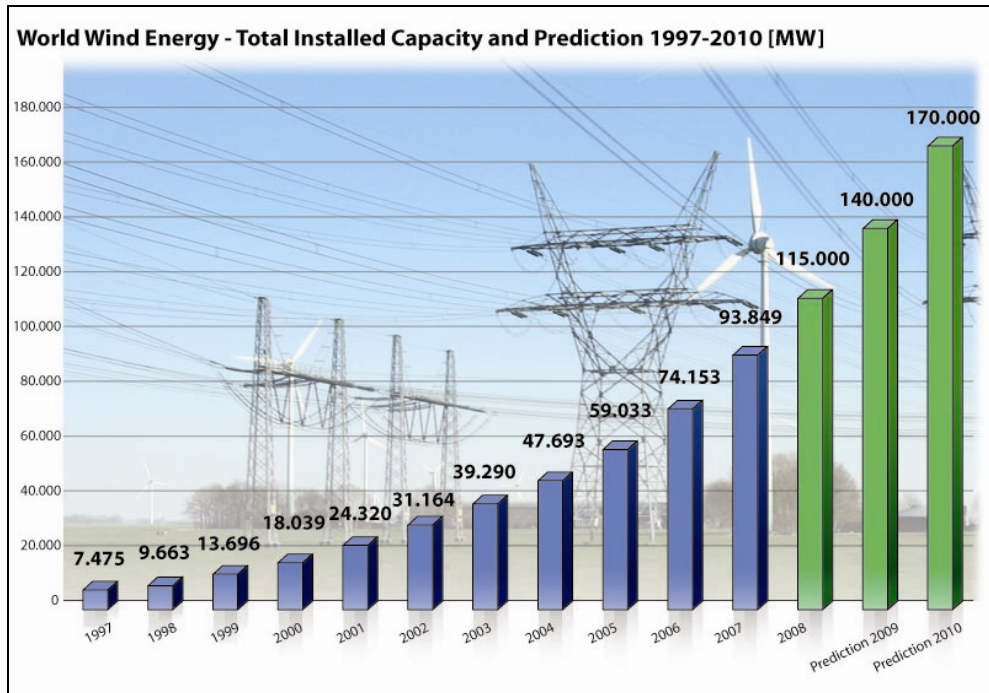


Figure 1.3. Total installed wind power capacity in the world in megawatts until 2007 and the prediction for 2008-2010. Data provided by the World Wind Energy Association.

Globally, in 2007, the total installed wind power capacity is roughly 94000 MW and, as can be seen in Figure 1.3, the prediction for the next years is to almost double that capacity.

In the Netherlands, the installed wind power capacity currently is approximately 1500 MW. The goals of the Dutch government are to increase this capacity to 3000 MW in the next few years. In 2020, the goal is to have 20% of the total output power be generated by means of sustainable energy, which for a significant part will consist of wind energy. This will mean that, by then, a total wind power capacity of 6000 MW will have to be installed, see [8].

1.3.1 Conventional methods

The most common and well known method of converting wind energy to electrical energy is through the use of wind turbines of the horizontal axis design, see Figure 1.4.



Figure 1.4. Wind turbines in the middle of the Dutch farming landscape.

Their current efficiency is around 50% at their rated speeds, which means they convert 50% of the available power associated with the wind. Currently, smaller turbines have power capacities around 250 kW, while the larger turbines are capable of delivering several megawatts to the grid.

Another rotation based method is the Darrieus wind turbine, shown in Figure 1.5, which is based on a vertical axis instead of the horizontal axis type that is used in the conventional wind turbine. This design has the advantage that it utilises wind from all directions.



Figure 1.5. An example of a Darrieus wind turbine.

1.3.2 Drawbacks of wind turbines

So, while wind turbines still are the main devices to convert wind energy to electrical energy, there are a number of drawbacks that limit the widespread use of wind energy. The main drawback is the high cost of maintenance. This need for maintenance arises primarily from the conversion of wind energy to electrical energy via mechanical energy, i.e. the rotational movement that drives the wind turbine. Especially gear box driven wind turbines are prone to wear and tear and need to be maintained on at least a yearly basis. Added to the cost of maintenance are the costs for, amongst other things, construction, land lease and permits which makes government subsidies a requisite to enabling wind energy projects. Thus, at this point, the choice for the wind energy is a political one [9].

Other drawbacks include the fact that conventional wind turbines are bound to circular surface areas, because of the rotational movement. This rotational movement is also the cause of noise and intermittent shadow nuisance. Another often heard complaint is that these wind turbines are responsible for what is called “visual pollution”, especially when large wind turbine farms in rural settings are involved. A solution for this problem is to build wind turbine farms at sea. This, of course, introduces problems such as increased construction and maintenance costs.

1.3.3 Alternative wind energy methods

There have been other developments in the field of alternative wind energy conversion. One example is the so-called “ladder mill” [10] which consists of a series of kites moving in a rotating manner while driving a generator.

Thus far, all of these developments are still in an experimental stage and have not been yet proven commercially successful. Also, they all have the common element that there are mechanically moving parts present in the design, which will lead to wear and tear, similar to wind turbines.

1.3.4 Use of wind energy

As many countries have stated in their long-term energy goals that they wish to increase their wind energy output, a question that often arises when any form of alternative energy production is mentioned is whether it can replace current energy production processes. With respect to wind energy, it can be said that, due to its intermittent nature and the limited means of energy storage in general, in the foreseeable future wind energy will not be able to fully replace fossil and nuclear based energy production.

Also, computational research using meteorological models as described in [11] suggest that the local and global climate could be altered by the use of large-scale use of wind energy, for example $1/10^{\text{th}}$ of the global electricity demand, by extracting kinetic energy and changing turbulent transport in the atmospheric boundary layer.

1.4 A new concept, a system with very little mechanical movement

As stated before, in all of the methods, that are used to convert wind energy into electrical energy, some form of mechanical movement occurs, which is the primary reason for maintenance and usually the primary cause of failure. Therefore, a concept in which there is very little mechanical movement would be ideal with respect to system complexity and maintenance costs.

The EWICON method (Electrostatic WInd energy CONverter) is a method which is based on the principle that the wind transports electrically charged particles or charge carriers in an electric field. Without going into great detail on how we will go about creating these charge carriers (this will be discussed in chapter 3), for now, we will discuss the principles of the EWICON method and its

possible implementations into an actual system. In principle, any object, that can hold or store a charge, could be used as charge carrier. At the end of this chapter, we will discuss in more detail what this, in practice, will come down to.

It is important to mention that the concept of converting wind energy into electrical energy by having the wind move charge carriers in an electric field is not new. There have been several patents that propose a similar idea, see for example [12] and [13]; however, most of these patents do not have an energy efficient solution for creating charge carriers.

1.4.1 Principle: work on charge carriers

When a force acts on a body that undergoes a displacement, that force does work on the body. In the case of the EWICON system, the body is a charged particle with a charge q and the force is the electric force on the charged particle due to an electric field E , given by

$$\vec{F} = q \cdot \vec{E} \quad (1-1)$$

which is illustrated in Figure 1.6.

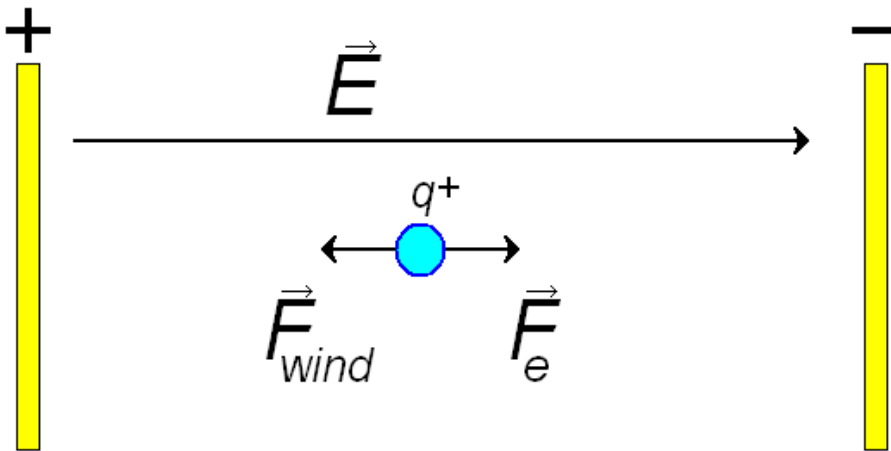


Figure 1.6. A positively charged particle is pushed towards the positive electrode by the wind against the direction of the electric field, thereby increasing the potential energy of the charged particle.

By allowing the wind to force the charged particles against the direction of this electric force, the potential energy of these charged particles will increase, similar to pushing a rock up a mountain against gravity.

$$dW = -dU \quad (1-2)$$

These charged particles with increased electrical energy can then be collected using one of the methods explained in the next section. In this way, wind energy is directly converted into electrostatic energy and the intermediate step involving the rotational movement, which takes place in conventional wind turbines, is taken out of the process.

1.4.2 Implementation of the EWICON method

Currently, there are two methods of collecting the charged particles, both of which will be explained together with their respective advantages and disadvantages:

1.4.2.1 Type A: the patent of Alvin Marks et al.:

As we can see in Figure 1.7, in this implementation of the EWICON system, the charged particles are created by a charging system, which usually consists of a number of nozzles and electrodes, which is grounded. A stream of charged particles, which can be considered as an electric current, is then transported by the wind to a separate insulated collector, which is initially neutral. When the charged particles touch the collector, they will deliver their charge to the collector. This causes the potential of the collector to rise.

This potential will have the same polarity as the charged particles cloud, thereby creating an electric field. Due to this field, an electric force will push the charged particles away from the collector. Initially, the wind force will be larger than the electric force and therefore the charged particles will still arrive at the collector. As long as this process occurs, however, the electric field generated by the collector will continue to increase, causing the charged particles cloud to either move back against the wind or around the collector. When the charged particles come in contact with the charging system or earth, the charge is lost and the net current decreases.

Therefore, the wind has to overcome this repelling electric force and depending on the speed of the wind, the size of the collector and the load, the collector potential attains a maximum that further depends on possible leakage currents to earth via the insulator surface. If all produced charged particles are captured by the collector, then the maximum power of the EWICON has been attained.

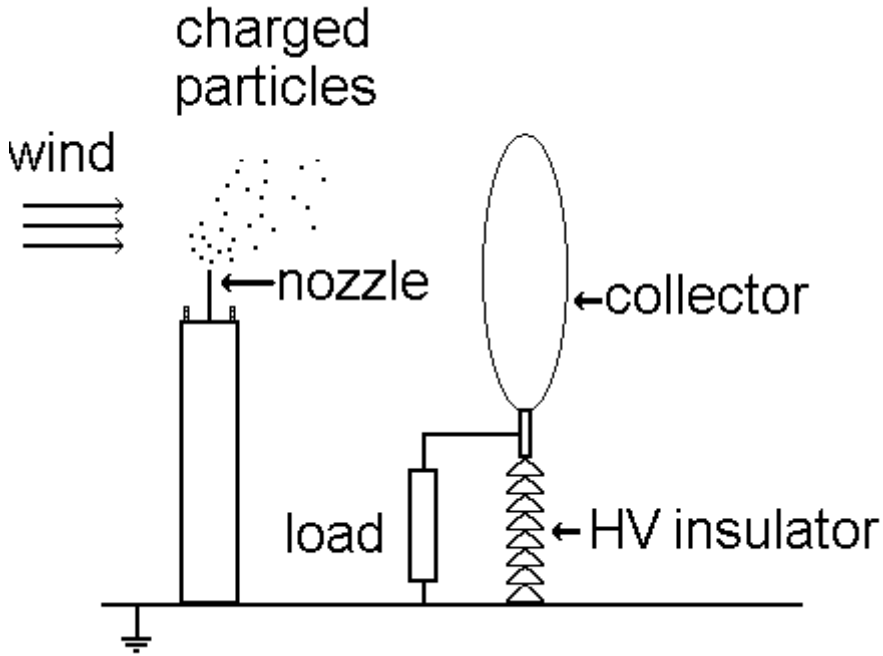


Figure 1.7. An example of a Type A implementation of the EWICON system with an insulated collector. The charged particles are created at the charging system consisting of nozzles and electrodes. The wind transports these particles to the collector. In previous experiments, the distances between nozzle and collector were in the order of one to two metres. A load can be attached to the collector.

Currently, research on this topic is also carried in Japan by Sato et al., see [14]. This work is only limited to implementations with a separate collector.

1.4.2.2 Type B: the collector-less EWICON system:

In this implementation, depicted in Figure 1.8, the charging system itself is insulated from earth. There is no separate collector present. Since the charging system starts in an electrically neutral situation, dispersing charged particles will cause the potential of the charging system to rise. To be more precise, the potential will rise in case of negatively charged particles, it will decrease in case of positively charged particles. However, this time, the polarity of this potential is opposite to the polarity of the charged particles. This means that in the absence of wind, the charged particles will be forced back to the charging system resulting in a charge loss or net current decrease.

Again, depending on the speed of the wind, the quality of the insulation of the charging system and the load attached to the system, the system itself will reach a maximum potential. Basically, the earth acts as the collector for the charged particles and if all of the charged particles are transported to earth, then the maximum power that can be delivered is attained.

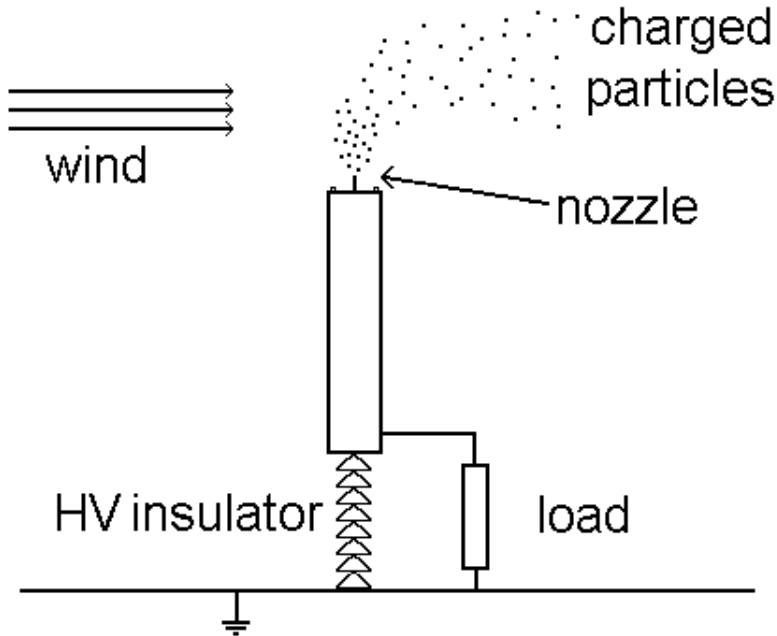


Figure 1.8. An example of a Type B implementation of the EWICON system. Here, earth acts as the collector. The charging system itself is insulated from earth and as a consequence, the dispersal of charged particles will result in the rise of the potential of the system. Again, a load can be attached to the charging system.

Also, in this case, an electrical load can be connected to the charging system.

1.4.2.3 Comparison of both implementations

Although the two implementations are equivalent from an electrical point of view, practical implications show that there is a preference for the Type B implementation. While the Type A implementation is conceptually simpler, it does require an external collector, which means extra building efforts. The drawback of a Type B implementation is that the charging system needs to be isolated from earth, which significantly increases the complexity of the EWICON. However, because there is no need for an external collector, the overall EWICON design

becomes simpler, effectively making the EWICON a one-unit system. This, for example, would make it relatively simple for the EWICON system to be aligned to the direction of the wind, whereas the working direction of a Type A implementation would be more or less permanent after building and placing the collector and the charging system. A platform could be designed on which both the collector and the charging system could be placed. In this way, the whole system could be aligned with changing wind directions.

Also, in the case of an external collector, due to the inherent varying character of the wind, a relatively large collector needs to be built to ensure that most of the charged particles are collected and even then, there is no guarantee that all of the particles will be collected. The percentage of collected particles depends on the size and shape of the collector. However, when considering Type B, the only requirement is that the charged particles do not return to the charging system. In this way, the rest of the surrounding environment acts as a collector.

A Type A implementation, by its nature, would lend itself for a (partial) particle recycling system, thereby reducing the amount of liquid used for energy production. This is an important issue to keep in mind when considering the Type B implementation, where the charged particles are dispersed into the surroundings. Therefore, from an environmental point of view, the charged particles cannot be harmful or toxic. One should note, however, that this problem would also be present when using the Type A implementation, since, as stated in the previous section, it would require a very large collector to catch all of the dispersed particles. Even then, there will inevitably be particles that would not reach the collector because of wind speed and direction and because of the fact that the collector would repel particles.

Table 1.1. Comparison of the two implementations of the EWICON system.

	Type A	Type B
Charging system	Grounded	Insulated
External collector	Yes	No
Extra building effort	Yes	No
Alignment with changing wind direction	Only with both charging system and collector on a single rotational platform	Yes

1.4.3 Expected advantages and disadvantages

The EWICON principle is expected to have several advantages over the standard conventional wind turbine systems, also listed in Table 1.2.

First of all and most importantly, apart from the floating charged particles, there are no moving/rotating parts present in the EWICON system. This means that wear and tear commonly found in the gearbox systems of wind turbines will not be present in the EWICON system. This will have a positive effect on the maintenance and investment costs.

Secondly, due to the lack of moving/rotating parts, there is less noise originating from the EWICON system. The noise would be comparable to that of wind flowing around and through tall buildings or structures.

Thirdly, since there are no rotating blades present, no intermittent shadows will be present. This is especially important for the placement of wind energy systems in the urban or rural settings.

Finally, since there is no rotational movement in the EWICON system, increasing the wind surface area does not necessarily have to go hand in hand with an increased circular wind area, as illustrated in the Figure 1.9.

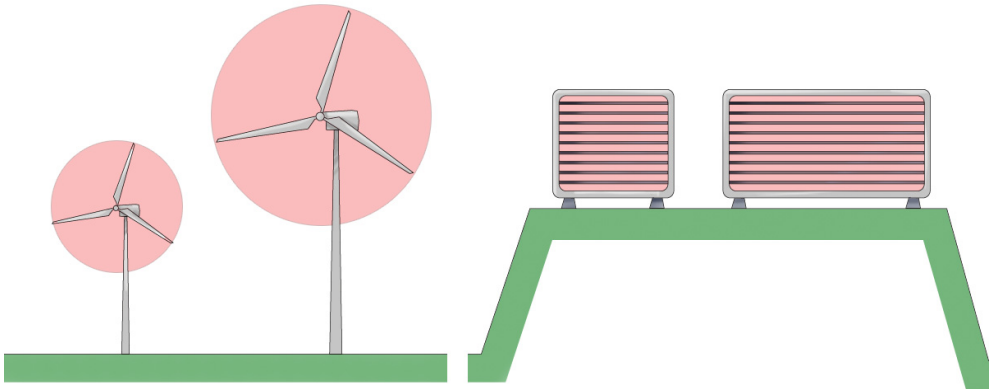


Figure 1.9. Using conventional wind turbines (left), increasing the wind surface area means the diameter of the circular area needs to be increased. Using an EWICON on for example a dam (right), the wind surface area is increased by stretching the width of the EWICON.

Due to the nature of the EWICON system, it is possible to extend the wind surface in one of the two dimensions, making a modular approach possible. This way, one could think of building long strips of EWICON modules along rooftops or dams, as illustrated in Figure 1.9. These long strips would, however, be static constructions and thus, less adaptable to the direction of the wind.

There are some issues associated with the conventional use of wind energy that cannot be solved by the EWICON system. We will see in the next chapter that the wind surface area is a restrictive parameter for the maximum of extracted power. This means that the EWICON system will have dimensions comparable to those of conventional wind turbines which will not solve the “visual pollution” problem due to size. However, because the construction and maintenance costs are expected to be lower than those of wind turbines, the placement of EWICON systems at sea might eventually be commercially more favourable than the placement of wind turbines farms.

In the introduction of this section, we briefly mentioned that, in theory, the charged particles could be any type of object that is able of storing electrical charge. However, in later chapters, we will see that using liquids particles or droplets as charge carriers currently is the most practical way of having the disposal of streams of charged particles. Considering the fact, then, that the EWICON system is based on liquid particles and that they are charged by electrodes, long term operation in humid and possibly saline environments, like at sea, might result in other problems than the usual wear and tear, like corrosion of the electrodes, electrolysis and clogging of liquid supply systems.

Finally, as we will see in chapter 3, creating the charged particles will require certain electrodes to operate on high voltage, see [15]. Therefore, attention must be paid to safety regulations and insulation issues. These problems will have to be addressed and taken into account when making the cost/benefit analysis.

Table 1.2. Comparison of an EWICON system with most conventional wind turbines.

	wind turbines	EWICON
Rotational mechanical movement	Yes	No
Noise	Yes	Comparable to noise of air flow along static buildings
Intermittent shadows	Yes	No
Modular expandable	Somewhat	Linearly, in both directions to a degree

1.4.4 Goals EWICON research project

The goals of this PhD research project were to investigate the theoretical and practical issues that have to be considered when designing and building an actual system based on the EWICON principle with both Type A and B implementations in mind. The research, needed to ultimately build an EWICON system, has been approached in the following manner:

- The dependence of the efficiency of an EWICON system on parameters like wind speed, type of liquid, droplet size and charge was determined, thus establishing a model that is able to provide an estimation of the output power.
- Suitable methods for creating the charged droplets were investigated and tested whether they are compatible with the requirements of an EWICON system.
- The electrical behaviour of the EWICON system due to the high voltage components was analysed in order to understand the interaction between the charged droplets and the power output of the system.

1.4.5 Contents and approach

Clearly, the stage of development of the EWICON is very early, in a sense that at the beginning of the current research, the proof of the principle had to be confirmed in practice.

First of all, the theoretical and practical feasibility of an EWICON system will be discussed. In chapter 2, an elementary model of the system, incorporating a number of charged droplets in an electric field and wind, will be developed which can be used to calculate the expected power output. With this model, we can then determine whether the EWICON system is able to achieve a net power output. Concurrently, a method must be devised to calculate the efficiency of an EWICON system based on the available wind energy, the energy needed to operate the EWICON system and the liquid consumption. This way, various implementations of the EWICON system can be compared.

Secondly, in chapters 3 and 4, based on results of simulations, both of the developed model and field analysis/droplet trajectories, a charging system has been designed. This will include the size and shapes of various electrodes, the geometric configurations, voltage potentials at which these electrodes need to be set. Also,

using the simulations, it will be obtained at what wind speeds the designed EWICON system is expected to function. Since charged droplets play an important role in this system, a method is needed to create droplets and to apply electrical charge to these droplets. Several methods will be discussed and analysed in terms of energy efficiency and liquid consumption.

Finally, in chapters 5 and 6, a laboratory version of an EWICON system will be built and tested and suggestions will be given for an industrial prototype and for a scaled up version. Also included in chapter 5, some consideration is given to the social, economic and medical issues surrounding the EWICON system.

1.5 Acknowledgment

The author wishes to acknowledge Dr. Piet Sonneveld of the Wageningen University and Research Centre for reintroducing the EWICON concept and for the close cooperation with the research project.

2

Theoretical basis and modelling

“In theory, theory and practice are the same. In practice, they’re not.”

– Lawrence Peter “Yogi” Berra

In this chapter, to help understand the basic principles of this concept, we will construct a model which we can use to make predictions of the operation and the efficiency of the EWICON system. This will involve assessing the power associated with the wind and how much of it can be used for the conversion. Based on the movement of the charged carriers under influence of the electric field and the wind, we can determine whether the carriers will be removed from the system and if so, how much electrical energy potentially can be gained. Using this model, we can determine which parameters are the most important for the efficiency of the EWICON system.

This model will be used as the basis for computational simulations. Quantitative results from this model can then be compared to experimental results and used to further improve and optimise EWICON system parameters.

Practical issues like the energy costs of all the equipment or devices needed for e.g. liquid supply or high voltage sources for the electrodes will not be taken into account during these theoretical considerations. All these issues will be addressed in chapter 4 and 5 where we will discuss the practical design of an EWICON system and the experiments conducted with the EWICON system.

At the end of this chapter, we will discuss in what way the efficiencies of various EWICON implementations will be determined. We will compare these implementations by defining a benchmark called the EWICON Performance Index or *EPI*. In the *EPI*, the energetic costs of the equipment and devices will be taken into account.

2.1 Energy and power contained in the wind

The kinetic power, P_w , contained by a flow of air is related to the 3rd power of its speed, v_w ,

$$P_w = \frac{1}{2} \cdot A \cdot \rho_a \cdot v_w^3 \quad (2-1)$$

in which A is the active surface area perpendicular to the direction of the wind flow and ρ_a is the air density. Not all this power can be used for the conversion of wind power to other forms of power because this would imply that the air flow would come to a complete stop just behind the converter.

This has been represented in Figure 2.1, where the original wind speed, v_w as stated in equation (2-1) is indicated as v_1 . The speed of the wind after it has passed through the converter has been indicated as v_2 .



Figure 2.1. Illustration of the Betz limit. The wind speed behind the wind converter, v_2 , should ideally be $\frac{1}{3}$ of the speed before it enters the converter, v_1 , while the speed just in front of the converter is $\frac{2}{3}$ of the initial wind speed.

By determining to what extent the wind would have to be slowed down by the converter and by calculating what the final wind speed would be, Betz [16] and Lanchester [17] both derived an expression for the maximum recoverable power, P_{max} , from the wind as a function of the prevailing wind speed v_w :

$$P_{\max} = \frac{8}{27} \cdot A \cdot \rho_a \cdot v_w^3 \quad (2-2)$$

In deriving expression (2-2), the wind speed, just in front of the converter, is $\frac{2}{3}$ of the original wind speed v_w and far behind the converter the wind speed is $\frac{1}{3}$ of the original wind speed v_w . A derivation of this expression can be found in appendix A. This distribution of wind speeds is the best compromise between using the power of the wind and maintaining a flow of air. The Betz limit basically states that there is an upper limit to the amount of power that can be extracted from the wind. More important, this limit is irrespective of the method of converting, which means that the EWICON principle is also bound by this limit.

Looking at the ratio between (2-1) and (2-2), we find that this limit is

$$\frac{P_{\max}}{P_w} = \frac{16}{27} \approx 0.593 \quad (2-3)$$

which basically states that this upper limit is almost sixty percent. The net power produced by the EWICON or any wind converting system for that matter will in part be assessed with respect to this limit.

2.2 EWICON model

In this section, we will look at the various aspects involved in the modelling of the EWICON concept. Such a model will consist of a number of charge carriers moving in an external electric field while different forces, mechanical and electrical, will act on these charge carriers.

Firstly, the charge carriers will be defined in terms of type, charge and size. Secondly, all the relevant forces will be specified, which, after calculations, will yield the trajectories of the charge carriers, i.e. positions and velocities. Finally, we will look at the constraints on the droplet parameters, the electric field and the wind speed, which must be observed in this model in order for the wind to transport the droplets away.

2.2.1 Rayleigh limit and droplet parameters

First of all, charge carriers have to be defined, which according to IEC norm no. 114-14-44 are “particles having one or more elementary electric charges”. In the previous chapter, we stated that, in theory, any object that can be wind-driven and hold an electrical charge is a useable charge carrier. However, based on the charge creation methods which will be discussed in the next chapter,

it turns out that using a liquid to create small droplets is a convenient way of creating charge carriers.

In this case, if a liquid is to be used as the source of charged droplets, there is a limit to the amount of charge that can be present on such a liquid droplet. This is because of the mechanical instability that will occur when the surface tension of the liquid and the electrostatic stress due to the repulsion of charges at the droplet surface are equal. If the charge on the droplet becomes too large, then the droplet will break up into smaller droplets. This occurs at the Rayleigh limit, which depends, among other parameters, on the droplet size. Therefore, the droplet size, and the ability to control it, will be important factors to consider when discussing methods for charged droplet creation in the next chapter.

This Rayleigh limit or the maximum charge, q_{max} , that can be present on a droplet just before it breaks up, is given by

$$q_{max} = 2\pi\sqrt{2\gamma \cdot \epsilon_0 \cdot d^3} \quad (2-4)$$

in which γ is the surface tension of the liquid of the droplet, ϵ_0 is the vacuum permittivity and d is the droplet diameter.

In Table 2.1, we can find values of q_{max} corresponding to a number of droplet diameters, for two types of liquids, water and ethanol, with $\gamma_{water} = 72 \cdot 10^{-3}$ N/m and $\gamma_{ethanol} = 22 \cdot 10^{-3}$ N/m. As we can see, for each droplet diameter, the q_{max} is lower for ethanol than for water due to the lower surface tension of ethanol.

Table 2.1. Example values of the maximum charges on water and ethanol droplets as specified by the Rayleigh limit as a function of the droplet diameter, with $\gamma_{water} = 72 \cdot 10^{-3}$ N/m and $\gamma_{ethanol} = 22 \cdot 10^{-3}$ N/m.

Droplet diameter (μm)	Maximum charge on droplet for water (C)	Charge to mass ratio for water (C/kg)	Maximum charge on droplet for ethanol (C)	Charge to mass ratio for ethanol (C/kg)
1000	$2.26 \cdot 10^{-10}$	$1.30 \cdot 10^{-2}$	$1.26 \cdot 10^{-10}$	$9.10 \cdot 10^{-3}$
100	$7.15 \cdot 10^{-12}$	$4.10 \cdot 10^{-1}$	$4.00 \cdot 10^{-12}$	$2.86 \cdot 10^{-1}$
10	$2.26 \cdot 10^{-13}$	$1.30 \cdot 10^1$	$1.26 \cdot 10^{-13}$	9.06
1	$7.15 \cdot 10^{-15}$	$4.10 \cdot 10^2$	$4.00 \cdot 10^{-15}$	$2.86 \cdot 10^2$
0.1	$2.26 \cdot 10^{-16}$	$1.30 \cdot 10^4$	$1.26 \cdot 10^{-16}$	$9.06 \cdot 10^3$

Also, for each droplet diameter, the maximum charge to mass ratio, CMR , has been calculated and included in Table 2.1, as given by

$$CMR = \frac{q_{\max}}{m_{\text{droplet}}} \quad (2-5)$$

This ratio illustrates the fact that, while the charge on a single droplet in absolute terms becomes smaller with decreasing droplet size as shown in Figure 2.2, the relative charge on a droplet increases significantly as shown in Figure 2.3.

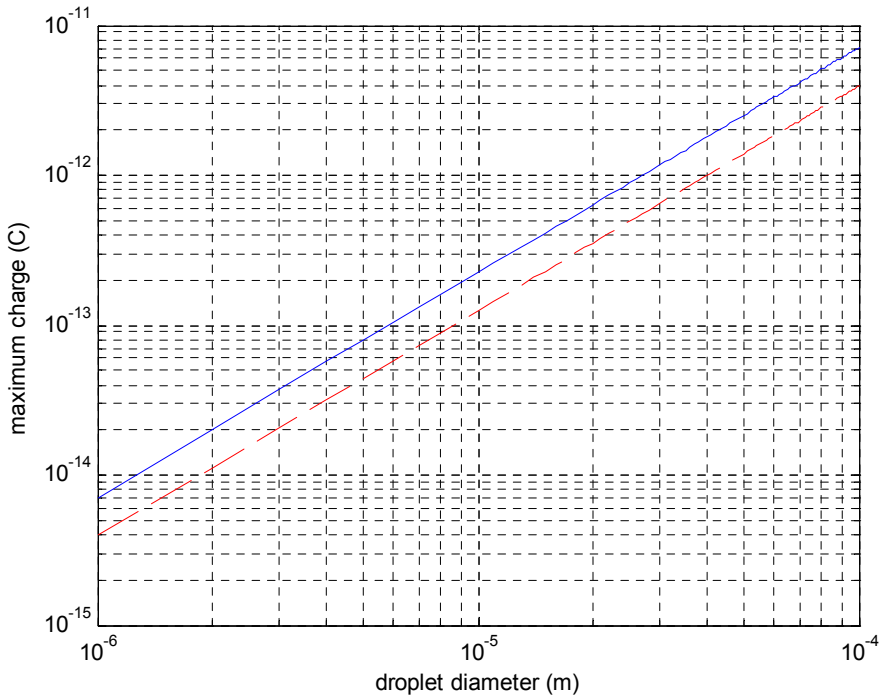


Figure 2.2. The maximum possible charge on a droplet as specified by the Rayleigh limit depicted as a function of the droplet diameter, ranging from 1 to 100 μm . Graphs are shown for water (continuous line) and ethanol (dashed line).

This means that with equal amounts or equal flow rates of a liquid, more electrical charge can be produced. Therefore, if all other factors are equal, the droplet diameter should be as small as possible. However, before we can say that with certainty, we will investigate in the next few sections, where we will discuss, amongst other things, constraints on droplet parameters, whether there are certain restrictions to the droplet diameter.

The maximum charge on a droplet as specified by the Rayleigh limit should also be carefully watched with respect to the evaporation of the liquid

droplet. Due to this evaporation, the droplet diameter will decrease over time. One of the main parameters governing the rate of evaporation is the difference between the velocities of the droplet and the surrounding air. As the droplet is moved along by the wind, the difference of droplet velocity with that of the wind decreases and, thus, does the rate of evaporation. This difference will be the greatest at the moment the charged droplet is created and released from the charging system into the moving air. Therefore, the rate of evaporation will be at its highest just as the charged droplet is starting its flight.

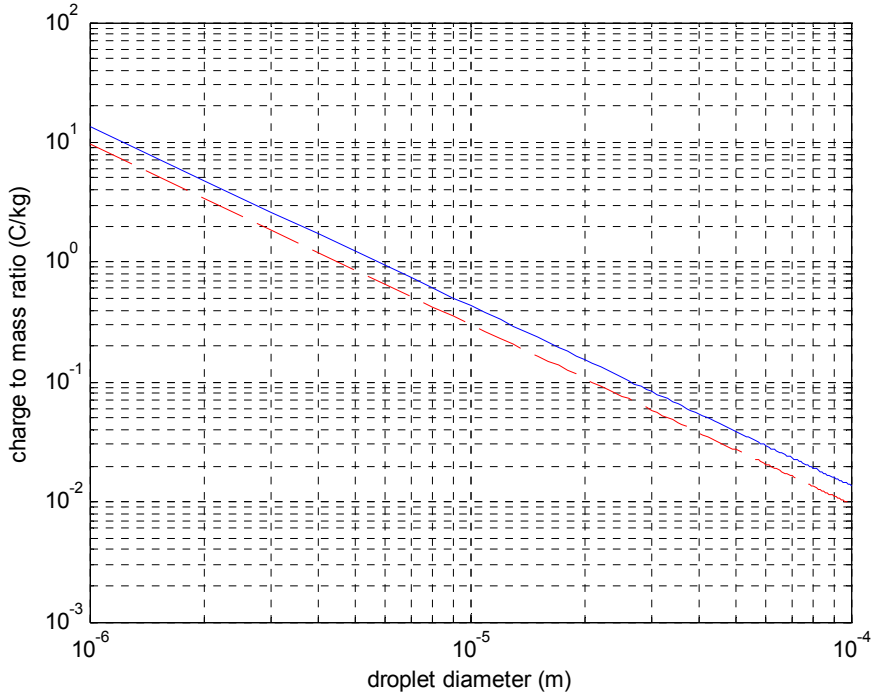


Figure 2.3. The charge-to-mass ratio, *CMR*, depicted as a function of the droplet diameter, ranging from 1 to 100 μm . Graphs are shown for water (continuous line) and ethanol (dashed line).

If the rate of evaporation is sufficiently high, the charge that is present on the shrinking droplet will reach the Rayleigh limit and, at this point, the charged droplet will break up into smaller droplets. If the rate of evaporation continues to be high, then the smaller charged droplets will continue to break up until only ions are left.

This break-up process is illustrated in Figure 2.4. The wind drag force, which among other things is dependent on the droplet diameter, decreases, while the opposing electric force remains constant. In other words, the electric mobility, which will be discussed in 2.2.3, is very high. Therefore, if the ions are still

sufficiently close to the charging system, the wind will not be able to transport the electrical charge that was initially stored in the original droplets.

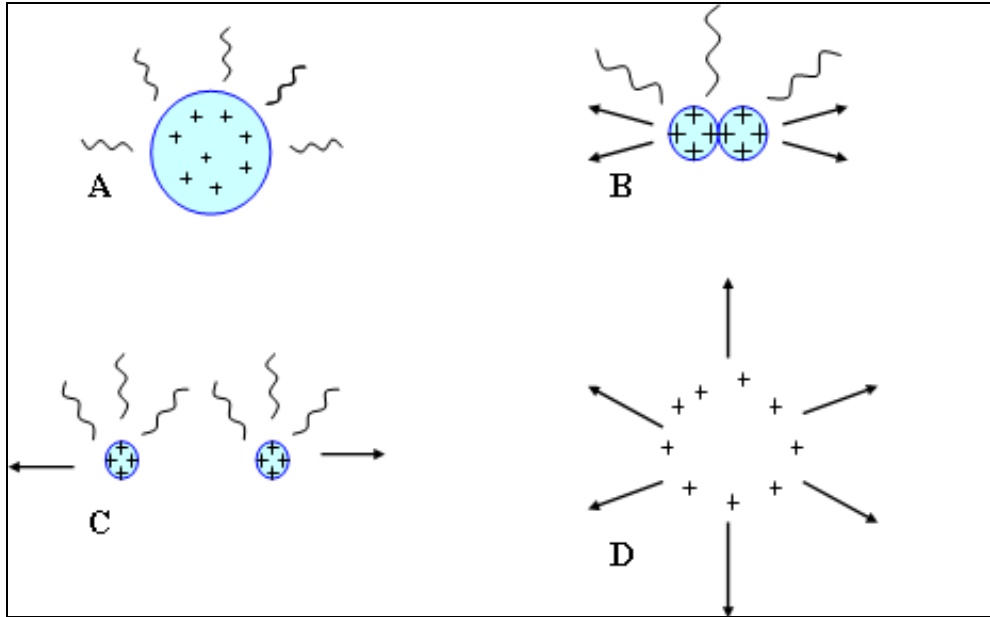


Figure 2.4. The break-up of charged droplets due to evaporation effects in combination with the maximum charge as specified by the Rayleigh limit. a) The droplet diameter decreases due to evaporation, b) the droplet breaks up into more droplets, c) due to continued evaporation, the newly formed droplet keep shrinking and breaking up until d) only ions are left.

Preferably, the charged droplets should survive as long as possible until they have reached the collector or the earth. Therefore, it is important to calculate the evaporation times, i.e. the time between state A and state D in Figure 2.4, of the charged droplets while they are being transported by the wind. In the next section, an analytical model will be derived, which can be used to calculate the flight times of the charged droplets. Comparing the evaporation times with flight times, we can determine whether the charged droplets can contribute to the conversion process.

Thus, in order to calculate the evaporation times of water droplets, the rate of evaporation has to be determined. This can be achieved in several ways, e.g. by using an energy balance method or by using mass transfer/diffusion methods. In this research, the latter method has been used which resulted in Table 2.2.

See appendix B for the set of equations and empirical relations that have been used to calculate the values in Table 2.2. The evaporation times of water

droplets with diameters varying from 1 to 100 μm have been calculated at a temperature of 20 $^{\circ}\text{C}$.

Table 2.2. The evaporation times of a water droplet as a function of the droplet diameter. Also, the relaxation time, τ , of the droplet has been calculated at 20 $^{\circ}\text{C}$ and a relative humidity of zero percent.

droplet diameter, d_d (μm)	evaporation time (s)	relaxation time, τ (ms)
1	0.001	0.003
10	0.076	0.304
20	0.31	1.21
30	0.69	2.73
40	1.22	4.86
50	1.91	7.59
60	2.75	10.93
70	3.74	14.88
80	4.89	19.43
90	6.19	24.59
100	7.64	30.36

In this table, we can see, for instance, that for droplets in the 20-50 μm range, the evaporation times vary from 310 milliseconds to almost two seconds if there is no wind present. If the air surrounding the droplet is moving, the evaporation time will be shorter depending on the difference between the speed of the droplet and the speed of the surrounding air. This means that water droplets need to be sufficiently far away or possibly collected by the earth before they are fully evaporated. These calculations have been conducted assuming that the relative humidity is zero percent.

In order to fully assess whether the evaporation will complicate the movement of the charged water droplets, we also have to consider the relaxation time, τ , of the droplets. In general, the relaxation time is the time required for a droplet to adjust to an equilibrium condition from a non-equilibrium position. In this context, it is the time it takes for the charged water droplet to attain the same speed as the surrounding medium i.e. the wind. As soon as that is the case, we only have to take into account the evaporation times as listed in the 2nd column of Table 2.2.

In appendix B, the reader can find the procedure for finding the relaxation times, but we will suffice by stating that these times for water droplets from 1 to 100 μm have relaxation times varying from $3 \cdot 10^{-6}$ to $30 \cdot 10^{-3}$ seconds, as can be seen in Table 2.2. In practice, this means that compared to the evaporation times,

the relaxation times are very small. This, in turn, implies that for practical matters we can take the 2nd column of Table 2.2 as the characteristic evaporation times which we can compare with the flight times. These flight times will be calculated in the next section and compared to the evaporation times.

2.2.2 Analytical model for simple configuration

In order to model the movement or trajectories of a number of the charged droplets as described at the beginning of this section, these droplets will be positioned in a simple electrode configuration, which means that the electric field will be modelled as a uniform field decreasing in the wind direction with $1/r^2$. The droplets will be assigned a polarity such, that the electric force they will experience, will be directed in the opposite direction of the wind, as shown in Figure 2.5.

First of all, equations must be given for the model, as complete as possible within reason.

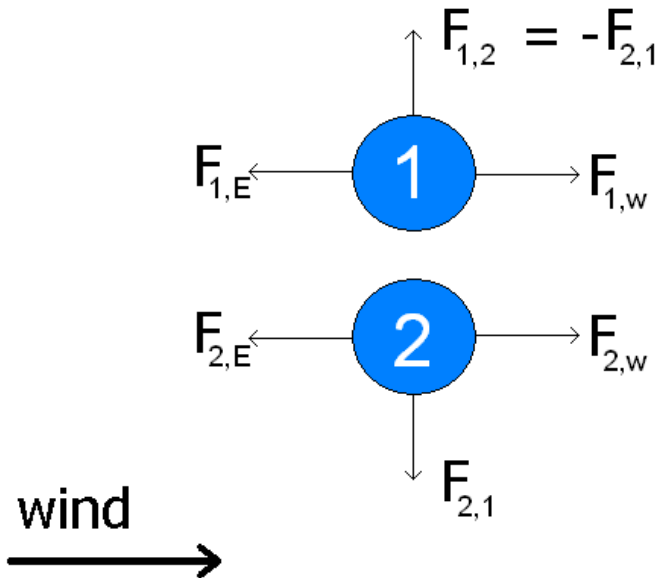


Figure 2.5. The schematic representation of the basic analytical model of charged droplets in a uniform electric field in which there is also wind present. Also, these charged droplets repel each other because of the like polarity.

There are several forces acting on the droplets, starting with gravity which obviously acts on all droplets,

$$\vec{F}_{i,g} = m_i \cdot \vec{g} \quad (2-6)$$

in which m_i is the mass of the i^{th} droplet and g is the gravity acceleration. In this model, for the time being, we will keep the mass of the droplet, m_i constant, thus disregarding evaporation effects. After droplet flight times have been calculated, we can compare them to the life times of the droplets and determine whether evaporation is a critical factor.

Because these droplets fall in air, there is also an upwards force acting on the droplets, the buoyancy,

$$\vec{F}_{i,B} = -\rho_a \cdot V_d \cdot \vec{g} \quad (2-7)$$

in which V_d is the volume of the droplet and ρ_a is the air density. Next, there is the drag force due to the wind which initially causes the droplets to move,

$$\vec{F}_{i,w} = \frac{\pi}{8} \cdot C_D \cdot \rho_a \cdot d^2 \cdot |\vec{v}_w - \vec{v}_d|^2 \cdot \frac{\vec{v}_w - \vec{v}_d}{|\vec{v}_w - \vec{v}_d|} \quad (2-8)$$

in which C_D is the drag coefficient, v_w is the wind speed and v_d is the speed of the droplet. This drag force will be zero when the droplet moves with the same speed as the wind. In specific cases, we can take out C_D and simplify (2-8) by looking at the Reynolds number.

The Reynolds number is an important dimensionless number in fluid mechanics and it is used to determine whether a flow process is turbulent or laminar by looking at the ratio of inertial and viscous forces. If the Reynolds number is lower than 1, which means that the viscous forces are dominant, then the flow process is said to be laminar,

$$Re = \frac{\rho_a \cdot d \cdot |\vec{v}_w - \vec{v}_d|}{\eta_a} < 1 \quad (2-9)$$

in which η_a is the dynamic/absolute viscosity of air. Laminar flow is often associated with smooth flow patterns as opposed to turbulent flow like e.g. the air flow around an airplane wing. When this happens, it is said that the flow process

takes place in the Stokes region and it can be shown that, in that case, Stokes' law can be used for the drag force,

$$\vec{F}_{i,w} = \frac{3\pi \cdot \eta_a \cdot d \cdot (\vec{v}_w - \vec{v}_d)}{C_c} \quad (2-10)$$

in which C_c is the slip correction factor by Cunningham, which becomes relevant for particles smaller than 1 μm . For particles with $d \gg 1 \mu\text{m}$, we can assume $C_c = 1$, see [18].

The electric forces acting on the droplets can be divided into two parts. The first part is the electric force due to the external electric field created by one or more electrodes present in the EWICON system, which will be represented by E_{ext} ,

$$\vec{F}_{i,E} = q_i \cdot \vec{E}_{ext} \quad (2-11)$$

in which q_i is the charge present on the i^{th} droplet. This charge will be expressed as a percentage of the Rayleigh limit and its value will depend on the spraying method used to create the charged droplets. The electric field, E_{ext} , is assumed to be decreasing in the wind direction with $1/r^2$ and pointed in the opposite direction of the wind. In this modelling, part of E_{ext} represents the field created by the charging system of the EWICON and, thus, the field that is responsible for the creation of the droplets.

The second part of the electric force due to the electric fields created by the other charged droplets is,

$$\vec{F}_{i,j} = \frac{1}{4\pi\epsilon_0} \cdot \frac{q_i q_j}{r_{i,j}^2} \cdot \hat{r}_{ij} \quad (2-12)$$

in which $r_{i,j}$ is the distance between droplet i and droplet j . It should be noted that all the created charged droplets have charge with the same polarity and, thus, they will repel each other.

In reality, the sum of the electric fields generated by all the charged droplets affects the electric field at the charging system, represented by E_{ext} , and that means that the charging and spraying process is changed. This, in turn, would mean that the created charge droplets could have different sizes, initial velocities and charges. In this model, we will not take this into account.

Summing all contributing forces, we find for the law of motion

$$\vec{F}_i = \vec{F}_{i,g} + \vec{F}_{i,B} + \vec{F}_{i,w} + \vec{F}_{i,E} + \sum_{j \neq i}^j \vec{F}_{i,j} = m_i \cdot \vec{a}_i \quad (2-13)$$

in which F_i is the total force on the i^{th} droplet and a_i is the acceleration of the charged droplet. Equation (2-13) can be solved, thereby giving us the velocity and position of every droplet at each point in time. In this equation, if we look at the orders of magnitude, then the total force is mainly dominated by the drag force and the electric force.

Using (2-13), the work done on the i^{th} droplet, W_i , by the wind can be found by using

$$W_i = \int (\vec{F}_i - \vec{F}_{i,w}) \cdot d\vec{\ell} \quad (2-14)$$

in which $d\ell$ is the displacement which follows the path of the droplet. From this, the potential energy difference for the droplet can be calculated and, when taking the sum of all the droplets, the total energy gained from the wind.

A number of assumptions have been made using this representation of the movement of charged droplets by wind in an electric field. Firstly, as has already been mentioned, we assume that there is no evaporation of the droplets. If these charged droplets do evaporate, then ions will be formed and there will be an ionic space charge field. If this occurs close to the charging system of the EWICON, then the influence of this field should be taken into account. Therefore, the evaporation times calculated in the previous section should be compared to the flight time of the charged droplets in order to verify whether the omission of evaporation effects is justified.

However, estimations show that in wet conditions the evaporation times are in the order of ten seconds. With a wind speed of e.g. 10 m/s, this implies that the ionic space charge field will be formed at distances of a hundred metres and its effect can be neglected.

Secondly, we assume that the size distribution of the droplets is monodisperse, i.e. all the droplets have the same size, and that the droplets each have the same charge. This, again, depends on the used spraying method and the way it has been implemented in the EWICON system. Thirdly, we assume that the droplets remain spherical at all times and do not deform when they are moved by the wind.

Finally, with respect to the wind speed, we assume that the flow of air is constant, laminar and unidirectional. In realistic scenarios, this is not always the case. However, during the experiments with similar systems, which will be discussed in chapter 5, the flow of air could be controlled such that it satisfied these assumptions.

2.2.3 Constraints on size and charge, electrical mobility

With the knowledge of the maximum charge, q_{max} , as described in section 2.2.1, we have to choose a certain value for the charge, q , on the droplet, which we will express in percentages of the Rayleigh limit. In practice, this will depend on the chosen charge creation method and the mode in which this method is operated. Some of these methods have the possibility to independently control the charge on the produced droplets, while other methods have size and charge dependency, see chapter 3 on methods for charge droplets creation for more information.

Regardless of which of the two implementations discussed in chapter 1 is used, for the EWICON system to operate successfully, the charged droplets need to be transported away by the wind completely. This flow of charge constitutes an electric current. The more charge can be transported per time unit, the higher the electric current will be and, in turn, the higher the output power will be, if we assume that the working voltage of the EWICON system remains constant during operation.

Therefore, it may seem favourable to assign as much charge to a droplet as possible and to make the droplets as small as possible, resulting in a high charge-to-mass, *CMR*, ratio, because in that case more droplets per time unit can be dispersed using the same liquid flow rate. However, these small highly charged droplets may have trouble to overcome the electric field which attracts them back to EWICON system and thus the question arises of what the optimal size of and charge on a droplet should be. Related to the answer to this question, it should also give an indication of the maximum of the electric field and/or the minimum wind speed needed to transport the droplets away.

If a charged droplet is released in a uniform electric field in vacuum, then the charged droplet will experience a constant electric force and, thus, will move with increasing speed, as indicated in Figure 2.6.

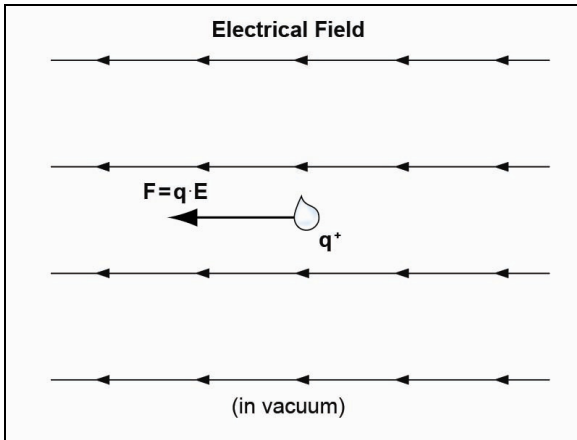


Figure 2.6. A charged droplet is released in a uniform electric field in vacuum. The droplet experiences a constant electric force to the left and will be constantly accelerated.

If a charged droplet is released in a uniform electric field in stationary air, then the droplet will experience not only a constant electric force, but also a drag force in the opposite direction, as indicated in Figure 2.7. This drag force is dependent on the speed difference of the droplet with the surrounding air. Therefore, the drag force will increase as long as the droplet is accelerated by the electric field until both forces are equal in magnitude. At that point, the droplet will move with a constant speed to the left.

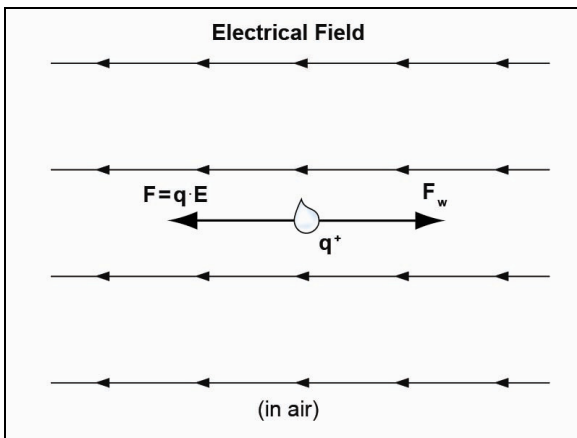


Figure 2.7. Here, a charged droplet is released in a uniform electric in stationary air. Now, the droplet will also experience a drag force, F_w , in the opposite direction, dependent on the difference between the speed of the droplet and the surrounding air and at the certain moment the two forces will be equal.

This situation is similar to that occurring at the nozzle of an EWICON system, where droplets are released in moving air flowing from the left to the right, as indicated in Figure 2.8.

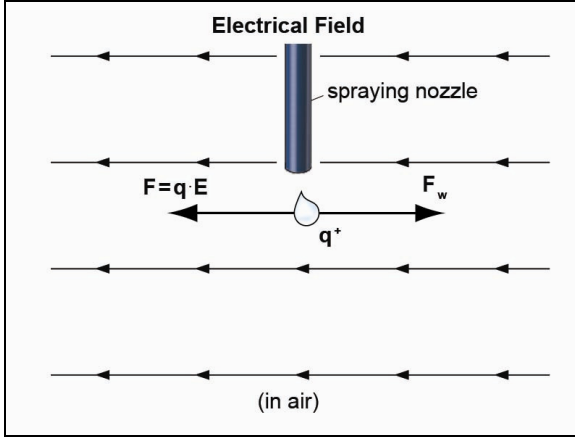


Figure 2.8. The situation in an EWICON system. A charged droplet is released in wind moving from the left to the right. In order for the wind to be able to move the droplet to the right, the wind speed needs to be higher than the constant speed that was reached by the droplet in Figure 2.7.

If the wind is to move the charged droplet to the right, then the wind speed must be higher than the constant speed or terminal electrostatic velocity, v_T , that was reached in stationary air in Figure 2.7. In order to calculate this terminal electrostatic velocity, we look at the mechanical mobility, μ_m , and the electrical mobility, μ_e , of the charged droplets which are defined as:

$$\mu_m \equiv \frac{v_T}{F_w} \quad (2-15)$$

and

$$\mu_e \equiv \frac{v_T}{E_{ext}} = q \cdot \mu_m \quad (2-16)$$

in which v_T is the terminal electrostatic velocity of the droplet or, in this case, the difference between the wind speed and droplet speed, $|v_w - v_d|$. F_w is the wind drag force and E_{ext} is the external electric field, in this case, generated by the electrodes present in the EWICON system. The latter part of equation (2-16) is derived when we equate the electric force to the drag force, which can be expressed in the form of equation (2-10) if the droplets move in the Stokes region.

If the Reynolds number is larger than 1, then the expression for the drag force becomes a bit more complicated. Again, we equate the electric force to the drag force, but this time, we use equation (2-8) for the drag force.

$$q \cdot E_{ext} = \frac{\pi}{8} \cdot C_D \cdot \rho_a \cdot d^2 \cdot v_T^2 \quad (2-17)$$

in which $|v_w - v_d|^2$ has been replaced with v_T^2 . Equation (2-18) can, if we solve for C_D and multiply by Re^2 , be rewritten to

$$C_D \cdot Re^2 = \frac{8 \cdot q \cdot E_{ext} \cdot \rho_a}{\pi \cdot \eta^2} \quad (2-18)$$

On page 57 of [18], we can find that for the terminal electrostatic velocity the following expression can be given

$$v_T = \left(\frac{\eta_a}{\rho_a \cdot d} \right) \cdot e^{(-3.070 + 0.9935 \cdot J - 0.078 \cdot J^2)} \quad (2-19)$$

in which

$$J = \ln(C_D \cdot Re^2) \quad (2-20)$$

For a range of droplet diameters and charges, one can calculate the terminal electrostatic velocities, v_T , of the droplets as a function of the electric field. This will give an indication whether the droplets have a too small or too big diameter or too much charge such that the wind is not able to transport them away. Also, this will give an indication on how to shape and grade the electric field to make sure it is not too high for the charged droplets to escape from. This is a point that will be addressed in detail in chapter 4.

As an example, in Table 2.3, we have calculated the maximum charge for four water droplets, each with a different diameter. In this table, for now, we have set the charge on the droplets to 70% of the Rayleigh limit maximum charge. In the next chapter on charged particle creation methods, we will see that there are methods available that can achieve these kinds of charging efficiencies.

Table 2.3. Various water droplet diameters with their respective maximum charge. In this example, the charge on the droplets, $q_{0.7}$, is set to 70% of the maximum charge which corresponds to charging efficiencies of one of the charged particle creation methods. These droplets are used to calculate the terminal electrostatic velocity in an electric field and air.

d (μm)	d (m)	q_{max} (C)	$q_{0.7}$ (C)
0.1	10^{-7}	$2.25 \cdot 10^{-16}$	$1.58 \cdot 10^{-16}$
1	10^{-6}	$7.12 \cdot 10^{-15}$	$4.98 \cdot 10^{-15}$
10	10^{-5}	$2.25 \cdot 10^{-13}$	$1.58 \cdot 10^{-13}$
100	10^{-4}	$7.12 \cdot 10^{-12}$	$4.98 \cdot 10^{-12}$

Continuing the example, while assuming that the flow process takes place in the Stokes region, we calculate the terminal electrostatic velocities for one of the droplet diameters mentioned in Table 2.3. In this example, we take 1 μm as the droplet diameter and we perform the calculations for different electric field strengths, of which the results can be found in Table 2.4.

Table 2.4. Terminal electrostatic velocities, v_T , for increasing electric field strengths.

droplet diameter 1 μm	E (V/m)			
	1	10^2	10^4	10^6
Stokes v_T (m/s)	$3.40 \cdot 10^{-5}$	$3.40 \cdot 10^{-3}$	$3.40 \cdot 10^{-1}$	$3.40 \cdot 10^1$
Re	$2.24 \cdot 10^{-6}$	$2.24 \cdot 10^{-4}$	0.02	2.24 too high ↓
Newton v_T (m/s)	-	-	-	24.47

For each of the terminal electrostatic velocities, the corresponding Reynolds number is calculated to ascertain the validity of the simple model. We can see in Table 2.4, that when the electric field varies from 1 to roughly 10^4 V/m, the Reynolds number is well below 1 and this gives us an indication that the calculated terminal electrostatic velocities are valid approximations.

However, when the electric field is in the order of 10^6 V/m, the Reynolds number is above 1 and that means the Stokes approximation does not hold anymore. It is said that the flow process takes places in the Newton region. Using equations (2-17) through (2-20), we can correctly calculate the terminal electrostatic velocity.

Furthermore, from Table 2.4, we can conclude the following. Firstly, when the electric field stays below roughly 10^4 V/m, the terminal electrostatic velocity is well below 1 m/s and this implies that any type of wind that is more than a light breeze ($v_w > 3.3$ m/s) should be capable of transporting this 1 μm charged droplet

away from the charging system. Secondly, however, as soon as the electric field is in the order of 10^6 V/m, the terminal electrostatic velocity of the droplet increases, even after correction for the Newton region, to approximately 25 m/s. For a $1 \mu\text{m}$ droplet to be transported away, a storm would be needed ($v_w > 25$ m/s).

The terminal electrostatic velocities for the other droplet diameters listed in Table 2.3 have been calculated as well. This has been plotted in Figure 2.9, where the black dots indicate that at the specified electric field the Reynolds number is equal to 1. At higher electric fields, the Stokes approximation is not valid. When the droplet diameter is increased to 10 or $100 \mu\text{m}$, the Newton region is entered at a lower electric field.

When the electric field is lower than 10^5 V/m, the maximum terminal electrostatic velocities of the droplets vary between 1 to 15 m/s, which is within the transporting capabilities of normal everyday occurring wind. As soon as the electric field is in the order of 10^6 V/m, the terminal electrostatic velocities vary from 20 to over a 100 m/s. Wind speeds of those magnitudes are much rarer and, thus, for everyday operation this will pose a problem.

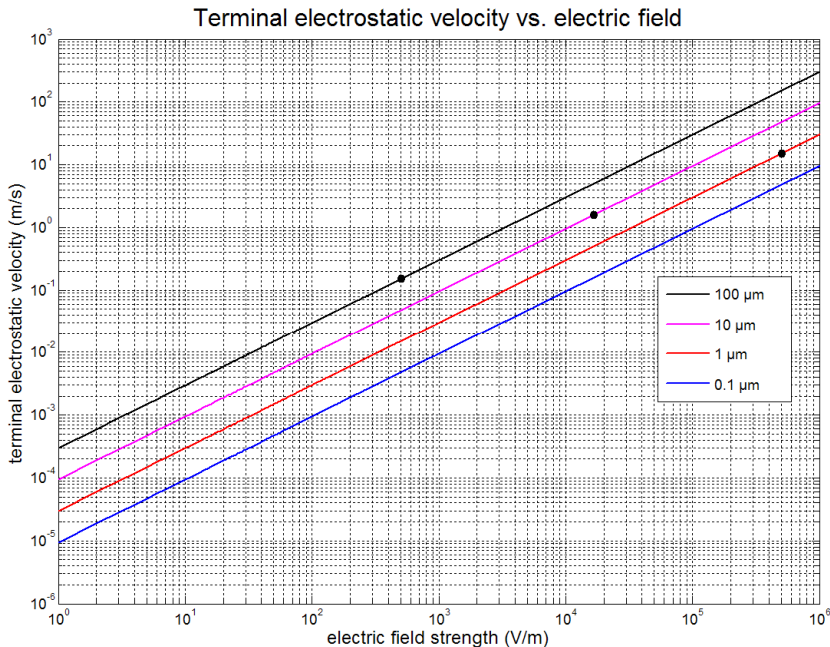


Figure 2.9. The terminal electrostatic velocities of a water droplet as a function of the electric field. The velocities have been plotted for droplet diameters of 0.1, 1, 10 and $100 \mu\text{m}$. The black dots indicate when the Reynolds number is equal to 1.

From all this, we can draw a number of conclusions which are useful when designing an EWICON system. First of all, it is apparent that the electric field should not be higher than 10^6 V/m anywhere in the trajectory of the charged droplets. This means that the electrodes in the charging system should be designed and graded, such that the charged particles creation process can still take place without the high fields occurring near the place where the charged droplets are dispersed. It also means that, when the EWICON system is in operation, its operating voltage should not rise to a magnitude that the system as a whole generates an electric field high enough to prevent transportation by the wind.

Another conclusion is that from the range of droplet diameters, for which we have calculated the terminal electrostatic velocities, most of them are suitable for charge transportation, depending on the prevalent electric field. If we calculate the electric mobility of these droplets, we find that it varies from $3 \cdot 10^{-5}$ to $3 \cdot 10^{-4}$ $\text{m}^2/\text{V}\cdot\text{s}$ for 0.1 to 100 μm droplets respectively. This partly agrees with the analysis of Cloupeau [19], who had concluded that for efficient power generation to take place, the charged droplets need to be created with a low electric mobility in the order of 10^{-6} $\text{m}^2/\text{V}\cdot\text{s}$. This value was based on a one-dimensional theory, see [20]. However, in [19] experiments were still conducted with a Type A EWICON implementation using droplets with mobilities of $3 \cdot 10^{-5}$ $\text{m}^2/\text{V}\cdot\text{s}$. Cloupeau concluded that wind power conversion with positive efficiency was possible, stating that actual two-dimensional effects were not taken into account by the one-dimensional model.

If we were to calculate the electric mobility of droplets for even smaller or bigger diameters, we would see that the mobility would increase and, therefore, those droplets would not be suitable for the EWICON system.

2.2.4 Computation & numerical values

Using equations (2-6) through (2-14), a numerical procedure was constructed which has been entered into MATLAB. For the calculation of the various quantities such as position, speed and the trajectories of the droplets, a numerical scheme called Velocity-Verlet has been used. This is a time integration method that is normally used in molecular dynamics simulations and it is favoured over other algorithms like Euler integration because of its higher stability and accuracy or over the Runge-Kutta method because of its relative simplicity.

Without going too much into detail, these methods use a Taylor expansion of the positions of the particles/droplets as a function of time. In general, based on the values of the position, velocity and acceleration of these particles and the potential function at time-step t_n , the values of the four quantities can be calculated at time-step t_{n+1} . After this, the potential function is recalculated using the newly

found values for the three quantities and the process repeats itself. The main difference between the Euler and the Velocity-Verlet method is that the former is a first order approximation scheme, whereas the latter uses a second order approximation.

The actual listing of the MATLAB program used for these simulations can be found in appendix C. A 3D plot of the trajectories based on the numerical calculations can be seen in Figure 2.10.

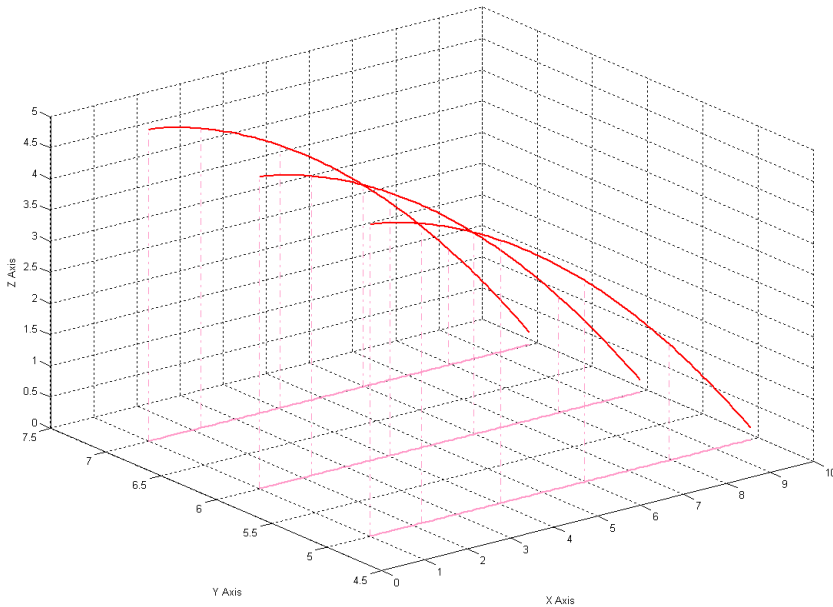


Figure 2.10. The resulting plot of the trajectories based on a simulation of three positively charged droplets in an electric field. The wind speed is set at 10 m/s in the positive x-direction, the electric field is set at $5 \cdot 10^4$ V/m in the negative x-direction.

In this simulation, we have set the wind speed at 10 m/s in the positive x-direction and the electric field at 50000 V/m in the negative x-direction. The droplets have a diameter of 10 μm and they are positively charged. The charge is set to 70% of the maximum given by the Rayleigh limit. The simulated time depicted in Figure 2.10 is 1 seconds.

We can see in Figure 2.10 that the wind is able to overcome the electric field and, thus, the droplets are transported in the direction of the wind, while falling down due to gravity. At this point, we look back at section 2.2.1, where we discussed the evaporation times of charged droplets. For a droplet with diameter of 10 μm , the evaporation time is 0.08 seconds, which means that in this simulation the droplet would have travelled 0.8 metres. In an EWICON system, this would

mean that extra measures would have to be taken before the charged droplets can reach earth. It can be calculated, however, that in the mist of charged droplets, the relative humidity is very high and this can prolong the evaporation time of these droplets up to 10 seconds, see appendix B and/or page 299 of [18].

In this simulation, the droplets have been placed far from each other and, therefore, the mutual electric repulsive force is not noticeable in the trajectories of the droplets. This is not the case in a simulation, of which the plot can be seen in Figure 2.11, where we have put the charged droplets very close to each other and, consequently, we can see that the repelling electric forces start to have a noticeable effect on the trajectories of the droplets while they are being transported by the wind.

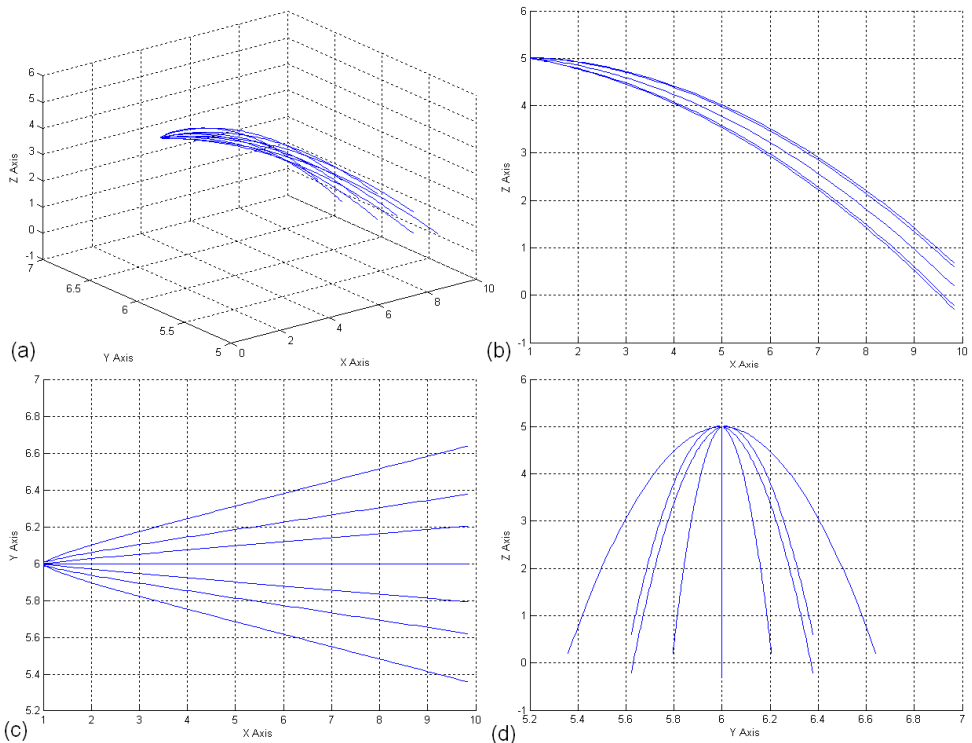


Figure 2.11. Plot of the simulation in which ten droplets of equal size and charge are placed closely to each other. Now, the mutual repelling forces start to affect the paths of the charged droplets. In the upper left-hand corner (a), an isometric view of the situation is given; in the upper right-hand side (b) a side view along the direction of the wind given. In the lower left-hand corner (c) a top view is given; in the lower right-hand corner (d) a side view in the direction of the wind is given.

Together with the plots of the trajectories of the charged droplets, the work on the droplets performed by the wind on the charged droplets according to (2-14) has been calculated and it was found to be $1.13 \cdot 10^{-8}$ J. If we assume that a spraying nozzle disperses roughly $1 \cdot 10^7$ droplets per second or 20 ml/hr, which, we shall see in the next two chapters, is not unreasonable to assume, then the power associated with this stream of droplets is 113 mW per nozzle. We will see in later chapters, that this is a reasonable estimation for the power delivered by a nozzle capable of producing these types of charged droplets.

We will take a closer look at scaled up EWICON systems in chapter 5, but for now we can imagine that if we were to pack 900, e.g. a 30x30 array, of these nozzles in a system with a wind surface area of 1 m^2 , the power associated with such a system would be 102 W.

2.3 Performance Index of the EWICON system

In order to compare the various implementations of the EWICON with the existing wind turbine technology and with each other, we have to clearly define numbers that characterise the system performance. This number, which will be called the EWICON Performance Index (*EPI*), should include the efficiency ratio, η_{EWICON} , of the converted output power, P_{out} , and the sum of the input power, ΣP_{in} ,

$$\eta_{EWICON} = \frac{P_{out}}{\sum P_{in}} \quad (2-21)$$

where ΣP_{in} consists of the maximum recoverable power in the wind, the electrical power needed to charge the droplets and mechanical power to pump the liquid to the desired height with the desired flow rate.

$$\sum P_{in} = P_{max} + P_{electrical} + P_{mechanical} \quad (2-22)$$

However, (2-21) does not completely represent the nature of the EWICON system. First of all, since the maximum output power of the EWICON system depends on the wind surface area, A , it stands to reason that the performance of a particular implementation is rated higher when it can convert more power from the same wind surface area.

Furthermore, since liquid droplets are used as charge carriers, the liquid flow rate, Q , also is an important parameter, which needs to be factored into the *EPI*. Lastly, in the case that the efficiency ratio, the liquid flow rate and the wind

surface are equal, we want to rate an implementation as higher when it is able to produce a higher output power.

All these considerations result in an *EPI* as follows

$$EPI \equiv \log \left(P_{out} \cdot \frac{\eta_{EWICON}}{A \cdot Q} \right) \quad (2-23)$$

where we have taken the logarithm to manage the otherwise high values of the *EPI*, which could occur if P_{out} reaches the order of current conventional wind turbines. Some example values of the *EPI* can be found in Table 2.5.

Table 2.5. Example values of the EWICON Performance Index. These four examples could be characterised as follows: the first two examples can be considered small prototypes, whereas the last two examples can be considered scaled-up versions. The last example is rated higher because it requires ten times less liquid to operate at the same output power.

ΣP_{in} (W)	Q (l/h)	A (m ²)	P_{out} (W)	η_{EWICON} (%)	<i>EPI</i>
10	1	0.1	1	10	2
100	1	0.1	10	10	3
10000	10	1	1000	10	3
10000	1	1	1000	10	4

2.4 Conclusions

We can conclude that from a theoretical point of view, the EWICON principle can be used to convert wind energy to electrical energy. The total energy that can be converted depends on the wind speed, the number of droplets, the amount of charge placed on these droplets and the strength of the electric field. Simulations have shown that the work performed by the wind on the droplets ultimately can lead to powers that are in the same order of magnitude as the power associated with the wind.

We have found that for a range of droplet diameters (0.1-100 μm), the electric field should not be higher than 10^4 - 10^6 V/m, if realistic wind speeds (up to 6 on the Beaufort scale) are expected to move the charged droplets away.

3

Charged droplet creation methods

“The noblest of elements is water.”

– Pindar, 476 B.C.

In order for the EWICON system to convert wind energy to electrical energy, the wind must be able to move charged carriers against the direction of the electric force on the carriers exerted by the electric field. In theory, these carriers can be any type of object that can be electrically charged. In the previous chapter, however, a number of requirements for these carriers, like charge and size, have been discussed and this means there are certain properties that the carriers ideally should have.

One of these assumed properties is that these objects should be droplets and this means that we need methods to create charged droplets from a liquid. For the sake of completeness, in this research, several experiments have been conducted using other types of charge carriers, like solid spheres. Without going into detail, these experiments have proven that the EWICON concept works with arbitrary types of charge carriers, but these experiments have also proven that most of these charge carriers are not ideal in terms of ease of creation, level of charging and power yield. Moreover, most of these non-liquid charge carriers would require some form of recycling procedure to reuse them. Therefore, the methods described in this chapter will all focus on the spraying and charging of liquid droplets.

Firstly, in section 3.1, we will look at the other requirements for the methods posed by the EWICON system, the first one still being that the medium is a liquid. Subsequently, in section 3.2, we will look at a number of charged droplet creation methods that have previously been considered and we will discuss the reasons why these methods have not been implemented in the EWICON system.

In sections 3.3 and 3.4, we will discuss the two main contending charged droplet creation methods. For each of these two methods, we will discuss the main working principles, some of the conducted experiments and the results thereof and

we will end with the conclusions with respect to their usability within the EWICON system.

Finally, we will discuss which of the methods are, in principle, most suitable for the EWICON system, where we should keep in mind that more than one method is possible, e.g. if the environmental conditions are different.

3.1 EWICON requirements on droplet creation

The efficient generation of charged droplets is probably the single most important aspect of the EWICON system. Therefore, the choice of the spraying method should be handled with extra consideration. The chosen spraying method(s) should at least try to adhere to the following set of requirements, which will then be explained per point in the following sections:

- low energy consumption with respect to the energy in the wind
- controllable charge, high current output
- monodispersity of the liquid droplets
- operable under windy condition
- environmentally friendly spraying liquid

3.1.1 Low energy consumption with respect to the energy in the wind

There are several methods available for creating charged droplets. Usually, these methods require high electric fields and/or high pressure to operate. Some of these methods require significant amounts of energy and this means that it would be more difficult to achieve positive conversion efficiency. Of course, the usability of a method depends on the prevailing wind speed at the site location and its distribution and on how much energy other components in the EWICON system need.

For example, if we take wind through a surface area of 1 m^2 with a speed of 10 m/s , then we know, by using equation (2-1), that the power associated with this particular wind is 647 W . Knowing, with Betz in the back of our mind, that roughly 60% of the power in the wind can be converted into electrical energy, this means that we can extract 383 W at most. So, if a particular spraying method would need e.g. 221 W to operate leaving 162 W as the net output, the maximum conversion efficiency would be 25%. This does not even include other factors like e.g. monitoring equipment or supplying the liquid to a certain height.

3.1.2 Controllable charge, high current output

In the previous chapter, calculations have been performed with respect to the electrical mobility of the charged droplets and the considerations made by Cloupeau 0. It was concluded that for a certain range of mobilities the performance of the EWICON system would be optimal. Therefore, the possibility to control the charge, that is present on a droplet, would give us a possibility to fine-tune the EWICON system such, that all the charged droplets would be transported away. Also, in the case that it would be relatively simple to adjust the amount of charge, the EWICON system could be designed in such a way that it could easily adjust to changing wind speeds.

The objective of the EWICON system is to convert as much wind power to electrical power as possible. This means that the current associated with the charged droplets should be as high as possible, assuming that the EWICON system operating potential is constant. This not only requires the droplets to be highly charged, but also that they are produced at a high rate.

In order to determine what is considered a high current, we will consider a small example. Using the information of chapter 2 as a guiding principle, we look at water droplets with a diameter of 5 μm that are sprayed from one nozzle. If these water droplets can be charged to 70% of the maximum charge given by the Rayleigh limit, then the current per nozzle can be calculated based on the flow rate of the liquid. At 20 ml/hr, the rate of charged droplets is $8.5 \cdot 10^7$ per second and this rate amounts to a current through the nozzle of 4.7 μA per nozzle. If we have an electrical load of 20 $\text{G}\Omega$, then this would imply an output power of roughly 0.5 W.

If we revisit the situation described in section 3.1.1, in which we wanted to achieve a conversion efficiency of 25%, then this would imply that we require 212 nozzles per m^2 to produce the current required to feed the load. Now, if we take droplets with a diameter of 15 μm , then the current drops to 0.9 μA per nozzle, which implies an output power of 17 mW. This would come down to roughly 5500 spraying nozzles per m^2 . In terms of liquid consumption, this equals going from 4.2 litres per hour for the former situation to 110 litres per hour for the latter situation.

3.1.3 Monodispersity

The production of monodisperse droplets means that droplets of only one size are created. Together with the requirement described in the previous section, we would have a droplet with one particular size and charge. This is advantageous for the EWICON system for a number of reasons. First of all, as we have seen in the previous chapter, the operation of the EWICON system is greatly simplified

regarding control purposes by only having to take into account one particular type of droplet.

Secondly, in monodisperse mode, the EWICON behaves like a near-ideal current generator, i.e. it can deliver a constant current to a load for any working voltage up to a certain maximum voltage. The fact that all droplets are created with equal size implies that they all have the same upper charge limit related to the Rayleigh break-up principle. This means that the droplets are all charged in the same manner, resulting in droplets with equal charge. In turn, this means that, on average, the force balance on each of the charged droplets, as described in the previous chapter, would be the same.

Therefore, if one charged droplet can be moved against the electric field by the wind, then all the droplets could be moved. Conversely, if one charged droplet is attracted back to the EWICON system, because e.g. the wind speed has dropped or the EWICON system potential has increased, all the droplets would be attracted. And thus, the output current would drop to zero at that potential. This does not take into account space charge effects, which causes charged droplets closer to the EWICON system to be pushed back by droplets that have been dispersed earlier.

In practice, there will always be a range of droplet sizes and, therefore, monodispersity as explained in the first paragraph will usually not occur. In aerosol science, a droplet distribution is defined as monodisperse when the geometric standard deviation σ_g or *GSD* of the droplet size distribution is smaller than 1.2, see e.g. [21],

$$\sigma_g < 1.2 \quad (3-1)$$

in which σ_g is given by

$$\sigma_g = GSD = \exp \sigma = \exp \left(\sqrt{\frac{\sum_{i=1}^n (\ln d_i - \ln \mu_g)^2}{n}} \right) \quad (3-2)$$

in which n is the number of measured droplets with a diameter d_i , σ is the standard deviation of the log-normal distribution and μ_g is the geometric mean defined by

$$\mu_g = \sqrt[n]{d_1 d_2 \dots d_n} \quad (3-3)$$

This assumes that the distribution of the produced droplets follows a log-normal distribution. For the measured droplets in the subsequent parts of this thesis, this will be determined by using statistical methods.

For large groups of droplets, calculating the *GSD* by using (3-2) and (3-3) can become laborious and, therefore, the *GSD* can also be estimated by

$$GSD = \sqrt{\frac{d_{84}}{d_{16}}} \quad (3-4)$$

in which d_{16} and d_{84} are the droplet diameters at the 16% and at the 84% size cut of the cumulative distribution. Equation (3-4) will be used, when the statistical fit of a distribution cannot be accurately determined.

After performing droplet size measurements, which will be discussed in this chapter and in chapter 4, the monodispersity of the produced droplets can be determined by using one of these methods.

3.1.4 Operable under windy condition

As we will see, there are a number of charging methods that provide a high current output and monodispersity in a wind-free environment which would suit the EWICON system, but these methods fail to deliver the same results when a flow of air is applied. Thus, for each method under consideration, it should be tested that the creation of charged droplets is not disturbed by the wind.

3.1.5 Environmentally friendly spraying liquid

The EWICON system is an open system, which means that it will be in contact with the surrounding environment, dispersing its charged droplets into it. Therefore, the spraying liquid needs to be safe for the environment if the EWICON is to be accepted as an alternative for the wind turbine. Preferably, the used charging method(s) should be able to make use of water, saline or fresh.

3.2 Previously considered creation and charging methods

There are several spraying and/or charging methods available and a number of these methods have been considered and tested in a previous EWICON research project, see [22]. We will list two droplet creation methods and one droplet charging method, give a brief description and explain why these methods have not been implemented in the current EWICON system.

3.2.1 Droplet creation - Ultrasonic atomisation

Ultrasonic atomisation is a method, with which droplets can be produced by using ultrasonic waves at the liquid-air interface, see e.g. [23]. These vibration forces, responsible for the atomisation, are generated by piezoelectric ceramic crystals. Two mechanisms are believed to be responsible for the droplet break-up, namely the capillary wave hypothesis and the cavitation hypothesis. The reader is referred to the references for these mechanisms. Droplets generated by this atomisation method have relatively small diameters, ranging from a few microns to a few tens of microns. Also, the distribution of the droplet size can be made narrow.

The main drawback of this atomisation method is that it is quite costly in terms of power dissipation. Devices capable of ultrasonic atomisation require 1 to 20 kilowatts to operate depending on the required flow rate. This would mean that an EWICON system would require a wind surface area of 2 to 50 m² operating at the Betz optimum conversion efficiency just to provide power for the droplet generation.

3.2.2 Droplet creation - Centrifugal or rotating disk atomisation

If a liquid is fed to the centre of a rotating disk in the form of a continuous jet at a small flow rate, then this liquid can be atomised, see [24]. Such a rotating disk can produce small droplets at high rotating speeds. Also, this technique can be modified to an electrified rotating disk in order generate electrospray.

The main drawback of this atomisation method is the fact that it is based on rotational movement and, hence, susceptible to wear and tear. This, of course, is the very reason why the concept of the EWICON system was introduced in the first place. Consequently, maintenance costs (together with purchase costs) of this type of atomiser are relatively high. Other drawbacks include the lack of monodispersity of the droplets.

3.2.3 Droplet charging - Corona charging

Both methods that are described in 3.2.1 and 3.2.2, in principle, only provide uncharged droplets (although for rotating disk a charging method has already been given). Therefore, they have to be combined with a charging method to obtain charged droplets.

Corona is a partial breakdown effect that occurs when the local electric field surrounding a sharp point, e.g. a charging electrode, becomes too high. When this happens, ionisation occurs because electrons are accelerated away (in case of negative potential) from the electrode, colliding with nitrogen or oxygen molecules, see [25]. This results in free electrons, which, in turn, can also collide with other molecules, leading to an electron avalanche. Typically, electrical breakdown occurs at electric fields of 3.0 kV/mm in air, but this also depends on the radius of the sharp point. In general, corona is an unwanted effect because it causes e.g. losses in high voltage lines or radio interference.

However, corona can also be used for the charging of particles and it is widely used in the coating industry or for the precipitation of dust. Therefore, this charging method has been considered for the application of charge on the droplets, which could be created by e.g. one of the two previously mentioned methods. The ions that have been created by the corona process will attach themselves to the droplets, a process called “ion bombardment”.

The power required to perform corona charging, P_{corona} , is given by

$$P_{corona} = V_{corona} \cdot I_{ion} \quad (3-5)$$

in which V_{corona} is the potential of the charging electrode at which the corona discharge occurs and I_{ion} is the current associated with the ionisation. Typical inception potentials for corona are in the range of 450 V to 15 kV per electrode for air depending on the polarity of the potential and the radius of the sharp edge of the electrode, see [25]. Currents associated with these potential are in the range of 200 to 1000 μ A, see [26]. Consequently, typical power requirements vary from 0.1 to 15 W per electrode.

One of the drawbacks of this charging method is that the created droplets need to be directed along the area where the corona is created for them to acquire charge. Inevitably, there will be a number of droplets that will not be charged. This, in turn, means that the current associated with the charged droplets will always be smaller than the current associated with the ionisation.

3.3 Electrohydrodynamic atomisation

Electrohydrodynamic atomisation, EHDA or electrospray, is a spraying and charging method which is e.g. used for coating purposes or medicine administering. Its main advantage is that very little energy is required for the creation of charged droplets.

3.3.1 EHDA principle

The EHDA spraying method is based on the principle that a strong electric field will deform the meniscus of the liquid leaving a spraying nozzle to a conical shape, i.e. the electric Coulomb force will interact with the surface tension of the liquid. Ions in the liquid will accelerate towards the cone apex and, due to this movement, the liquid itself is accelerated. At the cone apex, a liquid jet occurs which breaks up into droplets with a high charge density. Depending on the direction of the applied electric field, the net charge on the droplets will either be positive or negative. Usually, this electric field will be created using charging electrodes.

The droplet diameter, charge and initial velocity as well as the rate at which the charged droplets are ejected from the nozzle, all depend on the potential of the charging electrodes, the geometrical configuration of these electrodes and the properties and the flow rate of the spraying liquid.

Using EHDA, it is possible to spray droplets in different spraying modes, depending on the flow rate of the liquid and the shape and strength of the local electric field. The spraying modes of EHDA are separated into two general categories: modes that exhibit a continuous flow of liquid through the meniscus and modes that do not. The former consists of the simple-jet, the cone-jet and the ramified-jet, while the latter consists of the dripping, the micro dripping, the spindle and the intermittent cone-jet modes. The latter are often referred to as pulsating modes, see [27].

One of these continuous spraying modes is the cone-jet mode or Taylor cone mode, see Figure 3.1, and one of its main advantages is the fact that droplets are highly charged up to 70% of the maximum charge given by the Rayleigh limit, see [28]. Also, the droplet distribution in this cone-jet mode can be monodisperse.

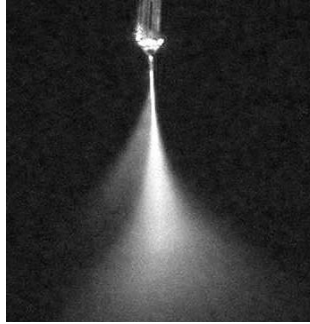


Figure 3.1. An example of EHDA spraying in the cone-jet mode, which is also referred to as the Taylor cone mode. Ethanol is sprayed under the influence of an electric field which results in a stream of charged droplets. The droplets all have the same polarity, which causes the expanding mist of droplets.

One drawback of EHDA, however, is that in order to spray in the cone-jet mode, the surface tension of the used spraying liquid should be relatively low. Using a conventional EHDA spraying set-up with demineralised water, continuous cone-jet spraying does not occur due to the high surface tension of water ($72 \cdot 10^{-3}$ N/m); see [29]. In order to actually achieve any spraying of charged water droplets, the electric field has to be increased to such a level, that it leads to a very unstable spray without monodisperse droplets. Part of this instability is caused by the fact that the charged water droplets reduce the electric field at the nozzle, thereby cancelling the cone-jet spraying as it has started. These charge relaxation times are usually in the order of 100 ms. This does not occur with ethanol, because, firstly, the electric field is not required to be as high as with water and secondly, the charged ethanol droplets have less charge on it than charged water droplets.

Also, in order to achieve such a high electric field, the charging electrodes have to be set on such a high potential that corona discharges start to occur. Ethanol e.g., on the other hand, has a much lower surface tension ($22 \cdot 10^{-3}$ N/m) and spraying in the cone-jet mode is easily achieved.

Liquid conductivity also plays a role in the feasibility of spraying in the cone-jet mode. According to Cloupeau [30], the flow rate at which cone-jet mode can be achieved decreases with increasing conductivity. A lower flow rate, however, could mean that a smaller number of charged droplets would be produced per time unit. Therefore, the advantage of spraying in cone-jet mode, i.e. higher charge per droplet, should outweigh the lower rate of produced droplets.

In practice, when using water, electrospraying will occur in one of the other aforementioned spraying modes of EHDA, each with their own characteristics. However, none of these spraying modes spray monodisperse droplets, meaning that we have to take into account that the droplet diameters will

follow a distribution. Also, none of these modes produce droplets that are charged as high as the droplets in the cone-jet mode.

3.3.2 Analytical model: EHDA

Several models exist for describing the EHDA spraying process. Using these models, it is possible to give an estimation of the droplet size and current output produced by the charged droplets as a function of the flow rate and/or the applied electric field. The model used in this research has been developed for the previously mentioned cone-jet mode and, therefore, it is only indicative for the other modes of spraying. Also, this model does not take directly into account the electric field. It assumes that the electric field has enabled cone-jet spraying and then it calculates the droplet size and charge.

The model, however, still can be used to gain a better understanding about how parameters like flow rate, surface tension, conductivity and (absolute/dynamic) viscosity affect the spraying process. We will not cover this model in detail, but we will state the important conclusions needed to effectively analyse and, ultimately, use EHDA spraying for the EWICON system.

Gañán-Calvo [31] found that the relations for the droplet size and current differ significantly depending on the aforementioned parameters, especially between highly conductive viscous liquids and liquids with a low viscosity and conductivity. Therefore, a viscosity number, VN , was introduced to determine which relation was valid for a given spraying liquid in the cone-jet mode,

$$VN = \left(\frac{\gamma^3 \epsilon_0^2}{\mu^3 K^2 Q} \right)^{\frac{1}{3}} \quad (3-6)$$

in which μ is the dynamic (or absolute) viscosity, K is the conductivity and Q is the flow rate. From VN we can see that for a specific liquid, the relation between the flow rate and the conductivity is given. The higher the conductivity of the liquid, the lower the flow rate should be to keep the viscosity number, VN , constant.

In the case of low viscosity and low conductivity, for liquids such as water and ethanol, the viscosity number, VN , likely will be larger than 1. In that case, the current and droplet size can be estimated using the following two relations [31],

$$\frac{d_d}{d_o} = 1.2 \left(\frac{Q}{Q_o} \right)^{\frac{1}{2}} - 0.3, \quad \frac{I}{I_o} = 11.0 \left(\frac{Q}{Q_o} \right)^{\frac{1}{4}} - 5.0 \quad (3-7)$$

in which d_d is the droplet diameter and I_o , d_o and Q_o are the characteristic current, droplet diameter and flow rate of the spraying liquid, given by the following set of equations

$$I_o = \left(\frac{\epsilon_0 \gamma^2}{\rho} \right)^{\frac{1}{2}}, \quad d_o = \left(\frac{\epsilon_0^2 \gamma}{\rho K^2} \right)^{\frac{1}{3}}, \quad Q_o = \frac{\epsilon_0 \gamma}{K \rho} \quad (3-8)$$

in which ρ is the density of the liquid. If we consider demineralised water with a conductivity of 2.0 $\mu\text{S}/\text{cm}$, then we can use equations (3-8) to calculate the characteristic current, the droplet diameter and the flow rate as shown in Table 3.1.

Table 3.1. Calculation of the characteristic current, I_o , droplet diameter, d_o , and flow rate, Q_o , of demineralised water with a conductivity, K , of 2.0 $\mu\text{S}/\text{cm}$, a surface tension of $72 \cdot 10^{-3} \text{ N/m}$ and a density of $998 \text{ kg}/\text{m}^3$.

I_o	$6.86 \cdot 10^{-3} \mu\text{A}$
d_o	$5.23 \cdot 10^{-1} \mu\text{m}$
Q_o	$1.16 \cdot 10^{-2} \text{ ml/hr}$

Using these three values together with equations (3-7), we can get estimations for the droplet diameter, d_d , and the current, I , associated with a droplet creation process in the cone-jet mode. For example, if we set the liquid flow rate, Q , at 1 ml/hr, then I and d_d become as shown in Table 3.2.

Table 3.2. The estimated current, I , the droplet diameter, d_d , and the Rayleigh percentage, q/q_{max} , when using EHDA spraying with demineralised water in the cone-jet mode for example flow rates, Q , of 1 and 20 ml/hr.

	$Q = 1 \text{ ml/hr}$	$Q = 20 \text{ ml/hr}$
I	0.20 μA	0.45 μA
d_d	5.66 μm	25.87 μm
q/q_{max}	70 %	78 %

We now have an indication of the magnitude of the currents per nozzle of an EWICON system that is fitted with an EHDA spraying system. We have also included the charge, q , on the droplet as a percentage of the maximum given by the

Rayleigh limit, q_{max} . As expected, this model predicts that when EHDA spraying is performed in the cone-jet mode, the droplets are highly charged.

Secondly, if we calculate VN using a flow rate of 1 ml/hr, then we find that it yields a value of 1.6, which is greater than 1 and, thus, we can legitimately use the relations stated in (3-7). However, if we increase the flow rate to, for example, 20 ml/hr, then we find that VN yields a value of 0.6, meaning that we have to use different relations, again from [31]:

$$\frac{d_d}{d_o} = 1.6(\epsilon_r - 1)^{\frac{1}{6}} \left(\frac{Q}{Q_o} \right)^{\frac{1}{3}} - 1.0(\epsilon_r - 1)^{\frac{1}{3}},$$

$$\frac{I}{I_o} = \frac{6.2}{(\epsilon_r - 1)^{\frac{1}{4}}} \left(\frac{Q}{Q_o} \right)^{\frac{1}{2}} - 2.0 \quad (3-9)$$

in which ϵ_r is the relative liquid permittivity, which in the case of water is 80.1 at 20°C. In Table 3.3, we have calculated I and d_d for a flow rate, Q , of 20 ml/hr. For comparison, in Table 3.2, we have also included I and d_d for the same flow rate using equations (3-7).

Table 3.3. The estimated current, I , the droplet diameter, d_d , and the Rayleigh percentage, q/q_{max} , when using EHDA spraying with demineralised water in the cone-jet mode for example flow rates, Q , of 20, 40 and 80 ml/hr. This time, the viscosity number has decreased to 0.6 or less, thus the calculations have been performed using equations (3-9) instead of equations (3-7).

	Q = 20 ml/hr	Q = 40 ml/hr	Q = 80 ml/hr
I	0.58 μ A	0.82 μ A	1.17 μ A
d_d	18.53 μ m	23.92 μ m	30.73 μ m
q/q_{max}	61 %	64 %	66 %

Finally, another observation, which can be made from Table 3.3, is that when the liquid flow rate is increased, the current follows, but not proportionally. As we can see, the flow rate needs to be quadrupled to double the current. Apparently, increasing the flow rate in the cone-jet mode causes the droplet diameter to increase and this means that the charge to mass ratio decreases. This is an important effect linked with some of the spraying modes produced with EHDA, which should be kept in mind when the electric current production needs to be increased in order to make use of higher wind speeds.

The extra wind power conversion that could be gained from the current increase should thus be weighed against the disadvantages of supplying liquid at a higher flow rate; which are amongst other things more dispersed liquid and more pumping power. We will discuss this in more detail in chapter 4 using the EWICON Performance Index as defined in chapter 2.

3.3.3 EHDA implementation and experiments

The goal of the following experiments was to determine how to actually establish EHDA spraying. We will look at the basic principles of EHDA in practice and analyse and design a system that will be able to electro spray various liquids. We will, then, measure the produced current associated with the spraying process, which will give us an indication of its potential use in the EWICON system. The question of whether the following EHDA spraying methods will actually perform as expected when there is wind present, will be discussed in chapters 4 and 5, where the overall EWICON design and the accompanying experiments are treated.

The principle in practice

In principle, a charging system based on droplet creation should consist of one or more spraying nozzles, a reservoir for the spraying liquid and electrodes to generate the electric field to establish the spraying process. These principles also apply to an EHDA based spraying system and, here, we will first look at a configuration with a single nozzle and a single electrode, schematically depicted in Figure 3.2.

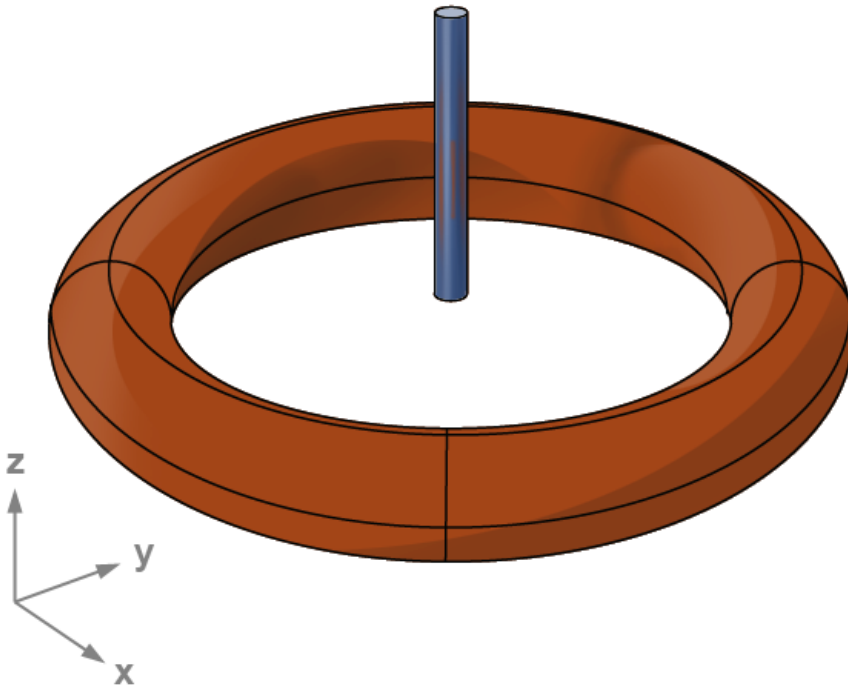


Figure 3.2. Schematic depiction of an EHDA based spraying system. The liquid is supplied through a stainless steel needle nozzle, while the electric field is generated by a copper ring electrode connected to high voltage source. In this case, the inner diameter of the ring was 2.0 cm and the needle was placed in the centre.

An actual implementation of such a configuration, called the “Delrin” nozzle because of its construction material, can be found in Figure 3.3. A stainless steel needle nozzle connected to a syringe pump has been used to supply liquid to the system. The testing liquids were demineralised water, ethanol and various mixtures of both, because mixing ethanol with water lowers the surface tension of the liquid.

Flow rates have been tested varying from 1 to 40 ml/hr. A copper ring acting as the charging electrode positioned around the nozzle was connected to a high voltage DC source. The potential on the electrode was varied from ± 1.0 to ± 7.0 kV. The spraying needle is connected to earth potential and this means that the electric field schematically will resemble the situation depicted in Figure 3.4a and Figure 3.4b. The charged droplets were sprayed towards a metal plate that was connected to ground.

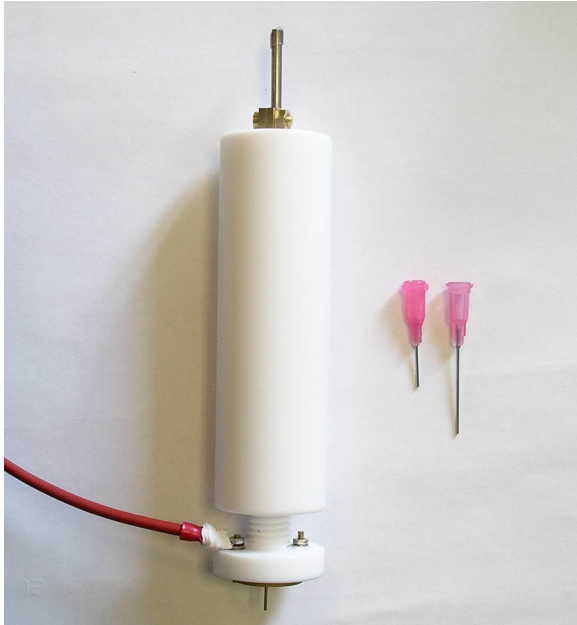


Figure 3.3. One of the possible implementations of an EHDA spraying system, called the “Delrin” nozzle. Two needle nozzles of different lengths are displayed on the right. The liquid is fed through connection on the upper side of the device. The ring electrode and the connection to the HVDC source are shown on the lower side.

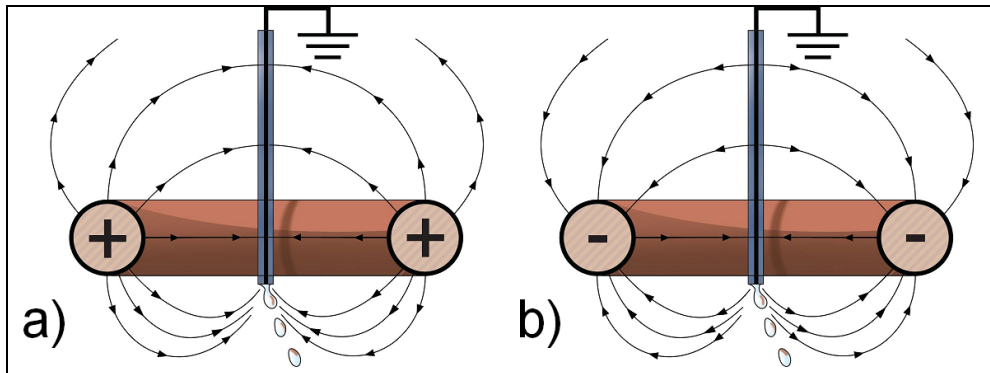


Figure 3.4. The approximate direction of the electric field in an EHDA spraying system. In both case, the spraying needle is connected to earth. In a) the charging potential is positive, so the electric field points inwards. In b) the charging potential is negative and the electric field points outwards.

Electrospray was achieved using this simple configuration, but stable spraying, however, was only observed when pure ethanol or water/ethanol mixtures were used as the spraying liquid. Cone-jet mode was only achieved with ethanol.

Since no wind was present during this stage of the testing, all the created charged droplets were instantly attracted back to the charging electrode.

Visual inspection with laser light of the spraying process resulted in Figure 3.5, in which, on the left-hand side, the process is shown for a positive charging potential. On the right-hand side, we can see the process for a negative charging potential.



Figure 3.5. A photo of the spraying process using water/ethanol as the spraying liquid. Both a positive charging potential, on the left, and a negative charging potential, on the right, was used. The spray is illuminated with laser light. Note the presence of a fine mist on the right.

For both negative and positive charging potentials, currents were measured up to $0.5 \mu\text{A}$ with a 70%/30% water/ethanol mixture per nozzle. The higher currents were obtained using a flow rate of 20 ml/hr. Higher flow rates than 20 ml/hr did not significantly increase the currents. When demineralised water was used, the currents were less than $0.1 \mu\text{A}$.

In order to get an indication of the electric field needed to establish electro spraying, a simulation software package called LORENTZ has been used to calculate the electric field generated by the ring electrode as shown in Figure 3.2, see appendix E. On average, electro spraying commenced when the ring electrode was on a potential of -4.0 kV . The electric field 1.0 mm underneath the nozzle tip was found to be $7.75 \cdot 10^5 \text{ V/m}$. At -6.0 kV , where the electric field is $1.16 \cdot 10^6 \text{ V/m}$, the current levelled off.

During these experiments, the current flowing from the charging electrodes to the high voltage DC source was also measured. This was found to be lower than $0.05 \mu\text{A}$ for a charging potential of -6.0 kV and, therefore, the power dissipation associated with the EHDA spraying process is estimated to be in the order of a few nanowatts per nozzle.

On the right-hand side of Figure 3.5, we can also see the presence of a fine mist. Since this mist apparently did not affect the produced current, we will not discuss it in this section. Instead, we defer the discussion of this mist and its effect on droplet transportation in chapter 4, when wind is introduced into this EHDA system.

Measuring the size, velocities and charge of the droplets

Using a Laser Phase-Doppler analyser (LPDA), we were able to determine the droplet diameter and velocities of the EHDA spraying system. In Figure 3.6, the droplet diameter distribution is given for the Delrin single nozzle system spraying demineralised water using a flow rate of 20 ml/hr.

For the measurement data collected by the LPDA the geometric mean, μ_g , and the standard deviation, σ were calculated. According to (3-2), the geometric standard deviation, GSD or σ_g , can be derived by taking the exponential of the standard deviation. For this particular measurement, the GSD was calculated to be 1.6, which means that the droplet distribution is not considered monodisperse.

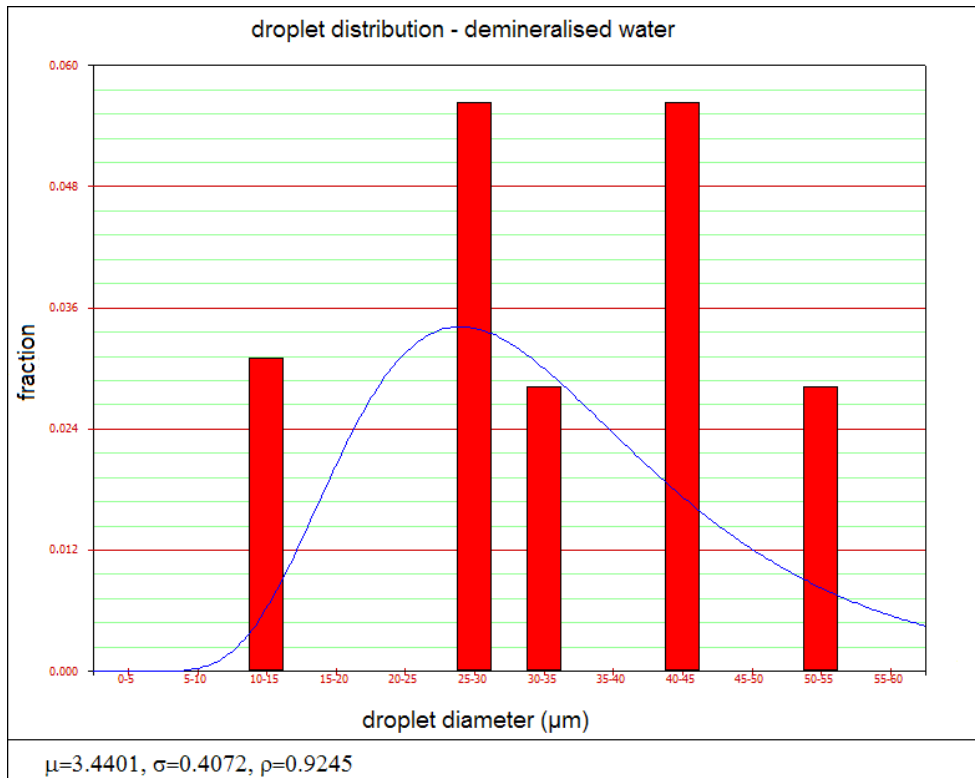


Figure 3.6. The droplet diameter distribution as measured by a Laser Phase-Doppler set-up with water. The calculated GSD of this distribution is 1.6. However, it is more likely to be higher, because very small and large droplets have not been registered by the LPDA.

This does not paint the whole picture, though, because not all droplet sizes have been measured. As previously stated, electro spraying water by conventional

methods is a very chaotic process, and therefore, a significant part of the droplets, smaller than 10 μm and larger than 100 μm , are not registered by the measuring volume of the LPDA. If these droplets are also taken into account, the *GSD* of this distribution is likely to be higher than 2-2.5.

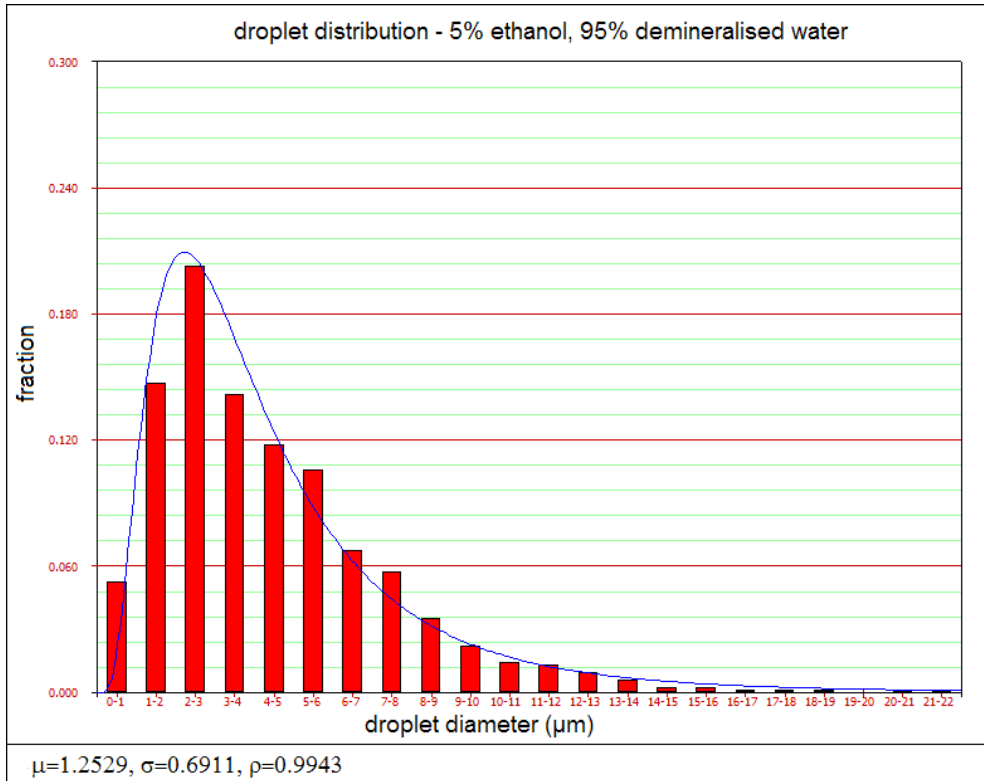


Figure 3.7. The droplet diameter distribution as measured by a Laser Phase-Doppler set-up with water/ethanol. The *GSD* of this distribution is 2.0.

In Figure 3.7, the droplet diameter distribution is given for the Delrin single nozzle system spraying demineralised water mixed with ethanol using a flow rate of 20 ml/hr. Now, the *GSD* was calculated to be 2.0. Again, this means that the droplet is not considered monodisperse.

During these same experiments, the velocities were also measured in the directions as specified in Figure 3.8. The velocities in the x-direction were found to be varying between 1 and -1 m/s. In the z-direction, the velocities were found to be varying between 1 and 5 m/s.



Figure 3.8. The velocities of the droplets have been measured in the z and x direction.

Also, by using a system called ELPI (Electrical Low Pressure Impactor), we were able to obtain a rough indication of the charging efficiencies on the droplets produced with EHDA spraying and whether these efficiencies varied as a function of the droplet diameter. In the ELPI, the droplets are collected in different impactor stages according to their diameter and the electric charge carried by the droplets into each impactor stage is measured in real time by sensitive electrometers. For more information, see [32].

These measurements indicated that the water droplets created with EHDA were charged up to 30% of the maximum charge as given by the Rayleigh limit. In section 3.3.1, we stated that the electric field strength is reduced by the creation of the charged droplets, thereby preventing the water spraying process to enter the cone-jet mode. This reduced electric field is also the reason that the water droplets are not as highly charged as expected with the cone-jet mode.

Affecting the surface tension reduction of the liquid by CO₂

Earlier, the surface tension of demineralised water was lowered by adding ethanol. However, this is not a long term solution if the EWICON system is to be used for large scale commercial use, both from an environmental and financial point of view. Therefore, other methods have been devised to lower the surface tension of water. One of these methods involves the use of CO₂, since the surface tension depends on the two media between which the surface is formed.

In [33], the surface tension of water was lowered from $72 \cdot 10^{-3}$ N/m to $57 \cdot 10^{-3}$ N/m as CO_2 was added to water. This implies that the electro spraying of water could be improved by using gaseous water. Experiments have been conducted, of which the results will be briefly given.

Carbonised water with a conductivity of $105 \mu\text{S}/\text{cm}$ has been sprayed in a Delrin nozzle system using similar parameters as used with demineralised water and the water/ethanol mixtures. This yielded a current of $0.1\text{-}0.2 \mu\text{A}$ per nozzle, whereas spraying pure demineralised water yielded less than $0.1 \mu\text{A}$ per nozzle. Using carbonised water in this particular EHDA system gives significantly better results compared to demineralised water in terms of produced net current.

However, technical difficulties arose while the carbonised water was fed to the spraying nozzle. In the water reservoir, the CO_2 escaped from the water causing extra pressure that increased the flow rate of the liquid. This led to fluctuations in the produced current. On occasion, large CO_2 bubbles entered the tubing system, which led to interruption of the liquid flow. This meant that no charged droplets could be produced and the current was zero.

Cylindrical electrode/nozzle configuration

When it became apparent that the stable electro spraying of (demineralised) water was not possible with the previously discussed configuration, a more detailed analysis was made in LORENTZ of the potentials and electric field distribution in the existing system. In Figure 3.9, results of the equipotential analysis are shown for the standard Delrin electrode configuration.

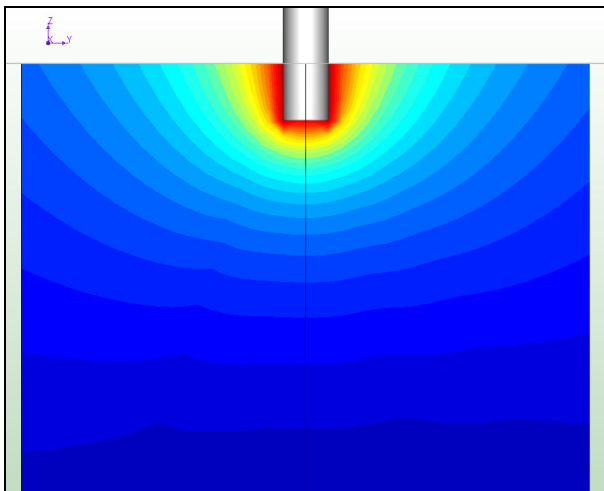


Figure 3.9. Equipotential plot around the tip of the spraying needle of an EHDA set-up. The charging electrode set at -4.0 kV is not shown in this plot. It was set at -4.0 kV. The spraying needle was connected to earth potential.

In this plot, the charging electrode was set at -4.0 kV and the spraying needle was set at earth potential. For the sake of clarity, the electrode is not shown in Figure 3.9. In order to analyse the effect of the electrode, this analysis was conducted without the liquid present.

If we look at the equipotential lines in the plot shown in Figure 3.9 around the tip of the needle, the field concentration is limited, due to the distance of the electrode to the spraying needle tip, which was approximately 2.0 cm in this case. Hence, in order to achieve some level of stable spraying the potential of the electrode would need to be increased, but, as previously mentioned, this would lead to corona discharges.

This knowledge was used to investigate whether spraying water is possible using a somewhat more complex electrode system. This led to the concept of a cylindrical electrode, partly based on [34] with a diameter of 4 mm that was designed around a stainless steel needle nozzle. The advantage of having such a small diameter was the fact, that the electric field could be focussed on the tip of the spraying nozzle, while keeping the electrode itself on a relatively low potential. In this way, corona discharge effects could be kept to a minimum. A photo of this cylindrical electrode/nozzle configuration can be seen in Figure 3.10. The tip of the needle sticks out approximately 0.5 mm.

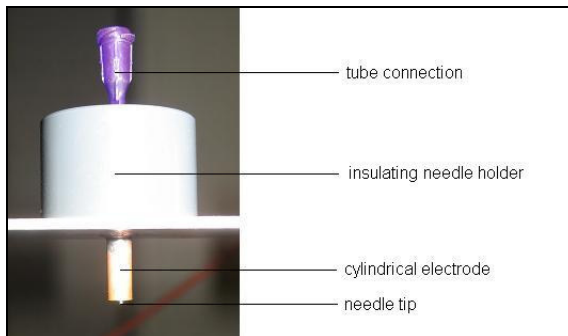


Figure 3.10. A spraying needle with a cylindrical electrode. The cylindrical electrode has a diameter of 4.0 mm and the spraying needle sticks out 0.5 mm.

Again, an equipotential plot was made of this needle/cylindrical electrode configuration with the cylindrical electrode set at -2.0 kV and the needle set at earth potential, see Figure 3.11. In this plot, we can see that the lines are concentrated around the tip of the needle, ensuring that a high electric field is present only at the tip of the spraying needle.

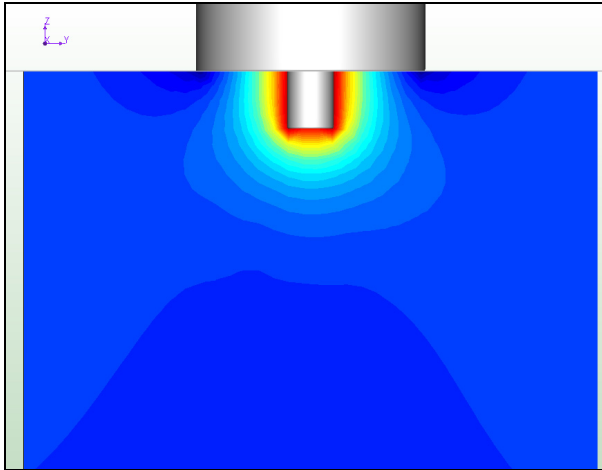


Figure 3.11. Equipotential plot of the cylindrical electrode EHDA set-up designed to spray water. Part of the cylindrical nozzle can be seen with the tip of the spraying needle sticking out. The cylindrical electrode potential was set at -2.0 kV. The spraying needle was connected to earth potential.

Experiments have been conducted with a configuration as depicted in Figure 3.10. The first and most important observation was that stable electro spraying with demineralised water was achieved. Stable spraying in this context means that droplets were sprayed downwards in a non-intermittent manner. However, the spraying was not in the cone-jet mode.

For a flow rate of 20 ml/hr, the measured current was 0.3 μA compared to the less than 0.05 μA found with the Delrin nozzle system.

Using similar spraying parameters as for the Delrin nozzle system, the droplet diameter distribution has again been determined using the LPDA, of which the results can be seen in Figure 3.12. This time using (3-4), the *GSD* was found to be 1.24, which means the droplet diameter distribution is considered to be nearly monodisperse. Thus, as far as electro spraying demineralised water is concerned, this is a significant improvement over electro spraying water with the Delrin nozzle system, as was shown in Figure 3.6.

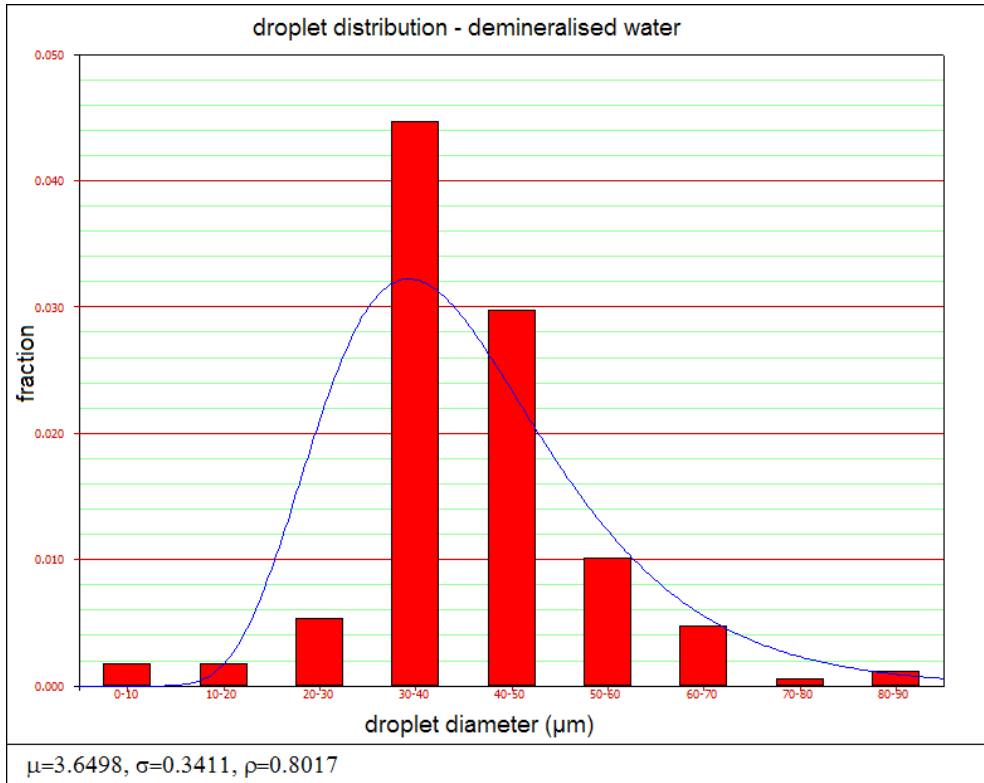


Figure 3.12. The droplet diameter distribution as measured by a Laser Phase-Doppler set-up with demineralised water using the improved spraying system. The GSD of this distribution is 1.24, which means that the distribution is nearly monodisperse.

Stable spraying with tap or saline water, however, was still not possible as the high conductivities of both types of water caused very chaotic spraying. Typical values are $5 \cdot 10^4$ $\mu\text{S/m}$ for tap water and $5 \cdot 10^6$ $\mu\text{S/m}$ for sea water as compared to the 200 $\mu\text{S/m}$ for demineralised water. This is mainly due to the fact that with electro spray high conductivities lead to unstable electric dripping modes.

According to [29], this situation can be partly resolved by decreasing the flow rate of the tap or saline water to a few millilitres per hour. However, this would mean that the number of nozzles needs to be increased by a factor of at least 10 to maintain the produced current. Another solution that is given in [29] is to increase the electric field by increasing the potential on the electrodes. However, the required potentials would need to be in the order of 20 kV. In this cylindrical electrode configuration, this would inevitably lead to discharges.

3.3.4 Conclusions on EHDA based spraying systems

First of all, the experiments have shown that EHDA can create droplets suitable for an EWICON system in terms of droplet size and charge. Monodispersity was not present for any tested liquid except pure ethanol. Using a 70%/30% water/ethanol mixture, the size distribution was found to be narrower. Unfortunately, the degree of monodispersity found with the electro spraying of pure ethanol was not achieved.

Electrospraying water mixed with CO₂ did yield higher currents than electro spraying with pure demineralised water. However, this did bring along other practical issues, which leads to the conclusion that, currently, this approach is not a viable solution for electro spraying water.

Finally, it has not yet been possible to electro spray water in cone-jet mode. Stable electro spraying yielding a higher current, however, was achieved using a cylindrical electrode. Also, the droplet size distribution was found to be nearly monodisperse. This means that, with EHDA, an EWICON system can be designed that uses water as a spraying medium and, thus, no harmful liquids are dispersed into the environment.

3.4 High pressure monodisperse spraying¹

The second method of charged droplet creation that has been investigated is the method called high pressure monodisperse spraying (HPMS). This method is based on the principle that a liquid is forced through a device fitted with small micron-sized pores with equal size creating liquid jets with equal diameter. The high pressure that is applied is usually in the order of 10 to 15 MPa. The liquid jets break up into droplets due to the Rayleigh break-up principle, with the diameter of the droplet proportional to the diameter of the liquid jet.

This droplet creating method has primarily been developed for continuous inkjet printing and, as such, was designed to operate with all kinds of liquids, including saline water. Based on the preceding section covering the EHDA spraying method, we have concluded that the creation of nearly monodisperse droplets with water is possible, but requires a more complex spraying system. Only ethanol will result in actual monodisperse droplets. Therefore, with HPMS, there is already a significant advantage of this method over the EHDA method, because the intended spraying liquid is water.

¹ This work was conducted in close cooperation with Wietze Nijdam and Jeroen Wissink of Medspray XMEMS BV

3.4.1 HPMS principle

While the droplets are created, the droplets are charged by induction using charging electrodes. In general, an HPMS set-up will schematically resemble a configuration like depicted in Figure 3.13. Because the charging process is separated from the droplet creating process, this means that, in theory, the charged droplets could be fine-tuned more easily to suit the specific EWICON conditions.

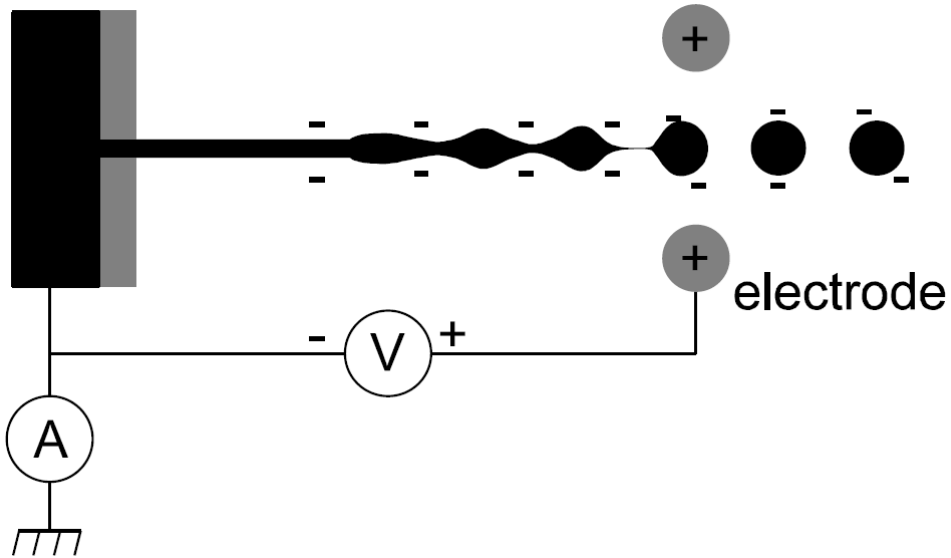


Figure 3.13. The working principle of the HPMS spraying method is depicted. A liquid is forced through a micron-sized pore resulting in a jet. This jet breaks up into monodisperse droplets while being charged by electrodes. In this case, the electrode is on a positive potential resulting in negatively charged droplets.

In this case, the liquid is connected to earth and the electrode(s) is set to a positive potential thus causing the droplets to be negatively charged. A negative charging potential, conversely, will yield positively charged droplets. Similar to the EHDA spraying method, these electrodes can be designed in several ways. The charging electrode depicted in Figure 3.13 can for example be designed as a ring electrode as shown in Figure 3.14. This has been analysed in LORENTZ.

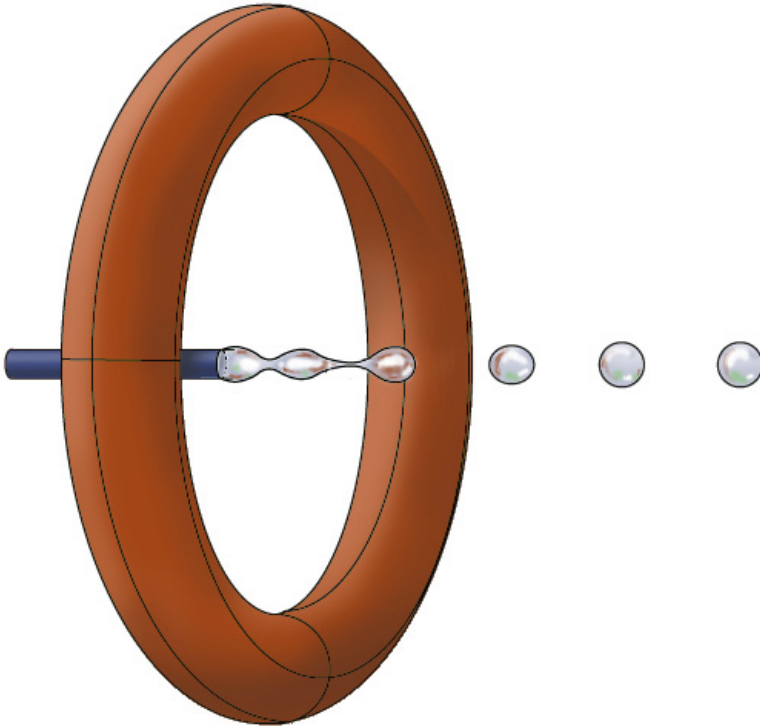


Figure 3.14. A ring electrode has been modelled for the water droplets created by the HPMS system. The droplets are charged by induction. The charge on a droplet can be determined by calculating the capacitance between the ring electrode and the droplet.

Another observation that can be made with respect to the charged droplets created by HPMS is the exit velocity. Whereas the droplets exiting the spraying nozzles in an EHDA based spraying system usually have a velocity of 1-5 m/s, the droplets in the HPMS system have a velocity of 10-20 m/s. Therefore, if we look at the calculations made in the last chapter on droplet mobility, maximum electric fields and minimum required wind speeds, we can expect that the charged droplet can be removed more easily.

3.4.2 Analytical model: HPMS

Firstly, we will calculate and predict the amount of current we can expect from this spraying system assuming a certain flow rate, a charge per droplet and droplet size. We will also look into the charging process itself.

These HPMS devices that have been tested in the current EWICON system were designed to produce droplets with a diameter of 20 μm . For these experiments, a flow rate of 71 ml/hr per device was used and, this means that

theoretically, the number of droplets per second that should be dispersed is $4.7 \cdot 10^6$. If we assume that these droplets can be charged up to 30% of the maximum charge as given by the Rayleigh limit, then the charge per droplet would be $1.9 \cdot 10^{-13}$ C. Thus, the current associated with the stream of droplets is $0.9 \mu\text{A}$.

The charging process of the droplets is similar to the process implemented in ink jet printer technology. In this technology, monodisperse ink droplets are firstly charged by charging electrodes and then guided to their place on the printing paper by deflection electrodes.

The charging of the droplets can be modelled by determining the capacitance $C_{droplet}$ between the droplet jet and the electrode.

$$q_{droplet} = C_{droplet} \cdot V \quad (3-10)$$

in which $q_{droplet}$ is the charge on the droplet and V is the potential on the charging electrode. The capacitance can either be obtained by analytical means or by using a simulation software package as LORENTZ as shown in Figure 3.14.

Firstly, we will give two analytical calculations. The first one is based on a sphere-plate configuration. The capacitance between a conductive sphere with a radius r_a and a metal plate at a distance d is given by [35]

$$C_{droplet} = 4\pi\epsilon_0 r_a \left[1 + \frac{1}{2} \ln(1 + 1/\xi) \right] \quad (3-11)$$

in which ξ is the ratio of the distance d to the radius of the sphere

$$\xi = \frac{d}{r_a} \quad (3-12)$$

If we take the radius r_a to be $10 \mu\text{m}$ and the distance d to be $250 \mu\text{m}$, then the capacitance between the sphere and plate becomes $1.13 \cdot 10^{-15}$ F.

The second analytical approximation is based on a model that is used in the ink jet technology, where a liquid jet breaks up in droplets inside a hollow cylindrical charging electrode. According to [36], the capacitance between the droplet to be formed and the charging electrode is given by

$$C_{droplet} = \frac{2\pi\epsilon_0 l}{\ln\left(\frac{D_c}{D_j}\right)} \quad (3-13)$$

in which D_c is the inner diameter of the charging electrode and D_j is the diameter of the liquid jet, which relates to the droplet diameter as $D_d = 1.89 \cdot D_j$. The value of l is set to the length of the jet forming one droplet, which in the case of these particular HPMS devices is $4.3 \cdot D_j$. With $D_c = 500 \mu\text{m}$ and the droplet diameter $D_d = 20 \mu\text{m}$, the capacitance between the charging electrode and the droplet is $0.65 \cdot 10^{-15} \text{ F}$.

Lastly, we can use the simulation software package LORENTZ to calculate the capacitance between the droplet and the charging electrode as shown in Figure 3.14. This yielded a value of $0.83 \cdot 10^{-15} \text{ F}$.

We can see that all three calculated capacitances are of the same order of magnitude and that the values provided by the ink jet model and the simulation in LORENTZ are close together. Since the situation as shown in Figure 3.14 is the most realistic approximation of the spraying system, we will use the latter value for the capacitance.

To calculate the potential of the charging electrode, we take the charge on a droplet as calculated at the beginning of this section and use it in equation (3-10). This yields that, theoretically, the charging electrode should be set on a potential of 229 V to obtain a water droplet of $20 \mu\text{m}$ with a charge of $1.9 \cdot 10^{-13} \text{ C}$, which should produce an output current of $0.9 \mu\text{A}$ per HPMS device as stated in the beginning of this section.

3.4.3 HPMS implementation and experiments

It was already known that the HPMS system is capable of producing monodisperse droplets and this has been confirmed by a high speed camera test set-up, where uncharged droplets were sprayed, as shown in Figure 3.15.

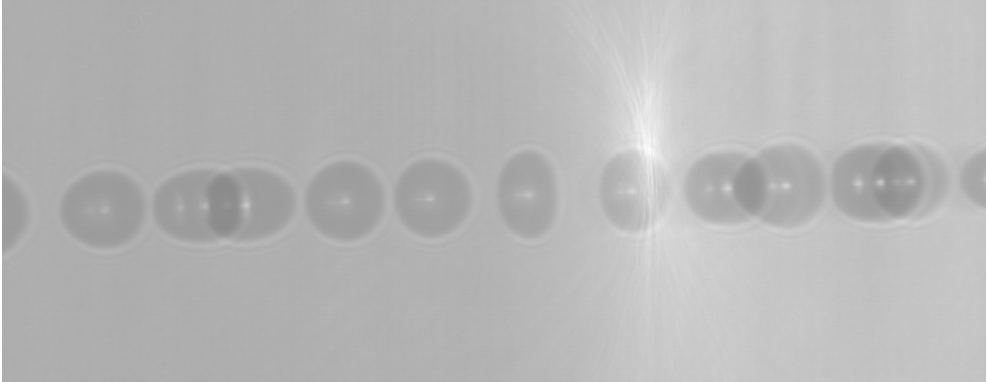


Figure 3.15. Image captured with a high speed camera of the spraying with the HPMS system. The spraying liquid is water+0.9% NaCl and the droplets are not yet charged. The droplets in this image have a diameter of 20 μm .

To illustrate the effect of the charging process, the potential on the charging electrode has been varied from 100 to 500 V. In Figure 3.16, where the charging potential has been set to 300 V, we can see that the charged droplets now repel each other. Another effect that was observed was that the repulsion between the charged droplets became stronger and more visible as the charging potential was increased.

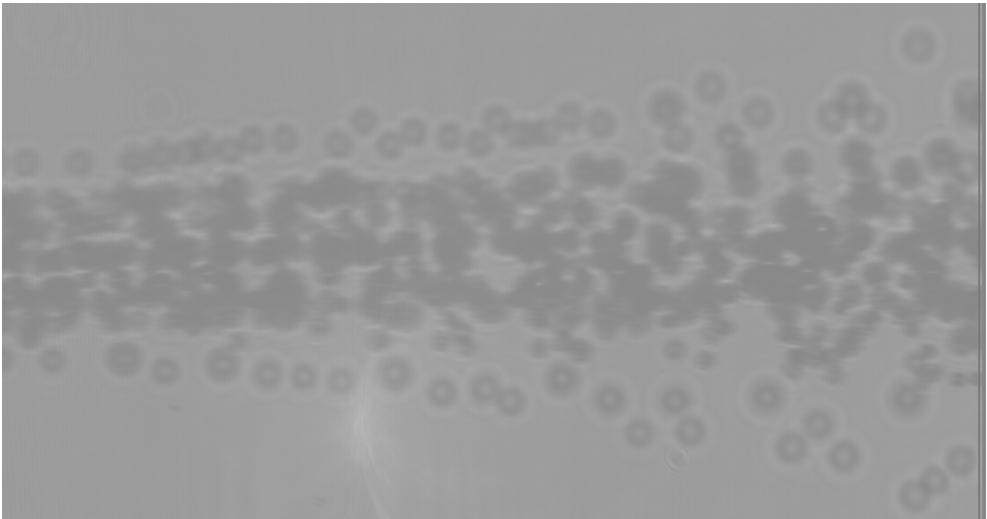


Figure 3.16. The charging electrode is set to a potential of 300 V. The droplets are sprayed from the left to the right. We can see that the droplets repel each other as they move to the right. The droplets in this image have a diameter of 20 μm .

The current has been measured for a single HPMS device using a set-up as shown in Figure 3.13. The potential of the charging electrode was set at 300 V and

this yielded a current of $0.1 \mu\text{A}$. This is lower than the predicted current calculated in the previous section by almost a factor of 10.

We can conclude that the droplets are not charged up to 30% of the maximum charge as given by the Rayleigh limit, but only up to 3-4%. This implies that the calculated capacitance is too high, which means that the electrode distance is estimated too small.

Also, measurements have been performed with a negative potential, creating positively charged droplets, on the charging electrode. For a single HPMS device, no significant difference in current was measured. However, we will see in chapter 4, where multiple HPMS devices are tested, and chapter 5, where these HPMS devices are implemented in the EWICON system, that a negative polarity results in slightly lower currents.

3.4.4 Conclusions on HPMS based spraying systems

From the images that have been taken with the high speed camera, we can conclude that the sprayed droplets are indeed monodisperse. These images also show that the droplets can be charged by induction, because the droplets start to repel each other.

3.5 Suitable charging method for the EWICON

3.5.1 Summarising conclusions

Both spraying methods have been investigated and both have been able to produce charged water droplets which are suitable for the EWICON system. While the EHDA spraying method was not able to produce monodisperse droplets with water as the spraying liquid, the associated current produced by electro spray was still in the same order of magnitude as the current produced by the HPMS devices. Testing with the EWICON will have to show whether the polydispersity of the EHDA produced droplets will affect the transportability by the wind.

It must be noted, that at this point in time, the effective wind surface areas for both EHDA and HPMS are in the same order, which allows that the currents can be compared.

Furthermore, the droplet creation for EHDA process required very little power, in the order of a few nanowatts per spraying nozzle. The power required for the HPMS method was in the order of a few milliwatts, but this spraying method did produce monodisperse droplets using saline water as the spraying liquid.

In addition, with both spraying methods, it was possible to control the charge on a droplet to a certain degree. With the HPMS method, the charge could be controlled independently from the droplet diameter. With the EHDA spraying method, however, there is some interdependency between the droplet charge and diameter.

3.5.2 Decision

Based on the conclusions in the last section, it was decided to implement both spraying methods in the EWICON system for further testing.

It could very well be thinkable that there will be a variety of different EWICON systems each incorporating a charging system that is best suited for its location. An EWICON system that is intended for operation at sea might be equipped with a HPMS based system, because of its favourable spraying capabilities towards saline water. An EWICON system that is intended for land-based operation, like e.g. on top of a building, might be equipped with an EHDA based charging system. However, in both cases, water can be used and this means that there is no risk to the environment.

4

EWICON system design

“A common mistake that people make when trying to design something completely foolproof is to underestimate the ingenuity of complete fools.”

– Douglas Adams

Now that we have taken a look at the different types of implementations of the EWICON system in chapter 1 and the theoretical background of charged droplets being generated and moved by the wind in an electric field in chapter 2, we shift the attention to the design of an actual EWICON system. A number of issues need to be addressed before a final EWICON system can be successful.

We will start in section 4.1 with the general design, which will be based on the implementation Type B, described in chapter 1, combined with either EHDA or HPMS as the spraying method, described in chapter 3. There will be differences in the design depending on the used spraying method. This design will then be the starting point on which further analysis will be performed. Also, it will be the blue print of the actual EWICON system.

In section 4.2, we will test the EWICON design with EHDA and HPMS in a wind environment in order to determine whether the wind is able to move the charged droplets away. We will also investigate whether the polarity of the charged droplets affects this transportation process.

The next issue is the increase of the produced current. In the ideal case, the EWICON system is expected to convert all of the Betz-limited power in the wind. Because the EWICON system acts as a current source, ideally, we want the EWICON system to be able to deliver a current that is matched to the power in the wind. This required current will have to be significantly higher than the current produced by a single spraying nozzle system, regardless of the charging method. Therefore, in the actual EWICON system, multiple spraying nozzles need to be combined in order to increase the rate of production of charged droplets and, thus,

the current. In section 4.3 we will look at extensions of both the EHDA and HPMS single nozzle systems.

Another issue, related to the movement of charged droplets, is the minimum required wind speed. For a simple system as described in chapter 2, we can determine analytically how much wind is needed to move the droplets against the electric field. However, in a more complex setting, where the electric field can not be calculated as straightforward, we have to resort to numerical methods. It appears that by analysing the droplet trajectories, we can find ways to lower the minimum required wind speed, thereby increasing the applicability of the EWICON system. This will be discussed in section 4.4.

In section 4.5, we will discuss some remaining issues. In chapter 3, the charged droplet creation methods have been analysed, assuming the charging system to be connected to earth. In the actual EWICON system, the potential of the whole system, including that of the charging system, will rise. We will describe how this will affect the behaviour of the charged droplets compared to the considerations made in chapter 2 and 3.

We will conclude with the final laboratory designs for the EWICON system, which will be described in section 4.6. Using these designs, a number of experimental set-ups were constructed, which were then used for experiments and measurements. These will be discussed in the next chapter.

4.1 General design

In Figure 4.1, we again take a look at the schematic overview of a Type B implementation, i.e. the EWICON system without a separate charge collector unit. The first thing that is apparent is that we need a platform that is isolated from earth. Basically, all the components on this platform will have their common earth point at this platform. Using switches, the platform can either be connected directly to earth or to an electrical load. In this chapter, we will look at the charge droplet transportation while the EWICON system is still connected to earth, i.e. in the case that the wind moves away the charged droplets, the platform and, thus, the EWICON system will not be charged.

Also, not explicitly mentioned before, the liquid has to be fed to the spraying nozzles, thus requiring some form of reservoir and a method of transportation of the liquid.

Lastly, the electrical devices, required to supply the high voltage and the liquid, need to be powered. Considering the fact that the charging system on the

platform is isolated from earth, a self-sufficient solution needs to be found for the power supply.

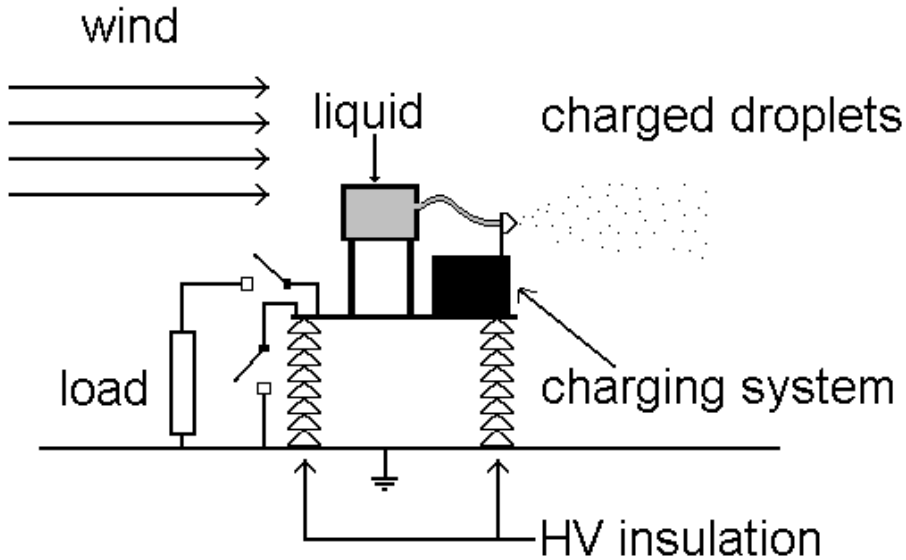


Figure 4.1. Schematic overview of a Type B EWICON implementation. A reservoir supplies the spraying liquid to the isolated charging system, where charged droplets are produced. The wind carries the charged droplets away, thereby increasing the potential of the EWICON system.

4.1.1 Platform and isolation

In both implementations of the EWICON system, during normal operation, there will be an electrically floating part or component that will be charged. In the Type A implementation, it is the separate collector unit and in the Type B implementation, it is the isolated charging system. If the EWICON system is operated without an electric load, the floating part that is charged can be represented by a capacitor. In the case that there is an electric load, this can be represented by a resistive impedance parallel to the capacitor.

Critical to the operation of a Type B implementation is the fact that the charging system needs to be isolated from earth. In practice, this means that all the additional components and devices have to be isolated from earth such that any leakage currents to earth are minimised. Therefore, in our experimental test set-up, a rectangular metal plate placed on a set of insulators was used as the basis for the charging system. This plate was sufficiently large to hold all the necessary components.

So, by using a metal plate as a holding platform, a capacitor was introduced in to the EWICON system. The value of the capacitance of the platform can be estimated by either using a parallel-plate approximation, by calculation in a software package such as LORENTZ or by measurement. The expression for the capacitance, in first approximation, is

$$C_{EWICON} = \epsilon_0 \cdot \frac{A}{d_{platform}} \quad (4-1)$$

in which A is the area of the platform and $d_{platform}$ is the height above ground. In this case, the surface area, A , is 2.45 metres by 2.00 metres and the height, d , is 1.13 metres. Rounding off the result, we get an indicative capacitance of 50 pF. However, equation (4-1) is only valid when d is small compared to the dimensions of the plate and in this particular case, we can see that d is in the same order as the surface area, A , of the plate. This means that, because the fringe fields existing at the edges of the plates will contribute to the capacitance, the actual value is likely to be higher.

Therefore, a platform with these dimensions was entered into simulation package LORENTZ, see Figure 4.2. The capacitance calculated by LORENTZ was approximately 125 pF. This was in agreement with experiments in which the AC impedance or capacitive reactance, X_c , of the system was determined by applying an AC voltage. The capacitance was then obtained by using

$$C_{EWICON} = \frac{1}{2\pi \cdot f \cdot X_c} \quad (4-2)$$

in which f is the frequency of the applied AC voltage, which in these experiments was set at 50 Hz.

If the charging process is established and the wind moves all the droplets away, the produced current will charge the EWICON, because the spraying nozzles are electrically connected to the platform. We can use the estimated capacitance of the system to calculate the rate at which the potential of the EWICON system will increase when e.g. one spraying nozzle disperses charged droplets with an equivalent current of 1 μ A. This is, as we have seen in chapter 2 and 3, a typical value for the current. The output potential is related to this charging current of 1 μ A by the following equation

$$I = C_{EWICON} \cdot \frac{dV}{dt} \quad (4-3)$$

in which I is the charging current, C_{EWICON} is the capacitance of the EWICON system and V is the measured output voltage potential of the EWICON system.

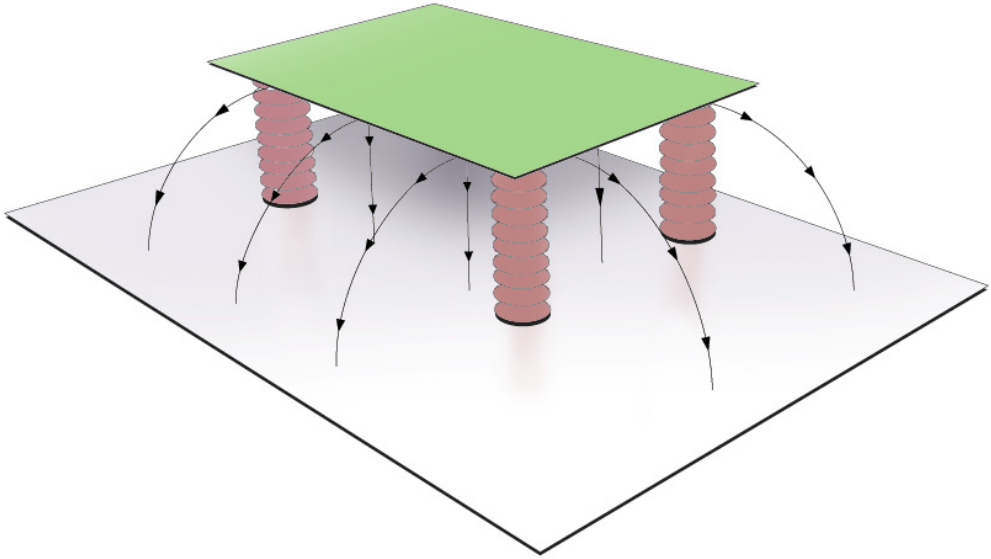


Figure 4.2. The capacitance of the platform, a metal plate (green), to the earth has been calculated by LORENTZ. The grey area represents earth or, in this case, the floor above which the platform floats.

From this equation, it follows that if the system is charged with $1 \mu\text{A}$ without an electrical load for 10 seconds, the potential of the EWICON system will reach 80 kV. Therefore, porcelain support insulators were used, which exhibited leakage currents in the several nanoamperes when stressed at DC potentials of 65 kV, implying a resistance in the order of tens of teraohms.

In the example, we assume that leakage currents present due to corona discharges or due to currents flowing over the surface of the support insulators are negligible. Also, we assume that the spraying behaviour of the charging system, i.e. the nozzle/electrodes configuration, remains unaffected and that the wind is still able to move the droplets away from the system.

4.1.2 Liquid supply system

In the previous chapter, we discussed the two main charging methods and found that typical flow rates vary between 1 and 20 ml/hr per spraying nozzle or pore. If we assume the output power per nozzle to be 50 mW, as we theoretically deduced in chapter 2, then for a 1 W rated system we would require a flow rate of 400 ml/hr. For a 1 kW rated system, a flow rate of 400 litres per hour would be required.

In the smaller systems, these flow rates can be provided by syringe pumps. However, as soon as we enter the kilowatts region, the liquid supply would have to be realised by pumping the liquid to a reservoir at a certain height, depending on the placement of the EWICON system. From the reservoir, the liquid flows to the spraying nozzles under the influence of hydrostatic pressure. The power, P_{pump} , associated with pumping liquid to a certain height, h , is given by

$$P_{pump} = \frac{dm}{dt} \cdot h \cdot g \quad (4-4)$$

in which dm/dt is the mass flow rate of the liquid and g is the gravity acceleration. As an example, we use water as the spraying liquid and this water needs to be pumped to a height, h , of 10 metres at a flow rate of 400 litres per hour. In that case, the minimum required pumping power will be 11 W, which is roughly one percent of the rated power. We also have to keep in mind that equation (4-4) only holds when the pump has a (theoretical) efficiency of a 100%. Currently, the maximum efficiency of water pumps is roughly 90% which means that the required power will actually be 12 W.

However, if the charging and spraying efficiency is lower and the output power per nozzle is, for example, 5 mW or 0.5 mW at the same flow rate, then the minimum required pumping power would be 121 W or 1.2 kW respectively. In the latter case, it is clear that the EWICON will not be able to convert wind power to electrical power with a positive efficiency. Therefore, in order for the EWICON to be self-sustaining, the chosen charging process needs to be optimised to the extent that the power associated with the required amount of spraying liquid is lower than the output power of the EWICON system. Another possibility is to use liquid that has reached the required height due to other processes, e.g. precipitation. We will touch upon this subject in chapter 6 on recommendations.

In our experimental set-up, however, we have chosen to use a syringe pump that can supply liquid to spraying nozzles in either an EHDA or an HPMS

based charging system. In this way, for research purposes, the liquid supply can be accurately established to the desired flow rate.

4.1.3 Electrical system

As said before, the Type B implementation of the EWICON system requires the charging system to be isolated from earth. This means that conventional means of electricity supply to the system cannot be used, since this would require an electric connection between the EWICON system and earth. This connection, in turn, would mean that the accumulated charge would flow back to earth and the EWICON system would be unable to drive a load.

Therefore, in order for the equipment in the EWICON system to operate, power is required, which has to be generated on the EWICON platform itself. In our experimental test set-up, we use a 12 V battery placed on the platform. Using a DC/AC converter, the voltage is converted to 230 VAC, which is required by all the components on the EWICON platform.

Among these components are the high voltage DC sources powering the electrodes, which are responsible for the electric field required to establish the spraying and charging process. These DC sources operate at potentials varying from ± 2.0 to ± 14.0 kV and are connected to the platform, just like the spraying nozzles. The reference potential of the platform is floating. Therefore, when the potential of the EWICON system rises, the potential of the electrodes and the spraying nozzles are lifted equally and, thus, the electric field in the vicinity of spraying nozzle remains constant.

4.2 Charged droplet transportation

The isolated platform, the liquid pump and the independent electrical system discussed in the previous section provide the basis on which the charging system will be placed. We now proceed to determine whether the wind is able to move the charged droplets away from the charging system. The current associated with the droplets that are moved away will be called the displaced current. Firstly, the wind generator will be described, after which the results of the implementations of both spraying methods, discussed in chapter 3, will be discussed.

In chapter 3, the various implementations of both charging methods were analysed in terms of produced currents associated with the charged droplets and, in the ideal case, all of these charged droplets will be moved away by the wind. If this is the case, then no charged droplets will come in contact with any of the electrodes

or the metal platform and, thus, no currents will be measured flowing back from the electrodes to the high voltage power supply.

If any of the charged droplets are attracted back to e.g. the charging electrode, then a flow-back current will be measured. Comparing these flow-back currents with the produced currents will then give an indication of the effectiveness of the wind to overcome the electric field.

4.2.1 Wind generator

The air flow in this research has been provided by a wind generator, as shown in Figure 4.3, which basically consists of a fan that forces the air through a system of small tubes. In this way, a laminar flow of air is obtained, which means that the wind speed at each of the spraying nozzles is roughly equal.

The wind speeds could be varied from 2 to 14 m/s (2 to 7 on the scale of Beaufort) for a circular wind surface area with a diameter of 35 cm. During the testing of the implementations discussed in chapter 3, the wind speed was first set at 10 m/s and then increased to 12 m/s.

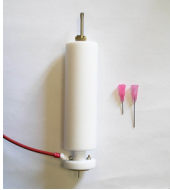
In the early stages of the research project, a smaller and less powerful wind turbine was available with a maximum wind speed of 8 m/s. Therefore, the experiments concerning the Delrin nozzle in this chapter and chapter 5 have been conducted with 6 and 8 m/s.



Figure 4.3. The wind generator which has been used to provide laminar air flow to move the charged droplets away from the charging system.

4.2.2 EHDA

- **Delrin nozzle**



The first implementation tested was the Delrin nozzle using a 70%/30% water/ethanol mixture which was configured to yield a produced current, I_N , of $0.5 \mu\text{A}$. The measuring set-up has been depicted schematically in Figure 4.4.

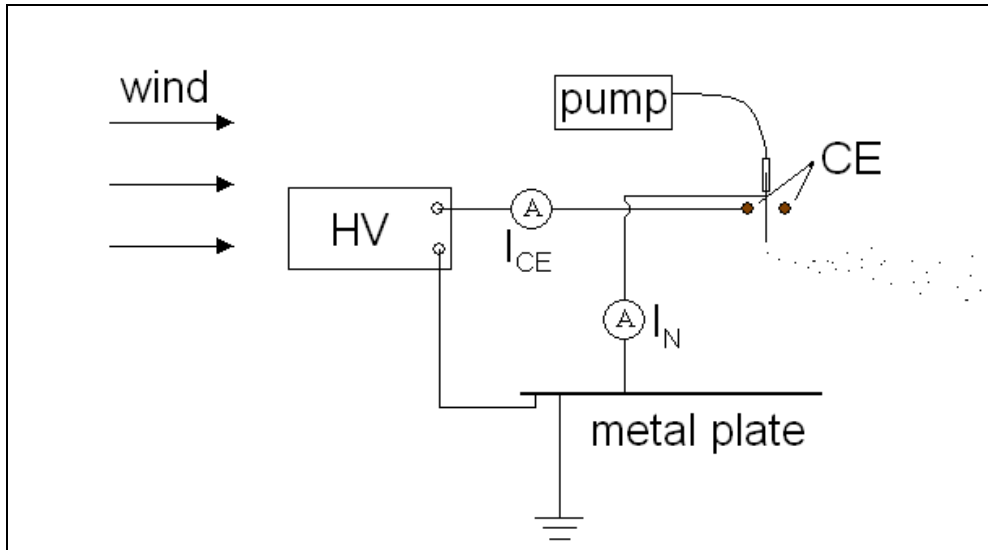


Figure 4.4. A schematic overview of the measuring test set-up for electrospaying charged droplets. The wind is blowing from the left to the right. Liquid is fed to the spraying nozzle using a pump. A high voltage DC source is used to power the charging electrode, CE. The current associated with the production of charged droplets, I_N , is measured using an ammeter. Any charged droplets that will be attracted back to the charging electrode, CE, will be detected as a flow-back current, I_{CE} .

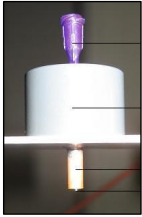
After the air flow was established, a flow-back current of $0.2 \mu\text{A}$ was measured. This implies that the wind was able to displace a current of $0.3 \mu\text{A}$ associated with the charged droplets. After the increase of the wind speed, the flow-back current decreased to $0.1 \mu\text{A}$.

When pure demineralised water was used as the spraying liquid, the produced current was approximately $0.1 \mu\text{A}$. After the air flow was established, a flow-back current of $0.1 \mu\text{A}$ was measured, implying that nearly all of the droplets were attracted back to the charging system. This, in turn, would mean that wind

was practically not able to displace a current. In this case, an increase of the wind speed did not result in a decrease of the flow-back current.

Part of the droplets created by the electro spraying of water are highly charged submicron droplets and even with the increased wind speed, the electric force pulling the droplets back is higher than the wind drag force.

- **Cylindrical electrode/nozzle configuration**



The second implementation that was tested was the cylindrical electrode/nozzle configuration, which was specifically designed to spray demineralised water. The measured current produced by the spraying process was found to be $0.3 \mu\text{A}$. After the air flow was established, a flow-back current of $0.1 \mu\text{A}$ was measured. This implies that the wind was able to displace a current of $0.2 \mu\text{A}$ associated with the charged droplets. After the increase of the wind speed, the flow-back current did not decrease.

Even though the electro spraying of water was improved with this new configuration, there are probably still a number of submicron droplets present. Similar to the situation described in the previous section, they cannot be moved by the wind because the electric force is higher due to the relative high charge on the small droplets.

- **Polarity of the charged droplets: EHDA**

As we have found in chapter 3, the polarity of the charging electrodes did not affect the magnitude of the produced current. During these wind experiments, the charging electrodes were set to a negative potential and this means that the droplets are positively charged. However, when the charging electrode was set to a positive potential, meaning the droplets were negatively charged, the flow-back current was found to be equal to the produced current. This implies that the wind was unable to move any of the charged droplets away from the EWICON system. This also implies that the EWICON system will not be charged, when the connection to earth will be cut. We will verify this in chapter 5.

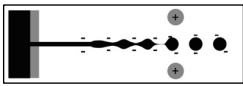
This effect was observed for all implementations that used the EHDA method, which also include the (still to be discussed) scaled-up versions. Also, this effect was observed with all tested spraying liquids, i.e. water, water/ethanol mixtures and ethanol.

According to Figure 3.5, a positive potential results in the presence of a fine mist, while this mist is absent in the case of a negative potential. While this

effect is not yet fully understood, the reasons could lie in the fact that the creation of the droplets is fundamentally different in both cases. When a positive potential is used, the OH^- ions are accelerated towards the apex of the cone. In the case of a negative potential, it will be the H^+ ions, which are smaller than OH^- ions. Therefore, it is likely that the droplets that break off of the cone due to H^+ ions will be smaller in diameter.

4.2.3 HPMS¹

- **Single HPMS device**



In chapter 3, a single HPMS device yielded a current of $0.09 \mu\text{A}$ associated with the charged droplets. After the air flow was established, it was observed that all the droplets were moved away from the EWICON system by the wind. This implies that all the charged droplets can contribute to the charging of the EWICON system.

- **Polarity of the charged droplets: HPMS**

During the wind experiments with the HPMS method, no flow-back current was measured regardless of the polarity of the droplets.

4.2.4 Conclusions: charged droplet transportation of both methods

For the single nozzle implementations of both spraying methods, we can conclude that the produced charged droplets can be moved by the wind against the electric field generated by the EWICON system. In the case of the EHDA method, the effectiveness depends on the sprayed liquid, the implementations and the polarity of the droplets, unlike in the case of the HPMS method.

With respect to the EHDA method, in terms of displaced currents, the increase of the wind speed in these single nozzle systems results in a higher current when water/ethanol mixtures are used as the spraying liquid. If demineralised water is used, the increase of the wind speed does not result in an increased displaced current, because of the submicron sized droplets.

¹ This work was conducted in close cooperation with Wietze Nijdam and Jeroen Wissink of Medspray XMEMS BV

4.3 Increased charged droplet production

The projected output power of a single spraying nozzle is in the order of tens of milliwatts, depending on which spraying method is used. Therefore, in order to increase the output power of the charging system to the order of kilowatts, the output current and, thus, the rate of charged droplet production needs to be significantly increased.

One straightforward method to increase the production of droplets is to simply connect multiple nozzles together. We will take a look at one- and two-dimensional expansions of the needle nozzle spraying system for EHDA. With this increased current production, there will also be more flow-back current. We will also investigate the net current as a function of the wind speed.

Subsequently, we will look at a spraying method that is based on the EHDA principle, but has no need for individual spraying needle nozzles. Finally, we will discuss the expansion of an HPMS system and the results of combining several of the spraying chips.

The experiments that will be discussed in this section are to determine the suitability of different concepts for up scaling droplet production in the EWICON system:

- EHDA: Multi-needle systems
- EHDA: Self-adjusting wire spraying system
- HPMS: Multi-chip system

4.3.1 EHDA: Multi-needle systems

The single nozzle version of the EHDA system was of the Delrin type and in order to obtain a multi-nozzle version of this system, a number of these casings would have to be placed next to each other. However, due to the size of each casing, a diameter of 3 cm, there would be room for only a limited number of Delrin nozzles in a small space.

Another strategy to designing a multi-nozzle system is to take only the spraying needles and place these in a grid. This could be achieved in numerous ways and in Figure 4.5 we have depicted one possible configuration in which the number of nozzles was expanded in one dimension.

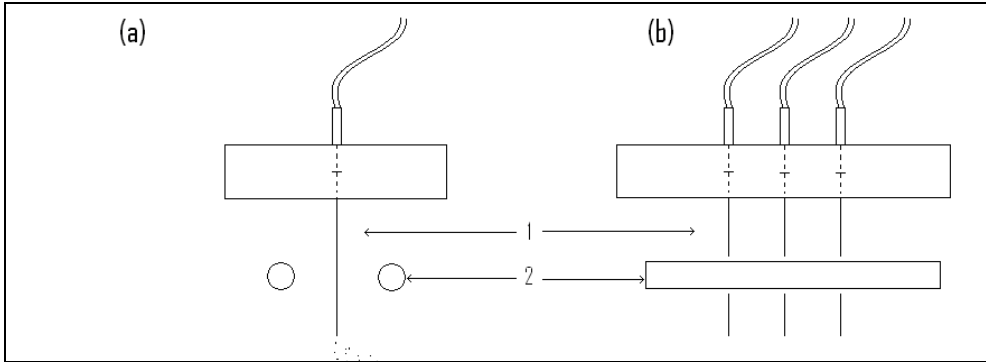


Figure 4.5. Schematic overview of a possible multi-nozzle set-up configuration. The spraying is fed through tubes to the needles (1) where EHDA spraying is achieved through the use of rod electrodes (2). (a) side view (b) front view.

Here, a row of nozzles have been positioned in an insulating material. The distance between the nozzles could be varied from 1.0 to 4.0 cm. Instead of individual ring electrodes for each needle, the electric field needed to establish the spraying process is now generated by two rod electrodes placed on both sides of the nozzles as depicted in Figure 4.5. A nine needle multi-nozzle configuration can be seen in Figure 4.6 where the spraying needles are 2.0 cm apart.

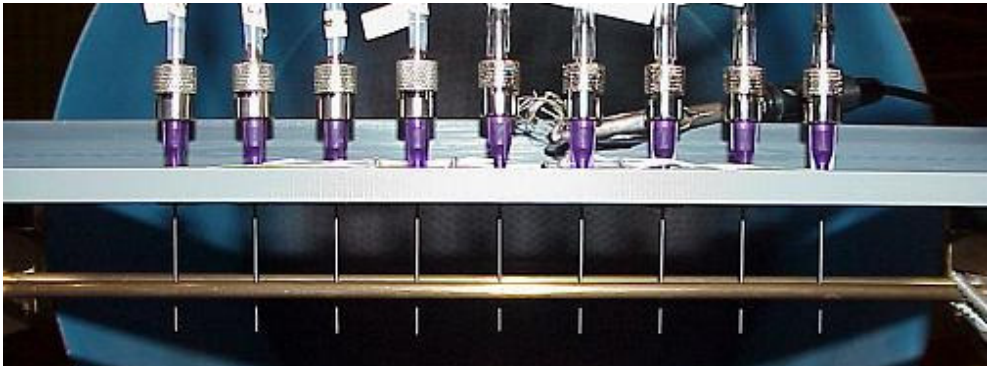


Figure 4.6. A nine needle multi-nozzle configuration using rod electrodes as the charging electrodes. In this configuration, the spraying needles are 2.0 cm apart.

Calculation of the electric field underneath the needles showed that without electro spraying the field increased with higher separation distances. This suggests that the current would be higher with a separation of 4.0 cm compared to 1.0 cm.

The experiments with the configuration shown in Figure 4.6 have been conducted using the same flow rate per nozzle and charging potentials as the single nozzle configuration. The flow rate was 20 ml/hr and the charging potential was -4.0 kV. Also, the separation distance has been varied from 1.0 to 4.0 cm.

The main conclusion is that the increase of the number of spraying nozzles led to an increase in the produced current as compared to a single nozzle in the same system. However, the current produced by each single nozzle was significantly lower compared to the single nozzle/ring electrode configuration. The maximum current per nozzle was $0.2 \mu\text{A}$ compared to $0.5 \mu\text{A}$ measured with the single needle nozzle configuration in the previous chapter. These results were obtained with separation distances of 2.0 and 4.0 cm.

When the separation distance was decreased to 1.0 cm, the current was measured to be lower per nozzle, $0.1 \mu\text{A}$. This is due to fact that the space charge of the sprayed droplets negatively affects the spraying process of the neighbouring nozzles. Therefore, a separation of 2.0 cm was chosen for subsequent multi-nozzle experiments.

- **Currents and electric field analysis**

One part of the explanation for this behaviour is the fact that the electric field generated by the rod electrodes is not as strong on the tip on the spraying needle nozzle as compared to the electric field generated by the ring electrode. Both systems have been modelled in LORENTZ with the electrodes set at -4.0 kV , after which the electric field right underneath the needle tip was found to be 2.6 kV/mm in the ring electrode set-up and 2.2 kV/mm in the rod electrode set-up. In these simulations the space charge effects of the droplets have not been included.

This problem can be partly resolved by increasing the potential on the rod electrodes to e.g. -6.0 kV , which increases the electric field to 3.3 kV/mm . This increased the current per nozzle to $0.3 \mu\text{A}$ while occasionally reaching $0.4 \mu\text{A}$, which still is lower than the current yielded by the single nozzle configuration. Another part of the explanation could lie in the fact that the electric field underneath the needle tip is not rotationally symmetric compared to the ring electrode configuration. This is illustrated in Figure 4.7 and Figure 4.8.

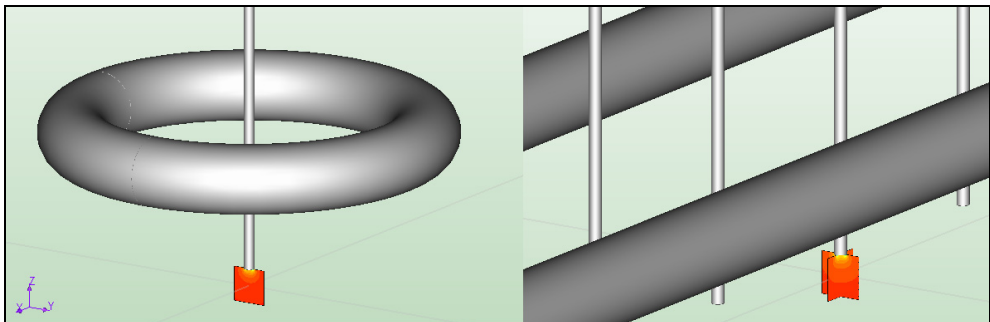


Figure 4.7. Both the ring electrode configuration (left) and the multi-nozzle with rod electrodes configuration (right) have been modelled in LORENTZ. The small orange coloured square indicate in which plane the electric field have been plotted.

In Figure 4.7 we can see the overall situation of both implementations, where the small orange coloured squares indicate in which plane the electric field has been plotted. These plots have been enlarged in Figure 4.8, in which Figure 4.8a is a plot of the field underneath the needle tip in the ring electrode configuration in Y-Z plane. Figure 4.8b is a plot in the same plane of the field underneath the needle tip in the rod electrode configuration. Both electric field plots are comparable in shape and magnitude.

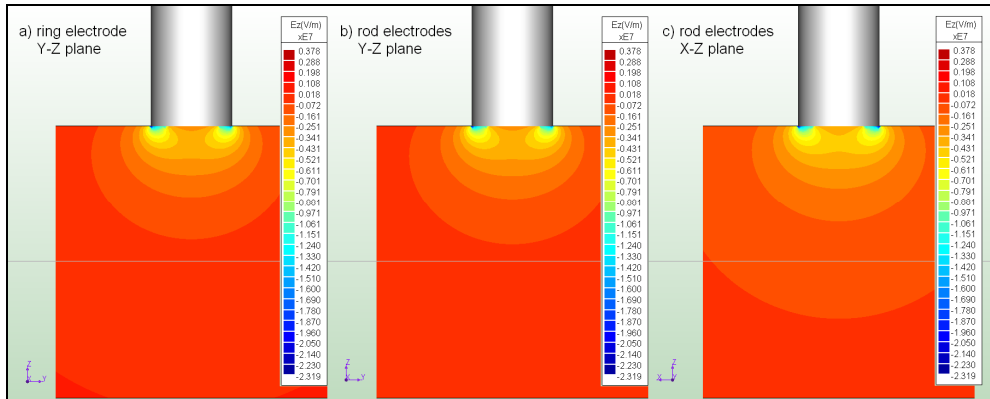


Figure 4.8. Plots of the electric field underneath the needle tip (a) in the ring electrode configuration in the Y-Z plane, (b) in the multi-nozzle rod electrodes configuration both in the Y-Z plane and (c) in the X-Z plane (right).

However, if we look at Figure 4.8c, which shows the electric field in the X-Z plane parallel to the rod electrodes, we can clearly see that the magnitude differ from the other two plots. Overall, this means that the electric forces acting on the ions in the Taylor cone are not symmetrical compared to the situation with the ring electrode and this could mean that the break-off process of the charged droplets is negatively affected. In [37] on the disintegration of water droplets, it is discussed that, theoretically, the formation of a Taylor cone can only occur when the electric field is azimuthally symmetrical. While the conditions that enable the forming of a Taylor cone are not a prerequisite for electrospraying in general, the fact that these conditions are not present with rod electrodes means that a lower current is to be expected.

Experiments with ring and cylindrical electrodes have proven to be more effective for EHDA based spraying and they seem to at least give credence to the above-mentioned discussion, see [38] and [39].

- **Non-linearity and two-dimensional system**

A concerning observation was the fact that while the produced currents could be added together, this process was not linear. The nine nozzle configuration, depicted in Figure 4.6, did not yield $2.7 \mu\text{A}$ as one would expect based on the individual nozzle result, but slowly reached $1.5 \mu\text{A}$ as the number of nozzles was increased.

In order to further investigate this non-linear effect, a two-dimensional charging and spraying system was constructed as shown in Figure 4.9. This system comprises of 3 rows similar to the one-dimensional multi-nozzle system each equipped with 8 spraying needles totalling 24 spraying units. Each nozzle had been individually tested to yield $0.3 \mu\text{A}$. In theory, this would mean that a total output current of $7.2 \mu\text{A}$ could be produced with this spraying system.

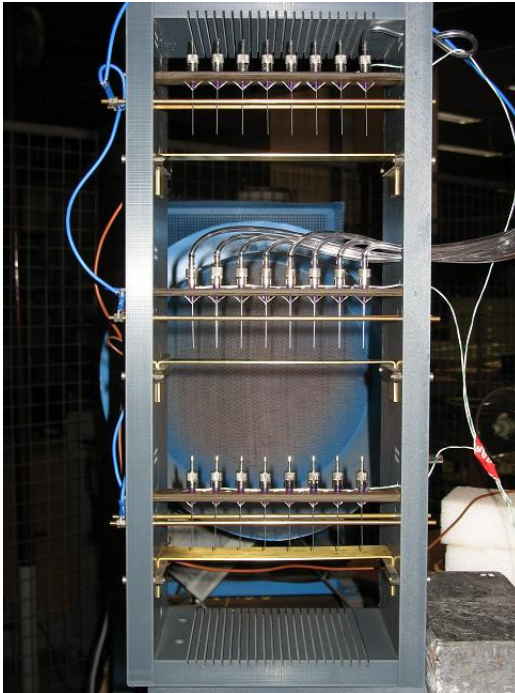


Figure 4.9. An EHD based charging test set-up equipped with a two-dimensional configuration of spraying nozzles. This spraying set-up employed 24 needles.

However, non-linearity was also present in this system. Each of the rows yielded a current of $1.5\text{-}1.6 \mu\text{A}$ and any combination of two rows yielded currents between 2.3 and $2.7 \mu\text{A}$. Finally, the full system yielded a current of $3.5 \mu\text{A}$, which is roughly half of the expected output current.

- **Multi-needle with rounded ring electrodes system**

A multi-needle system has been constructed in which each of the needles has its own ring electrode similar to the Delrin nozzle configuration, as depicted in Figure 4.10. Five rings have been shown, but the actual implementation was designed to fit up to 16 needles. These ring electrodes have been rounded in order to prevent corona discharges. This has been done to investigate whether the non-linearity also occurs if the electric field around each spraying needle is symmetrical.

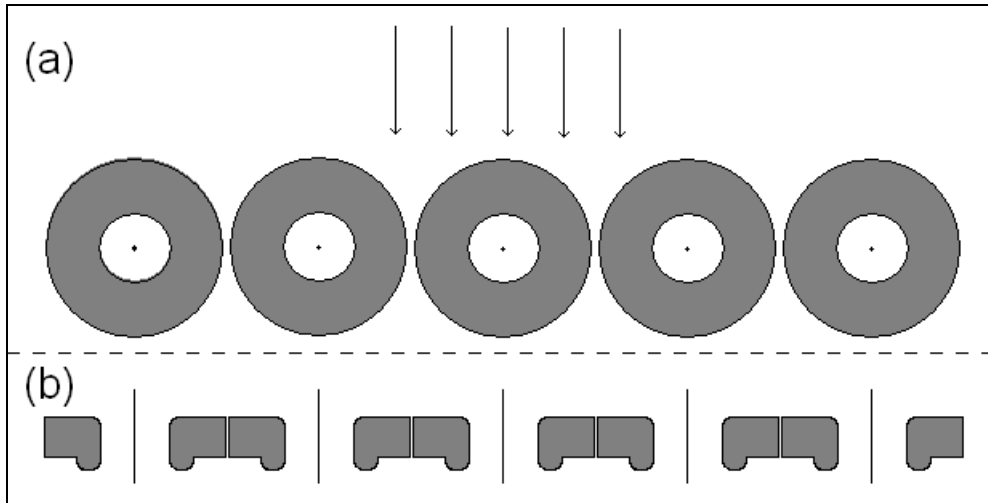


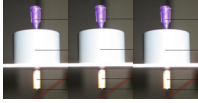
Figure 4.10. Schematic overview of the multi-needle with ring electrodes system. Each ring has an inner diameter of 20 millimetres. Five rings have been shown, but the actual implementation was designed to fit up to 16 needles. (a) bottom view (b) front view, the wind comes out of the paper.

This set-up has been tested using parameters similar to the previous systems. The sprayed liquid was a 70%/30% water/ethanol mixture with flow rate of 20 ml/hr. The wind speed was 10 m/s. One ring/needle configuration yielded a produced current of 0.5 μA . When 4 needles were connected, the produced current was found to be 2.0 μA . Thus far, the produced current is proportional to the number of ring/needle configuration. Connecting a 5th needle resulted in a total produced current of 2.3 μA , which is still within measuring inaccuracies. However, connecting a 6th needle resulted in a current of 2.5 μA , thus bring the current per needle to 0.4 μA . We will discuss these effects at the end of this chapter.

Up until this system, all the discussed multi-nozzle charging systems were tested with water/ethanol mixtures. They have been tested with demineralised water, but with little success in terms of produced current and stability of the spray

itself. However, spraying demineralised water in a 6 nozzle version of this system yielded a net current of $0.5 \mu\text{A}$.

- **Multiple needle with cylindrical electrode configurations**



A three nozzle version of the cylindrical electrode for spraying demineralised water, described in chapter 3, has also been constructed. In section 4.2.2, we found that for one nozzle, the produced current was $0.3 \mu\text{A}$ and the flow-back current was $0.1 \mu\text{A}$. Therefore, we expect that the produced current would be $0.9 \mu\text{A}$ and that the flow-back current would be $0.3 \mu\text{A}$, yielding an expected displaced current of $0.6 \mu\text{A}$.

During the measurements, the flow-back current was found to be $0.6 \mu\text{A}$, reducing the displaced current to $0.3 \mu\text{A}$. Apparently, non-linearity is also present in this case, however, this time, the non-linearity occurs due to the higher flow-back current. This could be attributed to the fact that charged droplets are pushed back by other charged droplets that have been sprayed a moment earlier. The fact, that there are 3 instead of 1 spraying nozzles, means that the charged droplets sprayed by the middle nozzle have less room to disperse.

This implies that in order to decrease the flow-back current, the wind speed should be increased. Therefore, the wind speed was increased from 10 to 12 m/s. This led to the flow-back current decreasing minimally by $0.1 \mu\text{A}$ to $0.5 \mu\text{A}$ and an increase of the displaced current increased to $0.4 \mu\text{A}$. However, if we allow for measurement inaccuracies, then the expected and actual displaced current do not differ by the same measure as the previously discussed multi-nozzle systems.

- **The displaced current vs. wind speed**

In the previous experiments with the single nozzle systems, we have already investigated whether an increase in the wind speed of 2 m/s would reduce the flow-back current. This has also been investigated for one of the multi-nozzle systems. In this case, a four needle version with the rounded ring electrodes configuration was tested.

The wind speed was varied from 6 to 12 m/s and the potential of charging electrode was increased such that the flow-back current was increased to be $1.4 \mu\text{A}$ when the produced current at the nozzles was $1.7 \mu\text{A}$. The results can be seen in Figure 4.11. As the wind speed increased, the flow-back current steadily decreases to $0.4 \mu\text{A}$. From this we can conclude, that the produced droplets vary in size.

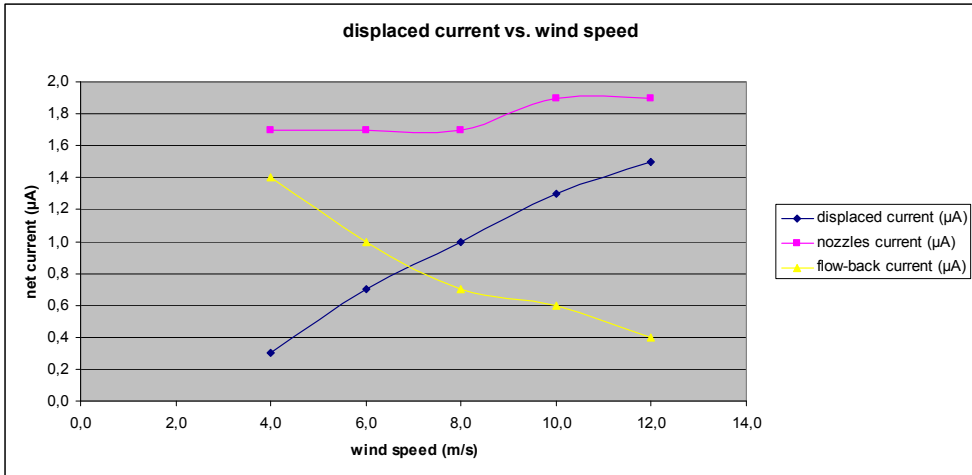


Figure 4.11. The displaced current as a function of the wind speed. The current measured at the nozzles stays roughly constant while the flow-back current decreases. Thus, the displaced current increases with increasing wind speed.

Another effect that can be observed in Figure 4.11 is the fact that the nozzles current increases at 10 m/s. This is due to the fact that at this wind speed, sufficient charged droplets are moved away from the nozzles and this leads to an increase in the local electric field. This, in turn, leads to the creation of droplets with a higher charge and thus a higher produced current.

4.3.2 EHDA: Self-adjusting nozzles wire spraying system

As we have seen, the expansion of the needle nozzles system leads to a higher, albeit at this time not proportional, current. The drawback is that this also means that more spraying needles and electrodes need to be implemented in the system. Concurrent with the research and design of multi-nozzle systems, research has also been conducted into other ways of spraying charged droplets. One of these methods, called high voltage wire spraying, is based on the observed phenomenon, that when a wet wire is set on a high potential, small EHDA-based Taylor cones start to appear.

For example, after rainfall, the wetted high voltage overhead lines appear to spray water droplets. This is schematically depicted in Figure 4.12.



Figure 4.12. Taylor cones formed as on a high voltage overhead line.

The main advantage of high voltage wire spraying is that the Taylor cones have been observed to be self-adjusting, i.e. because of the interaction between the liquid and the electric field generated by the electrodes and the charged droplets, the number of and the distance between the Taylor cones is adjusted according to parameters such as flow rate, electric field and wind speed. This ensures the optimal number and spacing of spraying nozzles which is not easily achieved using needles.

There are several ways to implement this wire-spraying technique, but we will discuss the final implementation which has been tested with ethanol as the spraying liquid, see Figure 4.13. A spraying system was developed which sprays charged droplets from Taylor cones formed from a liquid surface. This liquid surface is created by a strip of porous material in which an electrode is integrated, the length of this strip is 160 mm and the width is 4.5 mm. A number of standard spraying needles (not shown in Figure 4.13 but they are in Figure 4.14) are providing the liquid for the porous strip.

These porous strips were cut out of fluidising sheets manufactured by the company Porex.

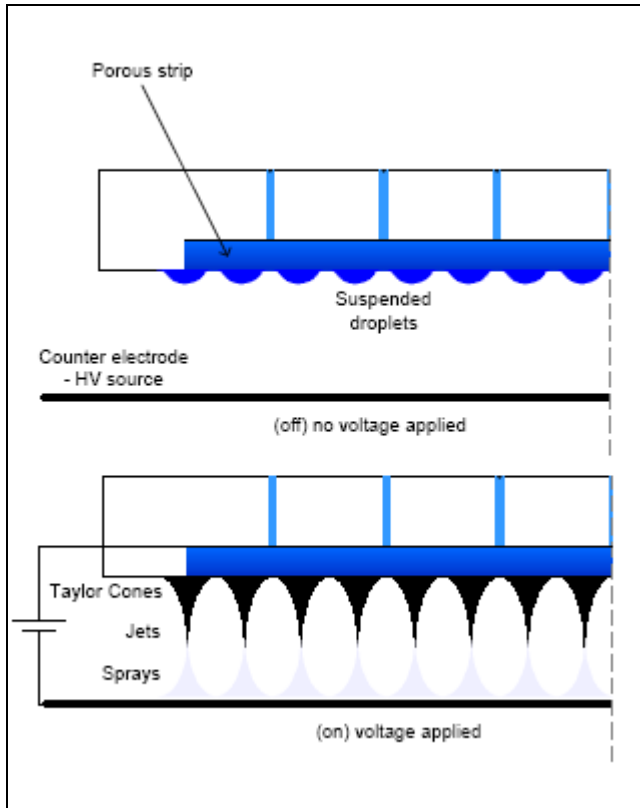


Figure 4.13. Schematic overview, taken from [40], of the self-adjusting multi-nozzle set-up, with and without applied voltage. Liquid is supplied to the porous strip, which evenly distributes it to a liquid film. Under the influence of gravity suspended droplets appear, see upper part. After the voltage has been applied, Taylor cones appear, see lower part.

Experiments have been conducted with this spraying system to test whether charged droplets would be created and whether the self-adjusting properties would be observed. In Figure 4.14, we can see a photo of the spraying process.

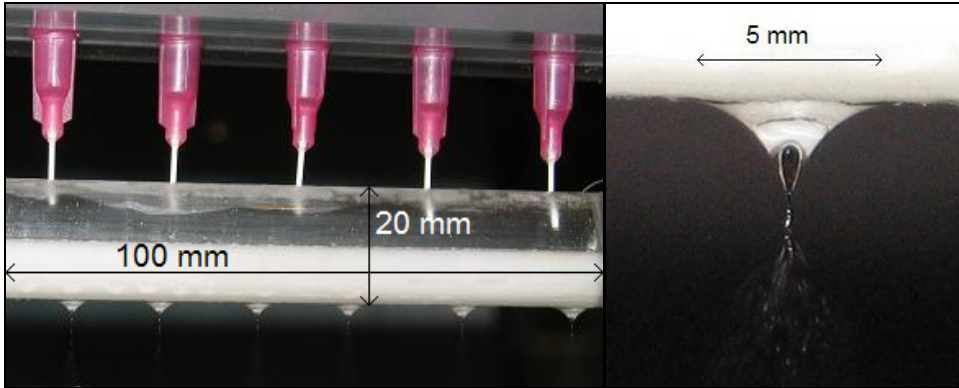


Figure 4.14. Photos of experiments with the self-adjusting multi-nozzle set-up. On the left-hand side, we can see the needle nozzles supplying liquid to the white porous strip from which the Taylor cones are created. On the right-hand side, we can see an enlargement of one these Taylor cones.

Using this system, the flow rate was set at 120 ml/hr, which is comparable to the flow rates in EWICON systems using multi-nozzle EHDA spraying. The charging potential was varied from 9.0 to 15.0 kV, which resulted in a charged droplet current increasing from 1.5 to 6.2 μA . The number of self-adjusting spraying sites went from 6 to 13. Another observed effect, while increasing the charging potential, was that the size, i.e. the length and width, of the Taylor cones decreased when their number increased, as depicted in Figure 4.15.

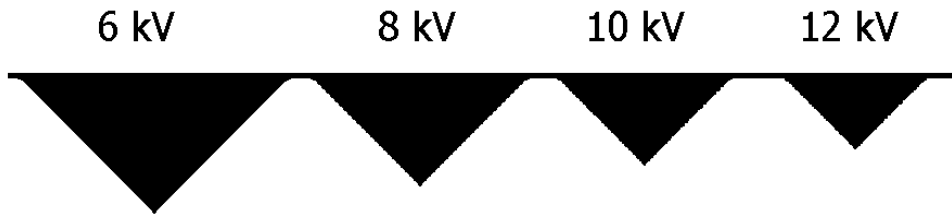


Figure 4.15. Increasing the charging potential leads to an increase of number of Taylor cones. Since the flow rate remains constant, the dimensions of the cones become smaller as schematically depicted.

Following these tests, the wind generator was turned on at a speed of 12 m/s. The first effect that could be observed was that the Taylor cones were strongly deformed by the wind. The second effect that could be observed was that the distance between the Taylor cones decreased. This could be explained by the fact that the wind transports charged droplets away, thereby effectively removing space charge from the vicinity of the cones. Normally, the presence of the charged droplets underneath would be responsible for the repulsion between the cones. However, with the removal of the droplets by the wind, the repulsive force decreases and, thus, the distance between the cones.

Theoretically, this would leave room for more cones, which could be achieved by increasing the flow rate at this point, thus increasing the produced current. However, due to safety reasons, this has not been tested and the spraying system as a whole needs to be modified such that the flow rate can safely be increased during the spraying process.

We can thus conclude that the Taylor cones are self-adjusting and will adapt to the prevailing parameters such as wind speed and charging potential.

4.3.3 HPMS: Multi-device systems¹

Three of the HPMS devices, each containing 35 spraying pores, discussed in the previous chapter have been combined in a way similar to the EHDA-based spraying needle nozzles. The output current of this three HPMS device spraying system has been measured to be 0.3 μA as compared to 0.09 μA for the single HPMS device spraying system. Therefore, the conclusion can be drawn that with respect to the number of spraying pores, the output current scales linearly.

4.4 Lowering required wind speed by field grading

In this section, we will investigate whether it is possible to grade the electric field in such a way, that the minimum required wind speed for effective EWICON operation can be lowered, while still maintaining the charged droplet creation process. To this end, the electric field is analysed and the droplet trajectories are calculated at different wind speeds. Subsequently, the electric field will be modified using one or more extra electrodes, after which the droplet trajectories will be plotted again.

As an example, we will look at a charging system that consists of the ring electrode with needle nozzle set-up used for the EHDA spraying. For HPMS at this moment, there is no need to lower the minimum required wind speed, because of the high exit velocities of the charged droplets.

4.4.1 Analysis of droplet trajectories

In Figure 4.16, the trajectories of droplets have been plotted as function of the wind speed, which is directed in the positive Y-direction and varied from 6 to 10 m/s. The needle nozzle is set at 0.0 kV, representing the fact that EWICON system is connected to earth, and the ring electrode is set at -4.0 kV. As we can see, the droplet escapes the charging system only when the wind speed is 9 m/s or

¹ This work was conducted in close cooperation with Wietze Nijdam and Jeroen Wissink of Medspray XMEMS BV

higher. Also, we can see that at 8 m/s, the wind manages to move the droplet, but still has insufficient time to accelerate the droplet to its terminal escape velocity.

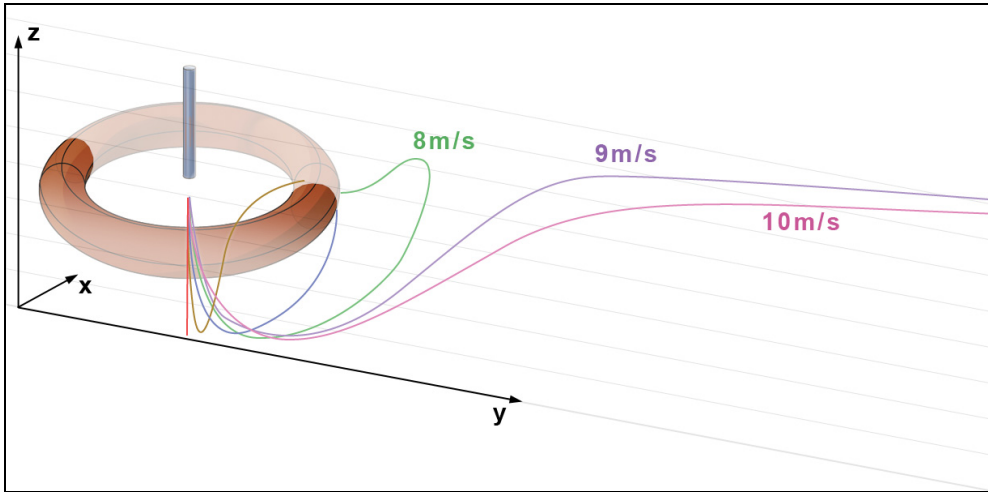


Figure 4.16. The trajectories of droplets are plotted as a function of the wind speed. The ring electrode is set at -4.0 kV and the needle is set at 0 kV. The wind speeds in this plot vary from 6 to 10 m/s. The droplet is moved away completely, only when the wind speed is 9 m/s or higher.

It should be noted, that in these simulations with LORENTZ, the wind is modelled as laminar air flow, similar to the MATLAB modelling performed in chapter 2.

Another example, which we will explore more in detail, is a charging system that uses the multi-nozzle spraying system described in section 4.3.1. In Figure 4.17, a five nozzle system with two metal rods as the charging electrodes has been depicted. Another component that is visible in the right lower corner of Figure 4.17 is a metal plate representing the platform as described in section 4.1.1. The orientation and placement of the platform depends on the actual implementation of a particular EWICON system.

The wind speed is set at 6 m/s and pointed in the positive Y-direction. The two rod electrodes are set at -4.0 kV and the nozzles and the platform are set at 0.0 kV, since they are electrically connected. For this simulation, trajectories of multiple droplets have been plotted.

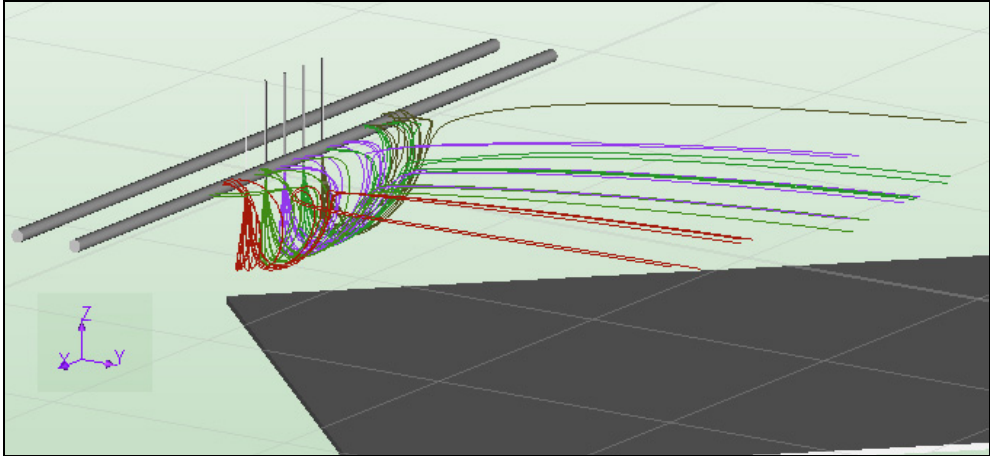


Figure 4.17. Result of the simulation of the EWICON system using a wind speed of 6 m/s. The two rod electrodes are set at -4.0 kV. The rectangular electrode represents the platform of the grounded EWICON system and is electrically connected to the needles. Most of the droplets are forced back to the charging electrodes.

As we can see in Figure 4.17, using a wind speed of 6 m/s (3 on the scale of Beaufort), the wind was unable to move all of the droplets away from the system. This has been verified in experiments where the leakage currents have been measured at the charging electrodes.

Revisiting the calculations in chapter 2, we found that if the wind speed was 3.3 m/s or more, then a charged droplet would be moved away by the wind, provided the uniform electric field nowhere is higher than 10^4 V/m. However, in this case, the volume underneath the spraying needles contains regions that have electric fields varying between 10^4 and 10^5 V/m. Also, the fact that there is a multitude of charged droplets present instead of one should be taken into account. Together, these are contributing factors to the fact that charged droplets are attracted back, even though the wind was assumed to be sufficient with a speed of 6 m/s.

Only when the wind speed was increased to 12 m/s (6 on the scale of Beaufort), which is even more than was needed in the case of the single needle nozzle/ring electrode configuration, the wind was able to move all the droplets away from the system, as is shown in Figure 4.18.

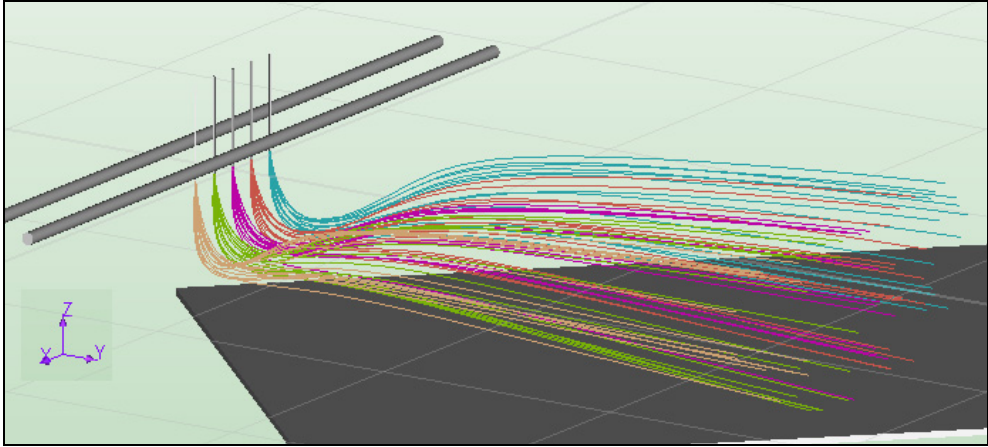


Figure 4.18. Result of the simulation of the EWICON system using a wind speed of 12 m/s. Only the presence of a much higher wind speed than 6 m/s results in the complete removal of all charged droplets.

In order to analyse in what way the electric field acts on the charged droplets, we take a look at a cross section in the Z-Y plane in an area around the spraying nozzles. We plot the z-component of the electric field, which results in Figure 4.19.

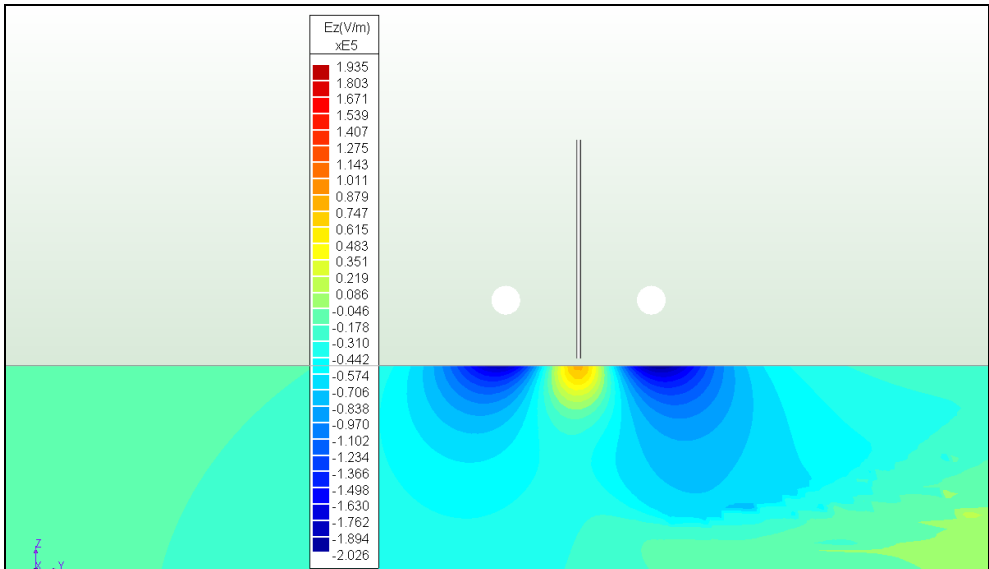


Figure 4.19. Plot of the z-component of the electric field present in the EWICON system. In the yellow/orange areas, the charged droplets are pulled downwards. In the dark blue areas, the charged droplets are pulled upwards.

In this plot, the yellow/orange areas represent the parts where the electric field is pointed downwards and, thus, positively charged droplets will be pulled downwards, which is consistent with the mechanism of EHDA droplet creation. The blue areas represent the parts where the electric field is pointed upwards and in these regions, the droplets will be pulled upwards one of the two rod electrodes. This is the effect we want to minimise. The underlying thought is to grade the electric field in such a way, that the wind actually has more time to act on the droplets before they can reach one of the electrodes.

4.4.2 Steering electrode(s)

One possible way of implementing that strategy is by introducing one or more steering electrodes, on a potential with a polarity similar to the charging electrode. The main thought is this steering electrode will change the electric field in such a way, that the electric force on the charged droplets pointing towards the charging electrodes will be lower. This means that the charged droplets will be attracted towards the steering electrode rather than the charging electrodes, travelling a different path. Also, this implies that in the case that there is no wind, most of the charged droplets would be pulled to the steering electrode.

In Figure 4.20, a plot of a simulation in LORENTZ has been made where there is no wind present. Most of the charged droplets are now attracted to the steering electrode, while a small remaining number of charged droplets are still attracted to the charging electrode. This is due to the mutual repulsion of the charged droplets, which causes some charged droplets to move in the +Y direction, thus being farther away from the steering electrode.

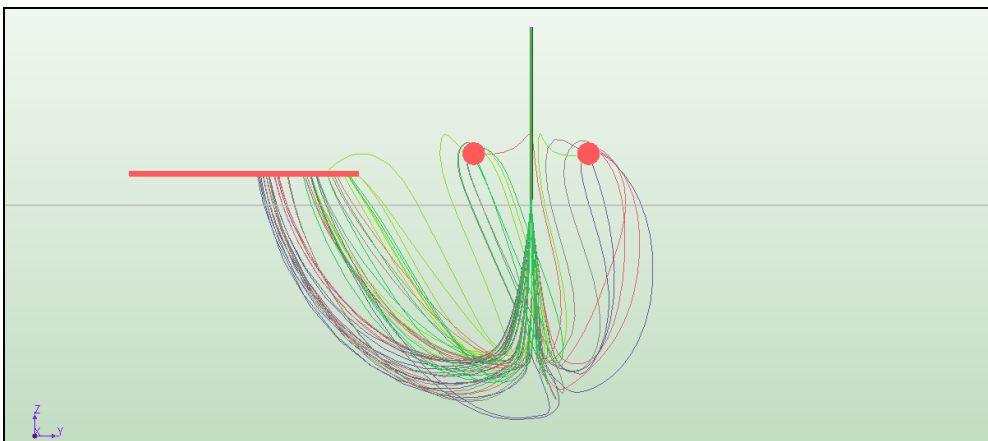


Figure 4.20. Result of a simulation of a charging system with a steering electrode when there is no wind present. Most of the charged droplets are attracted to the steering electrode while a small number of droplets are still attracted to the charging electrode.

If the distance covered by this different path to the steering electrode is longer than the path to the charging electrodes, then, presumably, the wind should have more time to act on those charged droplets. This, in turn, increases the likelihood that the charged droplets will escape the charging system and contribute to the produced current.

In Figure 4.21, we have plotted the electric field around the charging system. This time, a rectangular shaped steering electrode has been added to the system in front of the charging system with respect to the direction of the wind. We can see in the plot that by adding the steering electrode, the z-component of the electric field has decreased in the area where the charged droplets exit the nozzles. Therefore, the droplets will, first of all, travel a greater distance downwards and, secondly, be pulled back in the negative y-direction because of the steering electrode.

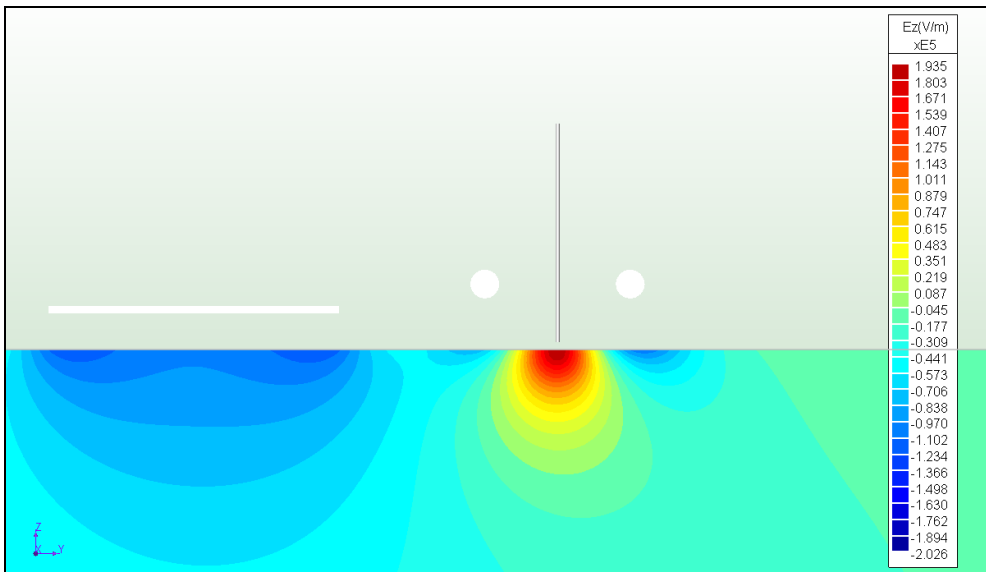


Figure 4.21. Plot of the z-component of the electric field present in the EWICON system. A steering electrode has been added and set at a potential of -10.0 kV.

Because of the fact that the charged droplets have to cover a greater distance before possibly colliding with one of the charging electrodes, the wind has more time to act on the droplets thus enabling it to remove most of the droplets from the system. This has been simulated again, as can be seen in Figure 4.22, in which the wind speed has again been set to 6 m/s.

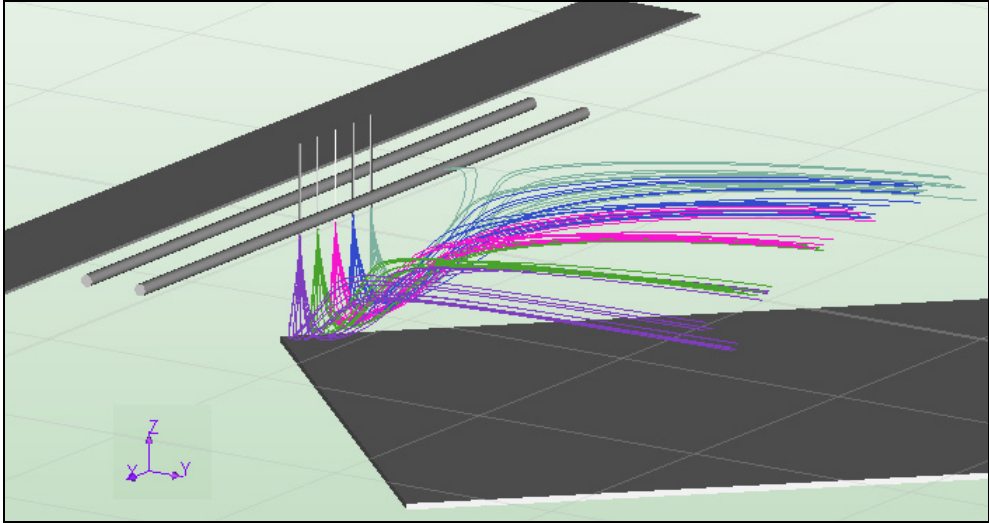


Figure 4.22. Result of the simulation of the EWICON system using a wind speed of 6 m/s. In this system, a steering electrode has been added and set at -10.0 kV. Practically, all of the charged droplets are now moved away by the wind.

We can see that practically all the droplets are removed from the charging system, which again was in agreement with the experiments.

4.4.3 Conclusions on field grading

The main conclusion is that the addition of at least one steering electrode already improves the usability of the EWICON system, with droplets created with the EHDA spraying method. Therefore, in all the future implementations of the EWICON, whether they are multi-needle or self-adjusting nozzle systems, steering electrodes should be considered to lower the minimum required wind speed.

It must be noted that adding an extra steering electrode, in theory, does not require any extra power after it has been charged up to its target potential, as long as no charged droplets come in contact with that steering electrode. Adding extra electrodes does, however, bring extra inconveniences with regard to the complexity of the EWICON system. These electrodes operate at different potentials and this means that the insulation between the various electrodes needs to be sufficiently high as to prevent any leakage currents to occur.

Another observed effect was the fact that, during spraying experiments, the potential needed on the charging electrodes was lower than if no steering electrode was used. The electric field at the tip of the spraying nozzles is raised by the electric field generated by the steering electrode. This is an advantage because this decreases the possibility of discharges at the charging electrodes.

Overall, LORENTZ is a useful tool to aid in the design of an EWICON system and to reasonably predict whether charged droplets will be moved away. However, in these simulations, we assumed monodispersity and the experiments have been carried out with water/ethanol mixtures, which exhibit monodispersity to a certain degree. Therefore, experiments will still be needed to confirm whether charged droplets will be moved away, especially when electro spraying of water is employed, where monodispersity is not yet achieved.

4.5 Rising EWICON potential and droplet movement

During all the experiments discussed in this chapter, the EWICON system itself was grounded while the charged droplets were sprayed and moved away by the wind. However, as soon as the EWICON system is disconnected from earth, it will charge up to a certain potential. As discussed in 4.1.3, the electric field in the vicinity of the spraying system remains constant during the charging process, because the potentials of the charging and steering electrodes will rise correspondingly. Therefore, the spraying process, either based on EHDA or HPMS, will remain undisturbed and the creation of charged droplets will continue.

This does not mean, however, that the electric forces acting on the droplets will remain constant. As the potential of the EWICON system rises, the attractive force back to the system is increased and at a certain point, the droplets will return to system. This means that the flow-back current increases and that the charging rate of the EWICON system decreases. Therefore, in the next chapter, in which we will conduct the charging experiments, we expect to observe the charging current to decrease while the charging potential will reach a maximum.

The behaviour still depends on the charging and spraying method, or more specifically, the size and charge distribution of the droplets. In 3.1.3, we briefly touched on the subject of monodispersity in that it implied that the force balance on the monodisperse droplets would be the same. It also means that, theoretically, at a certain potential, all the charged droplets would be attracted back to the system, thereby instantly reducing the current to zero. We expect this for the HPMS configuration.

Since EHDA does not provide monodisperse spraying for water and water/ethanol, we expect the charged droplets with a higher electrical mobility to be attracted back sooner than the charged droplets with a lower electrical mobility. Therefore, the charging current is expected to decrease gradually as function of the EWICON system potential.

4.6 Overall conclusions and final experimental set-up

4.6.1 Conclusions

We can conclude that it is possible to design the EWICON system in such a way that the wind can move charged droplets away. In the case of EHDA based spraying, the use of steering electrodes significantly lowers the minimum required wind speed. In the case of HPMS based spraying, steering electrodes were not needed, because of the high jetting velocity of the droplets.

Multiple-nozzle charging and spraying system, in one and two dimensions, with both the EHDA and HPMS method were designed and constructed. It has been possible to add the currents of the spraying nozzles together, even though for EHDA based systems this adding process was not linear.

The reason(s) why this non-linearity is present in these systems are still a topic of ongoing research and one of the most important issues that need to be resolved in order for the EWICON system to be scalable. The currents have been measured again more accurately using an oscilloscope instead of ammeters for a 1, 3 and 6 nozzles version of the rounded ring electrodes system.

The voltage has been measured over a 10 k Ω resistor resulting in Figure 4.23. We can see that in Figure 4.23a, that the voltage measured over the resistor connected to one nozzle is 3.110 mV, whereas in Figure 4.23b, the voltage measured over the resistor connected to three nozzles is 7.670 mV. Thus, the current produced by one nozzle is 0.311 μ A and the current produced by three nozzles is 0.767 μ A or 0.256 μ A per nozzle.

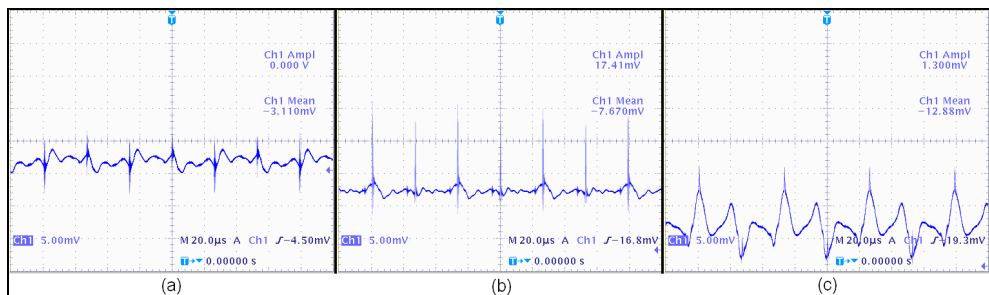


Figure 4.23. Results of the voltage measured over a 10 k Ω resistor in a (a) single nozzle (b) three nozzle (c) six nozzle version of the rounded ring electrodes system. The three nozzle version only yielded 2.5 times the current produced by a single nozzle version. The six nozzle version only yielded 4.1 times the current produced by the single nozzle version.

In Figure 4.23c, with 6 nozzles, the voltage measured over the resistor connected to 6 nozzles is 12.88 mV i.e. a nozzle current of 1.288 μA , which is higher only by a factor of 4.1 compared to one nozzle. Therefore, by also using more precise measurements, we can conclude that the increase of the current is not proportional to the number of nozzles.

The reasons for this non-linearity may lie in the fundamental nature in which the charge separation takes place. In the research of EHDA in general, the focus has mainly been on spraying particles in a controlled and predictable manner and less on the electrical implications that go hand in hand with the electro-spraying. Therefore, research should be conducted on the effect of the different materials at the nozzle/liquid interface on the charge separation process. In EHDA, the nozzle/liquid interface has always been a metal/water or metal/ethanol interface. In HPMS, the interface was always a dielectric/saline water interface and, up to now, no non-linearity has been found with HPMS. However, this was beyond the scope of this research project.

4.6.2 Final experimental test set-up

As it has been stated before, there are many ways to design and implement the EWICON system. For the majority of the conducted experiments described in this and the next chapter, the test set-up that was used is shown in Figure 4.24.

In Figure 4.24, we can see the isolated platform on which the high voltage DC sources have been placed. They are connected to the charging and the steering electrodes via ammeters. Also, on the platform, a 12V battery and a 12/240 converter are present, which power the HVDC sources and the syringe pump.

In order to facilitate the changing of the different implementations of the spraying systems, a separate isolated support structure has been constructed, seen on the right-hand side of the figure. The wind generator has been placed closely behind the support structure to ensure that the full width of the generator can be used for air flow.

The copper spheres (1), have been placed to minimise losses due to corona discharges, which would occur otherwise at higher EWICON system potentials. These rounded shapes can be seen throughout the whole set-up and all serve the same purpose. This rounding aspect is an issue that always needs to be considered when a scaled up version of the EWICON system will be designed.

The EWICON system potential has been measured with an electrostatic voltmeter (2). The potential is measured directly through electrostatic forces instead by measuring the current. In this way, the current losses are minimised.

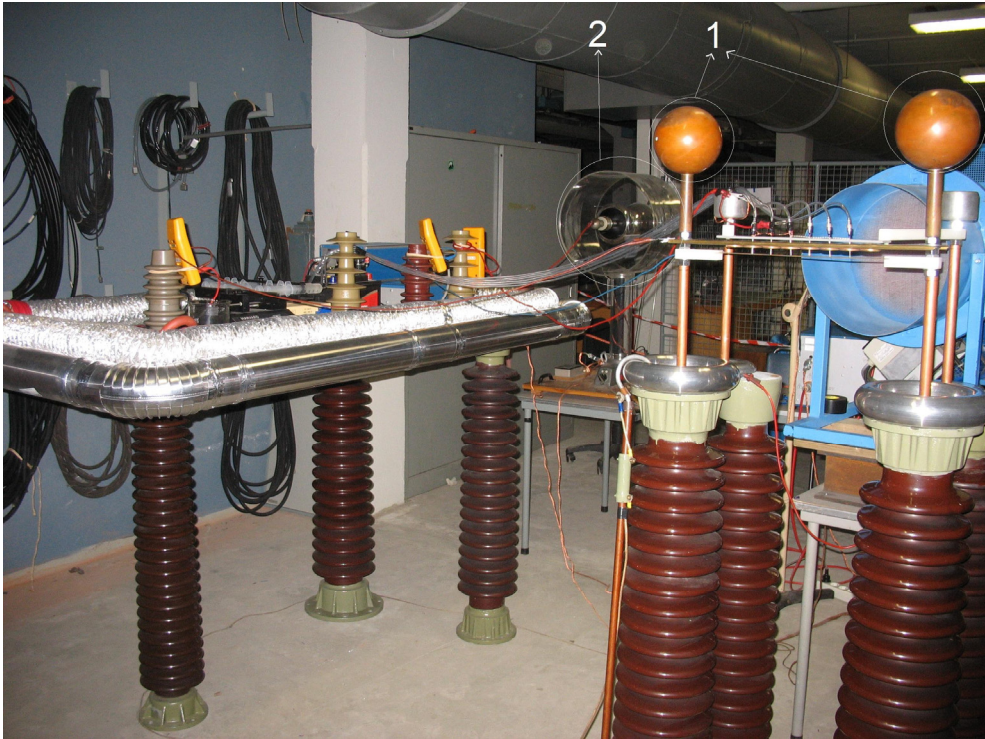


Figure 4.24. The final experimental test set-up of the EWICON system. On the left-hand side, the metal plate acting as the platform can be seen. On the right-hand side, the charging and spraying system can be seen.

5

Testing of the complete EWICON system

“It doesn’t matter how beautiful your theory is, it doesn’t matter how smart you are. If it doesn’t agree with experiment, it’s wrong.”

– Richard Feynman

In the previous chapters, the separate parts of the EWICON system, e.g. the charging system, the liquid supply system and the holding platform and its insulation have all been proven to operate as designed. In this chapter, experiments will be discussed that have been conducted on complete EWICON systems. The objective of these experiments was to determine whether the wind is able to move the charged droplets away such that the droplets can reach earth and if, by achieving that, the EWICON system can be charged.

Subsequently, upon having analysed the behaviour of the EWICON system without a load, it will be determined whether the EWICON system can be used to power an electrical load. We will analyse these results and determine whether the various EWICON configurations exhibit the expected behaviour. Summarising from the previous chapters, we expect the following:

- Using the EHDA method for charged droplet creation with water or water/ethanol mixtures, the charging or displaced current should decrease gradually as a function of the EWICON system potential.
- Using the HPMS method for charged droplet creation, the charging or displaced current should decrease rapidly to zero at a certain EWICON system potential.
- The maximum attained EWICON system potential should rise with increasing wind speeds.
- The EWICON output power should rise with increasing wind speeds.

All the experiments have been performed using a Type B implementation of the EWICON system, i.e. without a separate charge collector unit, see [41]. In section 5.1, the experimental method will be discussed. We will explain in what way the various types of currents and potentials were measured.

In the sections 5.2, 5.3 and 5.4, the experiments are described that were performed using different spraying methods. Some of the results of earlier measurements will be briefly stated, so that the results can be compared to results of more recent experiments. In section 5.5, we will analyse the results of the experiments and determine the efficiencies of the various configurations and in 5.6 we will summarise the conclusions.

In section 5.7, we will conclude this chapter with some considerations on up scaling of the EWICON.

5.1 Experimental method

In order to determine whether the EWICON system could be charged, the following steps were taken. Firstly, the wind turbine generator as described in chapter 4 was switched on and set to the desired wind speed. Secondly, the spraying and charging of the droplets was activated, in a similar way as described in chapters 3 and 4, depending on the used spraying system.

During this spraying phase, the holding platform of the EWICON system was still connected to earth. At this point, the optimal settings for the potentials on the charging and possibly steering electrodes, which were found during the testing described in chapter 4, were used. This also means that for different charging systems, e.g. the single nozzle/ring electrode system or the multi-nozzle/rod electrodes system, different potentials will be used. Therefore, it can be assumed that, in the next sections, the specified potentials are the ones that produce the highest net charging current.

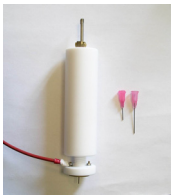
In the next phase, the holding platform was disconnected from earth, thus allowing the EWICON system to charge like a capacitor. During this charging process, the EWICON system potential was measured as a function of time. Using equation (4-2), we can indirectly estimate the magnitude of the charging current. The same procedure was followed to test the EWICON system with an electrical load attached. Finally, by using the results of these experiments, the output power of the various EWICON systems was calculated.

5.2 EWICON with single nozzle EHDA spraying systems

The first charging systems to be tested in the EWICON system are the spraying set-ups that consist of one single needle nozzle with one charging electrode. We will discuss the set-up equipped with the Delrin nozzle, the single nozzle version of the needle/rounded ring configuration discussed in chapter 3 and the set-up equipped with the cylindrical electrode, both of which were discussed in chapter 2.

5.2.1 Single ring electrode

- **Delrin nozzle (configuration #1 and #2)**



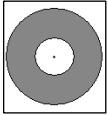
The first experiment using the Delrin nozzle with the ring electrode was performed using a 70%/30% water/ethanol mixture at a flow rate of 20 ml/hr. No steering electrode was yet implemented in this configuration. Similar to the Delrin nozzle experiments discussed in chapter 4, the wind speed was set at 6 m/s and the ring electrode was set on a potential of -7.0 kV, thus creating positively charged water droplets. The measured current from the needle nozzle was 0.5 μA and the flow-back current to the ring electrode was 0.2 μA .

After disconnecting the holding platform from earth, the potential of the EWICON system rose to a value of 6.0-6.5 kV in 5 seconds, where it remained steady for as long as the wind flow was present and the liquid was supplied. Connecting a load of 20.5 G Ω to the EWICON system resulted in a drop of EWICON potential to 2.0 kV. The current measured through the load was 0.1 μA , which means that the output power of this configuration resulted in 0.2 mW.

To illustrate the difference between positively and negatively charged droplets with respect to the transportation of said droplets by the wind, the ring electrode was set on a positive potential to create negatively charged droplets. The other parameters were kept constant. This time, after disconnecting the holding platform from earth, the potential of the system rose to approximately 1 kV in 90 seconds. Attaching the load to the EWICON system resulted in a drop of the potential to zero. In other words, this means that the load of 20.5 G Ω is too low compared to the internal impedance of the EWICON system. This effect has been noticed and tested for all EHDA based configurations with water, water/ethanol and pure ethanol as the spraying liquid. Therefore, from this point onwards, all the discussed results will only concern the experiments in which positively charged droplets were created and sprayed.

This experiment has also been performed with demineralised water. The measured current from the needle nozzle was approximately 0.1 μA and the flow-back current was also approximately 0.1 μA . After the platform was disconnected from earth, the potential of the EWICON rose to a 1000 V in 120 seconds. Connecting a 5.3, 10.3 or 20.5 G Ω load resulted in a drop of the potential to zero.

- **Rounded ring electrode (configuration #3)**



In this configuration, the holder with rounded ring electrodes has been used with only one spraying needle. In this way, the result can be compared to the results of configurations with multiple spraying needles. The flow rate was set at 20 ml/hr and the spraying liquid was a water/ethanol mixture of 70%/30%. The wind speed was set at 12 m/s. The measured current from the needle was 0.4-0.5 μA .

After disconnecting the holding platform from earth, the potential of the EWICON system rose to 45.0 kV in 60 seconds. The charging current has been indirectly determined using equation (4-3) and the progression of the EWICON potential over time, as can be seen in Figure 5.1. The theoretical output power reaches a maximum of 3.1 mW at 20 kV, which means that maximum power transfer would occur if a 130 G Ω load would be used. This load would then be equal to the internal source impedance of the current source.

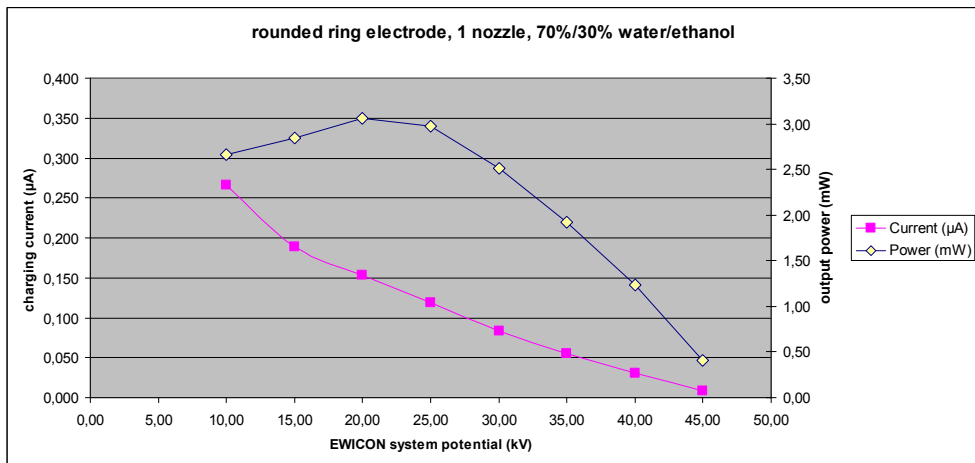


Figure 5.1. The indirectly measured charging currents and output power of a single nozzle while using ring electrodes as charging electrodes.

The charging current, I_c , vs. the EWICON system potential, U_{EWICON} , has been fitted with an exponential function in MATLAB, see appendix D, yielding the following expression for the charging current:

$$I_c(U_{EWICON}) = 0.501 \cdot 10^{-6} \exp(-62.31 \cdot 10^{-6} \cdot U_{EWICON}) \quad (5-1)$$

according to which $I_c(0)=0.5 \mu\text{A}$. This agrees with the current measured from the single needle nozzle. Based on (5-1), the calculated curves for the charging current and output power have been plotted, as shown in Figure 5.2.

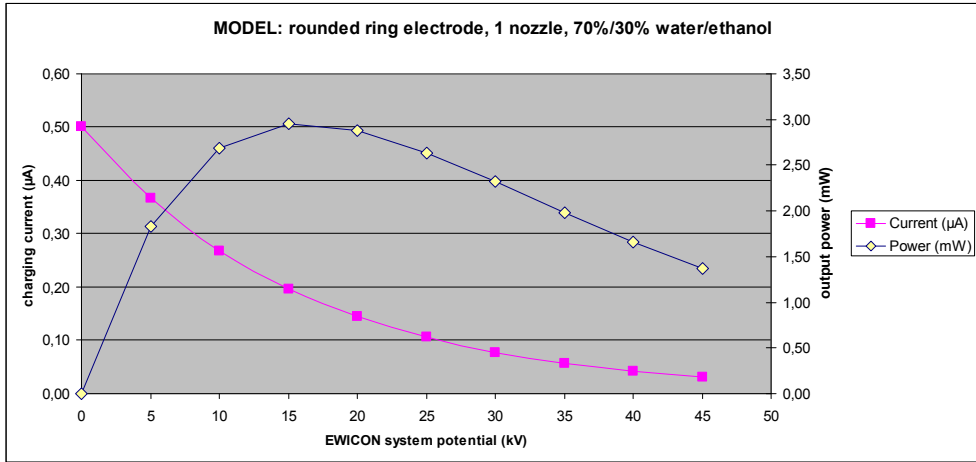
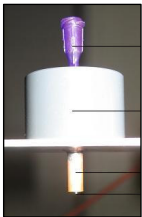


Figure 5.2. The calculated curves of the charging current and output power for the single needle nozzles version.

This suggests that the maximum power transfer will occur at 15 kV as opposed to the 20 kV derived from Figure 5.1. This discrepancy is due to the measurement error in the readout of the potential and the inaccuracy of the estimated parameters of (5-1).

5.2.2 Single cylindrical electrode

- **(configuration #4)**



This spraying set-up was used together with a steering electrode. The used liquid was demineralised water at a flow rate of 20 ml/hr. The wind was set at 12 m/s. During this experiment, the cylindrical charging electrode was set on a potential of -2.0 kV and the steering electrode was set on -9.7 kV.

After disconnecting the holding platform from earth, the potential of the EWICON system rose to 35.0 kV in approximately 5 minutes. The charging current has been indirectly determined as can be seen in Figure 5.3.

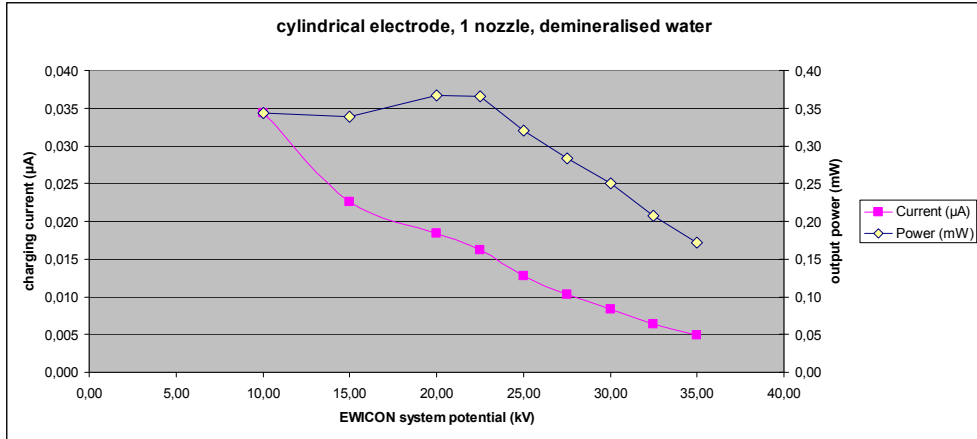


Figure 5.3. The indirectly measured charging current and output power of a single nozzle/cylindrical electrode configuration. The spraying liquid is demineralised water.

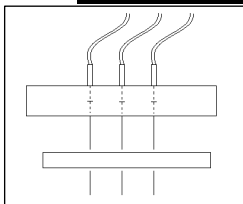
5.3 EWICON with multiple nozzle EHDA spraying systems

In this section, we will discuss the experiments performed with the EWICON system employing various spraying systems in which multiple spraying nozzles are present. In section 5.3.1, we will start with the multi-nozzle systems in which the charging electrodes are either rod electrodes or rounded ring electrodes as described in section 4.3.1.

Also described in section 4.3.1, is the multiple needle nozzle system with the cylindrical electrode configuration, of which the experimental results will be discussed in section 5.3.2. Finally, in section 5.3.3, the results of the final version of the self-adjusting nozzles configuration will be discussed.

5.3.1 Multiple needles with rod or rounded ring electrodes

- **Rod electrodes (configuration #5, #6 and #7)**



Eight spraying nozzles were used and the flow rate was set at 20 ml/hr per nozzle. The wind speed was set at 10 m/s. The rod electrodes were set on -5.0 kV and the steering electrode was set on -10.0 kV. Firstly, demineralised water

was used as the spraying liquid. This resulted in a net current just under 0.5 μA , while the EWICON system was still connected to earth. After disconnecting the holding platform, the EWICON system potential rose to 3.0 kV.

Secondly, the spraying liquid was changed to a 70%/30% water/ethanol mixture. This yielded a net current of 1.2 μA , while the EWICON system was still connected to earth. After disconnecting the holding platform from earth, the EWICON system potential rose to 9.8 kV. Connecting this configuration to a load of 20.5 G Ω yielded an output potential of 8.2 kV. The current measured through the load was 0.4 μA , resulting in an output power of 3.3 mW or 0.4 mW per nozzle.

Lastly, the two-dimensional spraying set-up described in 4.3.1 was used with the 70%/30% water/ethanol mixture. This set-up employed 24 spraying needles. This yielded a net current of 3.5 μA , while the EWICON system was still connected to earth. Connecting the 20.5 G Ω load to this configuration yielded in an output potential of 15.0 kV. The current measured through the load was 0.7 μA , resulting in an output of 10.5 mW or 0.4 mW per nozzle.

- **Rounded ring electrodes (configuration #8, #9, #10 and #11)**



Six spraying nozzles were used and the flow rate was set at 20 ml/hr per nozzle. The spraying liquid was a 70%/30% water/ethanol mixture. The wind speed was set at 12 m/s. The ring electrodes were set on a potential of -4.0 kV and the steering electrode was set on a potential of -10.0 kV. While the EWICON system still was connected to earth, the current measured from the six needle nozzles was 1.5 μA .

After disconnecting the holding platform from earth, the EWICON system potential rose to 45.0 kV in, on average, 30 seconds and ultimately reached 69.0 kV. Connecting this configuration to a load of 20.5 G Ω yielded an output potential of 16.0 kV in 10 seconds. The measured current through the load was 0.8 μA and this means that the output power of the EWICON system is 12.5 mW or 2.1 mW per nozzle. Also, electrical loads of 10.3 and 5.3 G Ω were connected to this configuration, which yielded an output potential of 9.7 kV with a current of 0.9 μA and 5.7 kV with a current of 1.1 μA respectively.

The current has also been determined indirectly in Figure 5.4.

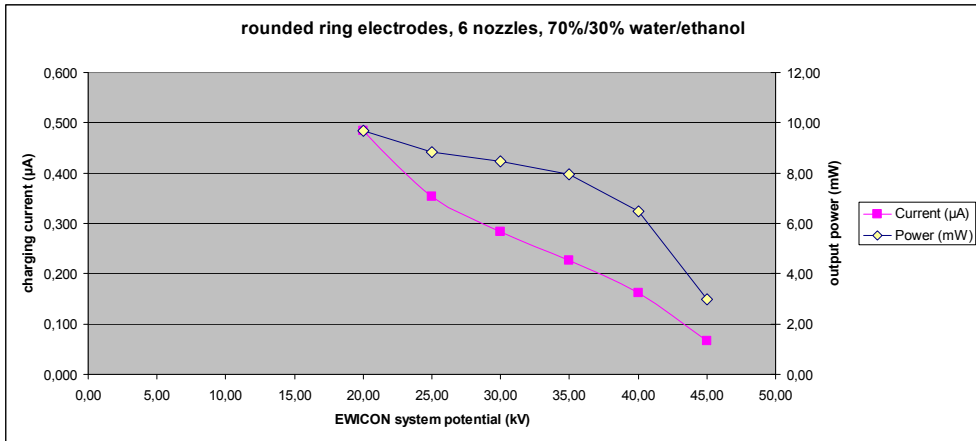


Figure 5.4. The indirectly measured charging currents and output power of six nozzles while using ring electrodes as charging electrodes. The spraying liquid is a 70%/30% water/ethanol mixture.

The charging current, I_c , vs. the EWICON system potential, U_{EWICON} , has been fitted with an exponential function in MATLAB, see appendix D, and this yielded the following expression for the charging current:

$$I_c(U_{EWICON}) = 1.581 \cdot 10^{-6} \exp(-58.85 \cdot 10^{-6} \cdot U_{EWICON}) \quad (5-2)$$

according to which $I_c(0)=1.6 \mu\text{A}$. This agrees with the current measured from the six needle nozzles. Based on (5-2), the calculated curves for the charging current and output power have been plotted, as shown in Figure 5.5.

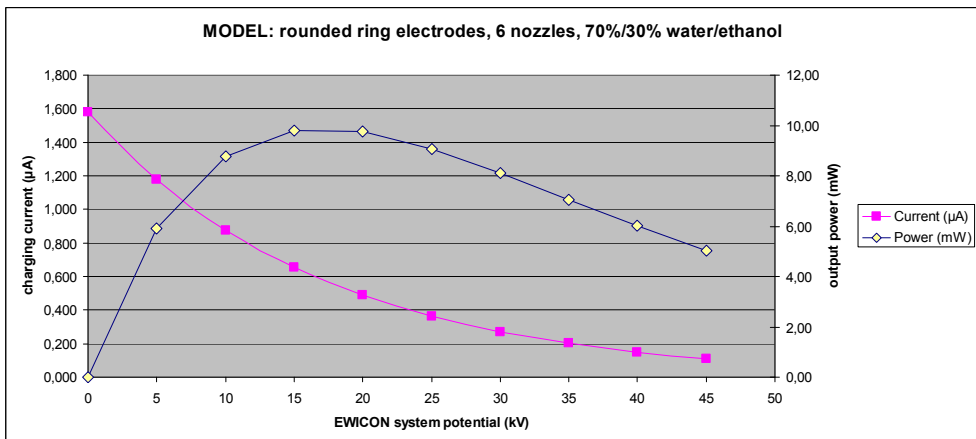


Figure 5.5. The calculated curves of the charging current and output power for the six needle nozzles version.

Similar to the single needle nozzle version, Figure 5.5 suggests that the maximum power transfer of 9.8 mW will occur at 15 kV. This is not in contradiction with the measurements, because in Figure 5.4, there is no maximum of the output power visible. Thus, the maximum power transfer occurs at a lower potential than 20 kV.

This experiment has also been performed with demineralised water. Six needle nozzles spraying with a flow rate of 20 ml/hr per nozzle. While the EWICON system still was connected to earth, the net current was 0.5 μ A. After disconnecting the holding platform from earth, the EWICON system potential rose to 33 kV in 60 seconds. The charging process is shown in Figure 5.6.

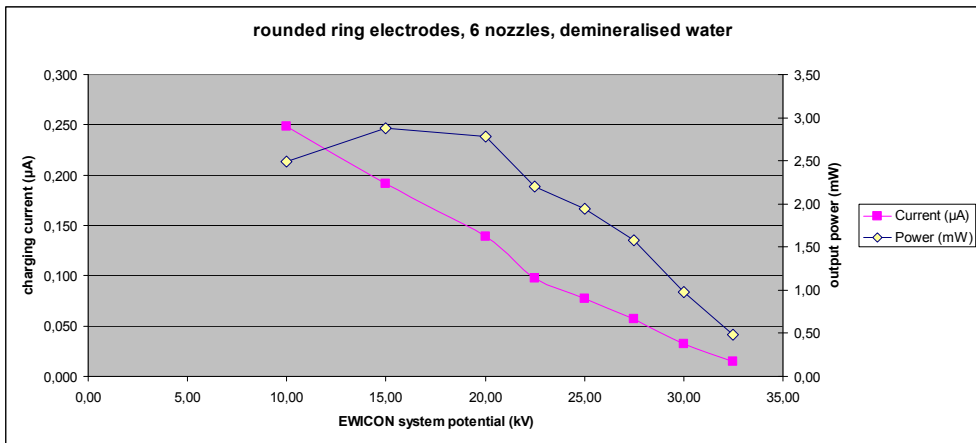
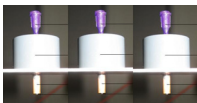


Figure 5.6. The indirectly measured charging currents and output power of six nozzles while using ring electrodes as charging electrodes. The spraying liquid is demineralised water.

As can be seen, the charging current and the output power that is produced with demineralised water are lower as compared to the case when a water/ethanol mixture is used.

5.3.2 Multiple needle with cylindrical electrode configurations



- **(configuration #12 and #13)**

Three of these cylindrical electrode nozzles have been used with a flow rate of 20 ml/hr per nozzle using demineralised water. The wind speed was set at 12 m/s. Similar to the single version of this type of nozzle, the cylindrical electrode was set on a potential of -2.0 kV and the steering electrode on -9.7 kV.

After disconnecting the holding platform from earth, the potential of the EWICON system rose to 35.0 kV in approximately 45 seconds, which is significantly quicker than using a single cylindrical electrode nozzle. The charging current has been determined as can be seen in Figure 5.7. The output power reaches a maximum of 2.7 mW at 20 kV or 0.9 mW per nozzle.

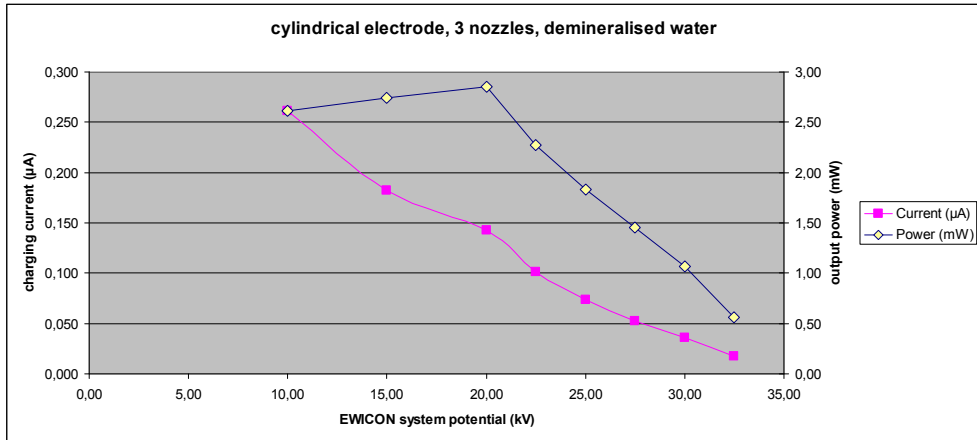


Figure 5.7. The indirectly measured charging currents and output power of three nozzle/cylindrical electrode configurations. The spraying liquid is demineralised water.

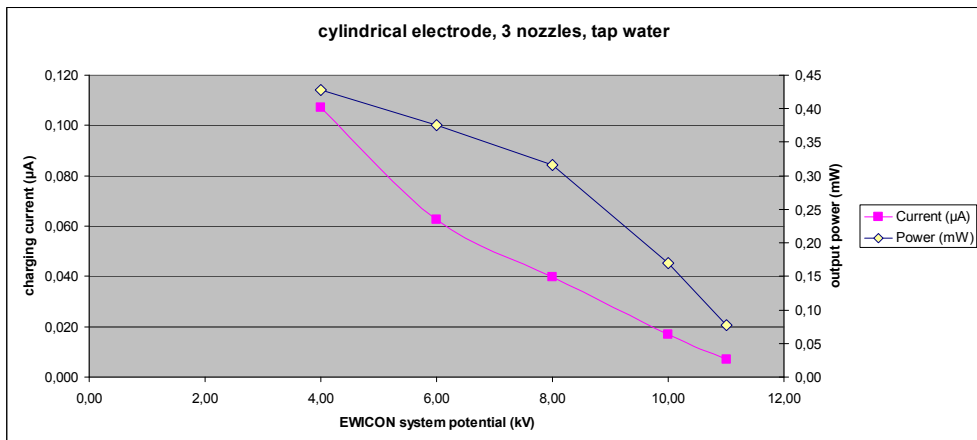
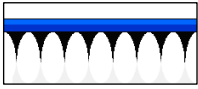


Figure 5.8. The indirectly measured charging currents and output power of three nozzle/cylindrical electrode configurations. The spraying liquid is tap water with a conductivity of 456 $\mu\text{S}/\text{cm}$.

In order to illustrate the fact that the chaotic spraying which occurs when tap water is used as the spraying liquid negatively affects the produced and displaced current, the previous measurement has also been conducted while using

tap water as the spraying liquid. Tap water has a higher conductivity than demineralised water, 456 $\mu\text{S}/\text{cm}$ in this case, and this will cause chaotic and unstable electrospraying. This will result in a lower charging current and, thus, in lower EWICON system potentials, which can be observed in Figure 5.8.

5.3.3 Self-adjusting nozzles configuration



- **(configuration #14)**

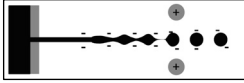
This configuration has only been tested with pure ethanol as the spraying liquid at a flow rate of 120 ml/hr, which roughly compares to six needle nozzles spraying at 20 ml/hr in the other EHDA configurations. At a charging potential of -15.0 kV, the current associated with the droplet creation process was 6.2 μA . No steering electrode was used in these experiments.

However, as has been mentioned in the previous chapter, the thirteen Taylor cones, which are responsible for the spraying of charged droplets, were strongly deformed by the wind. This was especially noticeable when the holding platform was disconnected from earth. The open output potential rose to 2.5 kV and fluctuated heavily between 2 and 3 kV.

The self-adjusting nozzles configuration was not yet aerodynamically optimised for the EWICON system. If this spraying system is to be used in the future, then a solution needs to be found such that the wind is able to move the charged droplets away without disturbing the spraying process. One possible solution is an airfoil that deflects the air flow such that the Taylor cones would be protected and the wind flows in the volume occupied by charged droplets alone.

Also, similar to the needle based spraying systems, the charged droplets still are inclined to move towards the charging system. Therefore, after analysis of the electric field using the same procedure as described in the previous chapter, steering electrodes can be implemented to facilitate the removal of charged droplets by the wind.

5.4 EWICON with HPMS system¹



The HPMS device was implemented in the EWICON system in a manner similar to the EHDA based spraying systems. As discussed in the previous chapters, the only spraying liquid used for the HPMS device(s) was saline water and the charging electrodes on the device were set on positive potentials as opposed to the negative potentials needed for EHDA spraying. Also, the fact, that the charged droplets are dispersed with a high velocity, facilitates the transportation of the droplets by the wind. Therefore, no steering electrodes were needed in this EWICON configuration.

5.4.1 Single spraying device

- **(configuration #15)**

In this experiment, one HPMS device has been used. The wind was set at 10 m/s and the flow rate of the water+0.9% NaCl was set at 35 ml/hr. The charging electrode was set to a potential of 100 V. The charging process can be observed in Figure 5.9. The potential of the EWICON system rose to 44 kV in 210 seconds. In Figure 5.9, we can also see that the output power reaches a maximum of 1.63 mW at 32.5 kV.

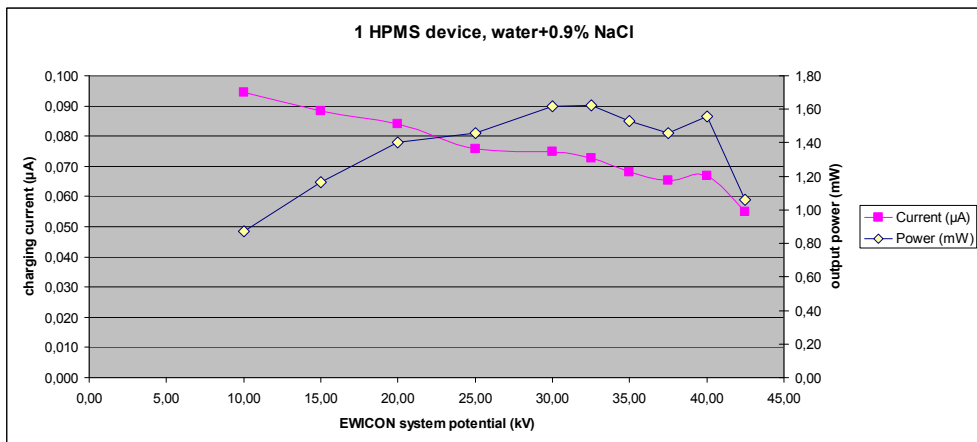


Figure 5.9. The indirectly measured charging currents and output power of 1 HPMS nozzle. The sprayed liquid is water+0.9% NaCl.

¹ This work was conducted in close cooperation with Wietze Nijdam and Jeroen Wissink of Medspray XMEMS BV

While conducting these experiments, various HPMS devices have been used. It should be noted that between the various devices, there have been variations in charging current and output power.

5.4.2 Multiple spraying devices

- **(configuration #16)**

In this experiment, three HPMS devices have been used. The wind speed was set at 10 m/s and the total flow rate of the water+0.9% NaCl was set at 105 ml/hr. The charging electrode was set to a potential of 100 V. In Figure 5.10, the charging current is shown as a function of the output potential of the EWICON system. There is no measurement data over 50 kV as the spraying system started to discharge at that moment. In Figure 5.10, we can also see that the output power reaches a maximum of 5.7 mW at 50 kV or 1.9 mW per HPMS device.

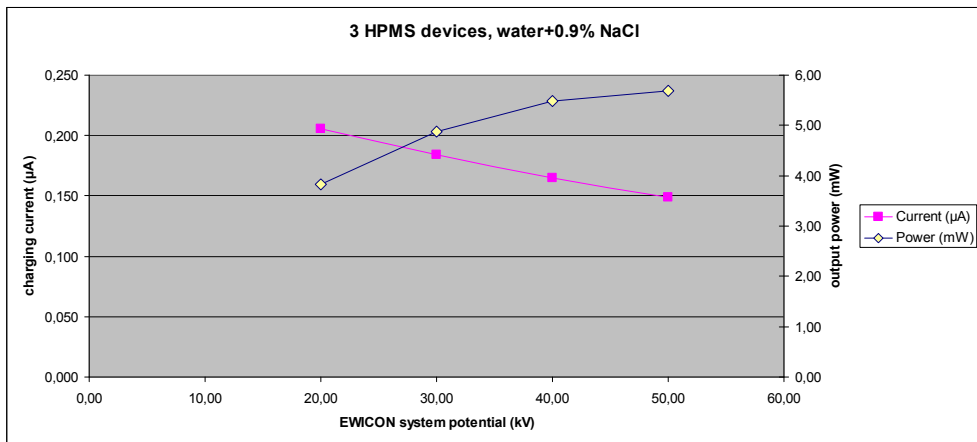


Figure 5.10. The indirectly measured charging currents and output power of 3 HPMS nozzles. The sprayed liquid is water+0.9% NaCl.

5.5 Analysis of the experimental results

In this section, we will summarise the charging processes and the output power of the various configurations of the EWICON system. We will compare these results with simulations of the equivalent circuit of the EWICON system in PSpice, of which the procedure will be briefly discussed first.

Subsequently, we will determine whether this output power increases linearly with the number of spraying nozzles which is of importance with respect to possible scale-ups of the EWICON system. Next, we will look at the dependence

of the output power of some of configurations of the EWICON system on the wind speed and we will conclude this section by calculating the efficiencies and EWICON performance indices (*EPI*).

5.5.1 EWICON circuit equivalent

In order to analyse the behaviour exhibited during the charging experiments, the EWICON system has been translated to a circuit equivalent. The configuration in this example is the charging system with the round ring electrodes spraying the 70%/30% water/ethanol mixture discussed in sections 5.2.1 and 5.3.1. Both the single needle nozzle and the six needle nozzles version will be analysed.

In this model, which can be found in Figure 5.11, the needle nozzle spraying the charged droplets has been modelled as a constant current source. The value of this current source is set at $0.4 \mu\text{A}$, which represent the net produced current produced by the spraying system. In reality, this current will decrease as the EWICON system potential rises. The source impedance of this current source has been set to $130 \text{ G}\Omega$.

The capacitance of the EWICON system was set at 130 pF and the resistance of the insulation of the EWICON system was set to $20 \text{ T}\Omega$. Finally, a resistance of $130 \text{ G}\Omega$ was added to model the electrical load, because this is the load value at which there is maximum power transfer as can be deduced from Figure 5.1.

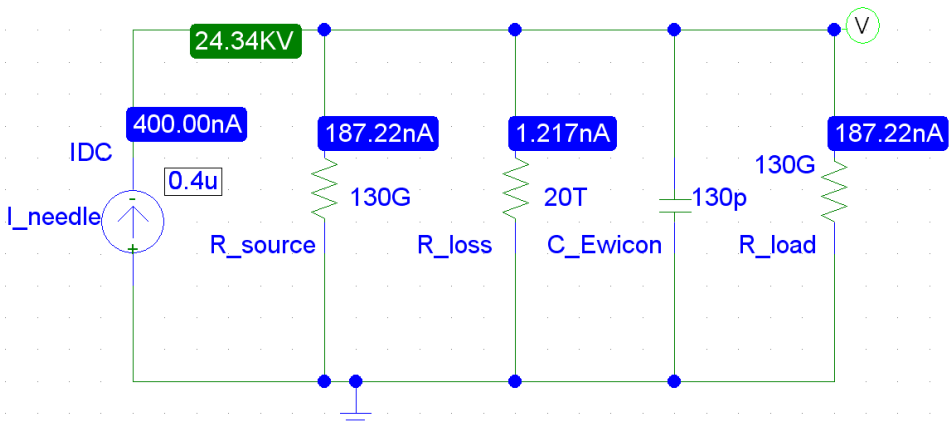


Figure 5.11. The circuit equivalent of the single nozzle EWICON system in PSpice. The needle nozzle has been modelled as a current source delivering, in this example, a current of $0.4 \mu\text{A}$ and an internal source impedance of $130 \text{ G}\Omega$. The resistance of the insulators was set at $20 \text{ T}\Omega$ and the capacitance of the EWICON system was set at 130 pF .

First of all, a bias point analysis was performed, i.e. the currents and potentials were determined while the EWICON system was at a steady-state. The results have also been displayed in Figure 5.11, where we can see that the EWICON system potential has reached 24.34 kV and the current through the load is 187 nA. This agrees reasonably well with the results discussed in section 5.2.1 and Figure 5.1, where the potential is 20 kV and the current is 153 nA.

Secondly, a transient analysis was performed, which gives an indication of the charging time and the potential of the system. The potential is determined at the node in Figure 5.11, indicated by the encircled “V”. A plot of the EWICON system potential as a function of time can be seen in Figure 5.12. We can see that the potential approaches 24 kV in 35 seconds, after which the system stabilises.

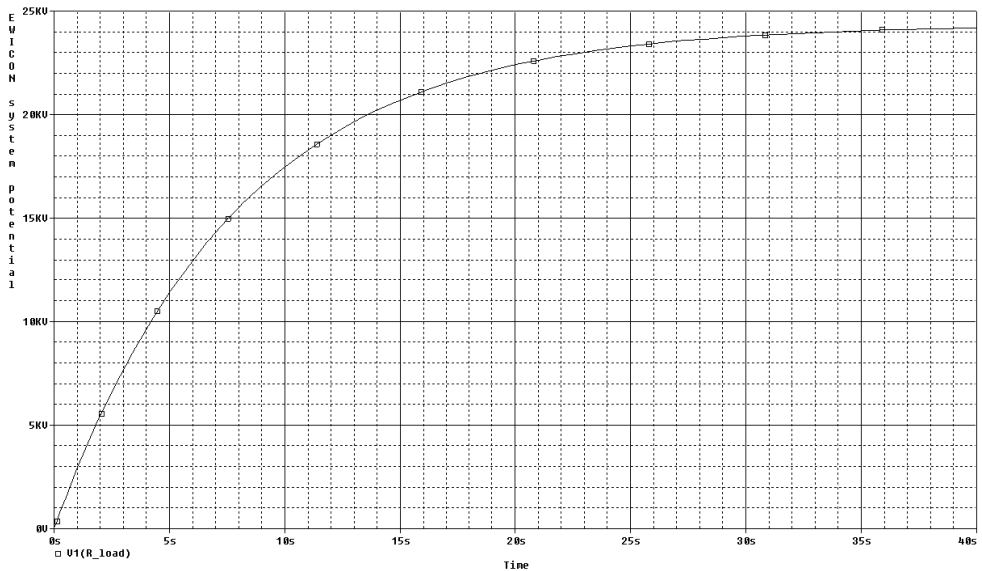


Figure 5.12. A plot of the charging process of the single nozzle EWICON system with a load of 130 GΩ. The needle nozzle is spraying a current of 0.4 μA. The EWICON system potential approaches 24 kV after 35 seconds after which the EWICON system stabilises.

If we now look at the six needle version of the rounded ring electrodes system, then the model in PSpice becomes as shown in Figure 5.13. Assuming that the source impedance of each needle nozzle is 130 GΩ, the total source impedance of the six needles spraying together is 22 GΩ. Also in Figure 5.13, the 20.5 GΩ load has been connected to the EWICON system similar to the experiment conducted in section 5.3.1.

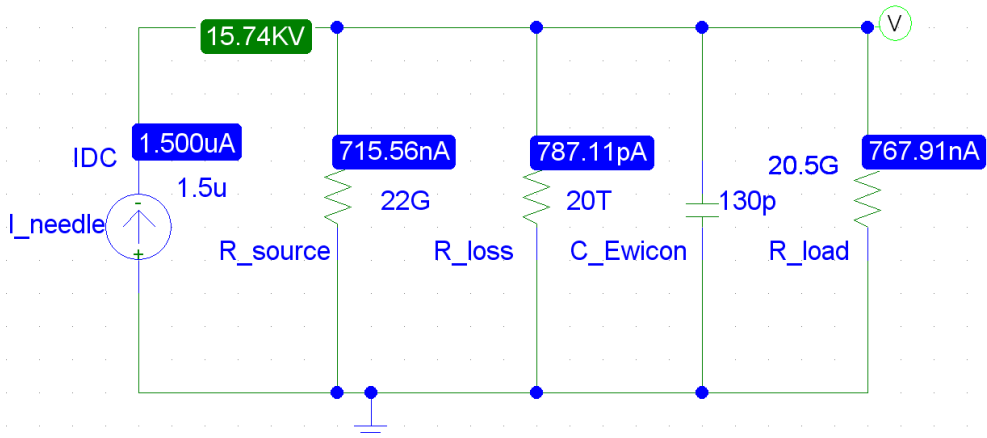


Figure 5.13. The circuit equivalent of the six nozzles EWICON system in PSpice. The six needle nozzles have been modelled as one single current source delivering, in this example, a current of 1.5 μA and an internal source impedance of 22G Ω . The resistance of the insulators was set at 20 T Ω and the capacitance of the EWICON system was set at 130 pF. Now, a load of 20.5 G Ω has been attached to the EWICON system

We can see that the potential reaches 15.74 kV which is in agreement with the 16 kV measured in section 5.3.1. The current through the 20.5 G Ω load has been calculated to be 0.78 μA , which is again in agreement with the measurements. The two other loads of 5.3 and 10.3 G Ω have also been entered in this simulation, of which the results can be seen in Table 5.1 together with the results of the 20.5 G Ω load.

Table 5.1. Comparison of the measured potentials and currents with the simulated potentials and currents as a function of the attached electric load.

load (G Ω)	measured U_{load} (kV)	simulated U_{load} (kV)	measured I_{load} (μA)	simulated I_{load} (μA)
5.3	5.7	6.4	1.1	1.2
10.3	9.7	10.5	0.9	1.0
20.5	16.0	15.7	0.8	0.8

5.5.2 Charging of the EWICON, output power

The results of the experiments in this chapter have been summarised in the order of discussion in Table 5.2. The output power P_{out} has either been given for the R_{LOAD} or for R_{Pmax} . R_{LOAD} is the actual electrical load that has been connected to

the EWICON system. R_{Pmax} has been calculated as the load at which the maximum power would be transferred.

Table 5.2. List of the calculated output power. “70w/30e” is the 70%/30% water/ethanol mixture and “demi water” is demineralised water. U_{EWICON} is the EWICON system potential and I_{out} is the current through the electrical load R_{LOAD} .

#	system	liquid	nozzles no.	U_{EWICON} (kV)	I_{out} (μ A)	R_{LOAD} (G Ω)	R_{Pmax} (G Ω)	P_{out} (mW)
1	Delrin	70w/30e	1	2.0	0.1	20	-	0.2
2	Delrin	demi water	1	0	0	20	-	-
3	rounded ring	70w/30e	1	20	0.15	-	131	3.1
4	cylindrical	demi water	1	20	0.018	-	1111	0.4
5	rod	demi water	8	3.0	-	-	-	-
6	rod	70w/30e	8	8.2	0.4	20	-	3.3
7	rod	70w/30e	24	15.0	0.7	20	-	10.5
8	rounded ring	70w/30e	6	16.0	0.8	20	-	12.5
9	rounded ring	70w/30e	6	9.7	0.9	10	-	6.4
10	rounded ring	70w/30e	6	5.7	1.1	5	-	3.3
11	rounded ring	demi water	6	15	0.19		79	2.9
12	cylindrical	demi water	3	20	0.14		143	2.7
13	cylindrical	tap water	3	4.0	0.11		37	0.43
14	self-adjusting	ethanol	13	2.5	-	-	-	-
15	HPMS	saline water	1	32.5	0.07	-	650	1.63
16	HPMS	saline water	3	50	0.15	-	268	5.7

5.5.3 Analysis of the charging current

- **EHDA**

In all the EHDA plots of the current as a function of the EWICON system potential, we can see that the current decreases in gradual manner as expected because of the polydispersity of the charged droplets. The charged droplets with a higher electric mobility are attracted back earlier than the charged droplets with a lower mobility.

- **HPMS**

In the plots of HPMS experiments, where the current was expected to decrease sharply at a certain system potential, we can see, however, that this is not the case. The reason for this behaviour is yet unclear and it was not only seen with increasing the potential of the holding platform, but also over time. The charging process may be influenced by local build up of charge in the nozzle and this requires more investigation.

5.5.4 Analysis of the output power

- **EWICON output power in general**

Compared to the results of the simulations discussed in chapter 2, the output power of the EWICON system is lower for all the implementations, both with EHDA and HPMS, averaging 2.0 mW per nozzle. In chapter 2, it was calculated that one nozzle spraying at 20 ml/hr theoretically should deliver an output power of 206 mW.

The main reason for this large difference is that the current associated with the creation of charged droplets is significantly lower than expected. On average, the measured current per nozzle was 0.2-0.3 μA , whereas the expected current was roughly 1.0-1.7 μA assuming that charging efficiencies of 70% of the maximum given by the Rayleigh limit were reached.

For both EHDA and HPMS, the spraying modes and droplet sizes were not optimal. With both spraying methods, the droplet diameters were larger than 10 μm . Also, for EHDA, cone-jet spraying for water has not yet been achieved, leading to lower charging efficiencies. For HPMS, the charging efficiency was in the order of 3-4% instead of 30-50%.

- **EHDA**

In the case of EHDA based spraying systems, in some cases, the output power is reasonably proportional to the number of spraying nozzles. In the case of the rod electrodes charging system, increasing the number of needles from 8 to 24 resulted in an output power increase from 3.3 to 10.5 mW, which is a factor of 3.2, which can be considered linear.

In the case of the rounded ring electrodes charging system increasing the number of needles from 1 to 6 resulted in an output power increase from 3.1 to 12.5 mW, which is a factor of 4.0.

In the case of the cylindrical electrodes charging system, increasing the number of nozzles from 1 to 3 resulted in an output power increase from 0.4 to 2.7 mW, which is a factor of 6.8. The reason that this factor is significantly higher than 3, is that the output power of the single nozzle version is lower. This is due to small corona discharges which occurred at the two needle tips of the non-spraying nozzles and thus causing a loss current.

In other multi-nozzle configuration, the single nozzle version could always be realised by removing the spraying needles. In the case of the configuration with the cylindrical electrodes this was not possible. Because the nozzles are connected to the platform, these nozzles will also rise in potential when the EWICON system is charged, which causes the corona discharge.

- **HPMS**

In the case of HPMS based spraying systems, in general, linearity of the output power was found. A single nozzle system yielded on average 1.6 mW, whereas a three nozzle system yielded 5.6 mW, which is a factor of 3.5.

5.5.5 The output power vs. the wind speed

In order to investigate whether a higher wind speed would result in a higher output power, an experiment similar to the one described in 4.3.1 was conducted in which the wind speed was varied from 6 to 12 m/s.

The used set-up in this experiment was a 3 needle nozzle version with the rounded ring electrodes. The spraying liquid was the 70%/30% water/ethanol mixture at a flow rate of 20 ml/hr per nozzle. The effective wind surface area was 0.06 m by 0.02 m. The output current through a load of 20.5 G Ω and the output potential of the EWICON system can be seen in Figure 5.14.

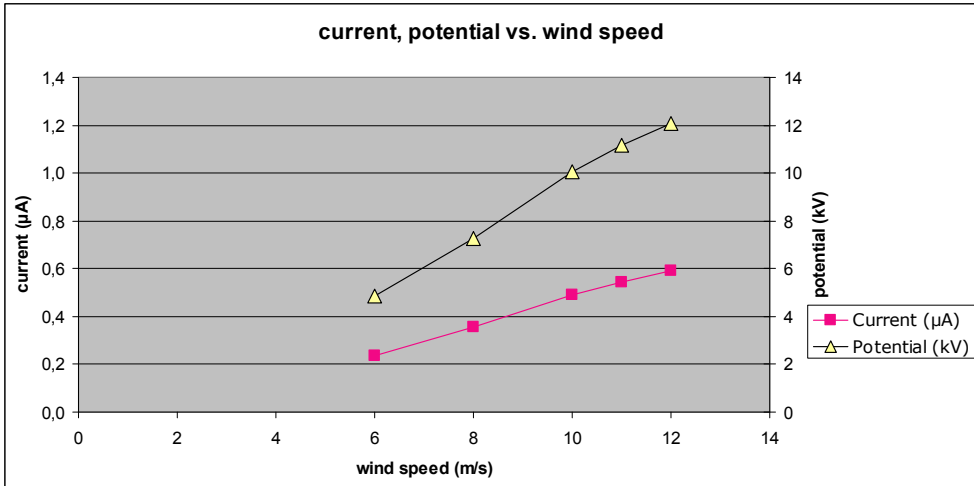


Figure 5.14. The output current through and potential over a load of 20.5 GΩ. This experiment has been conducted with an EHDA based EWICON system consisting of 3 spraying nozzles.

We can see that the current through the load increases with increasing wind speed, which is consistent with the results of the experiment in section 4.3.1. Consequently, the EWICON potential rises with the wind speed as well.

In Figure 5.15, the output power has been plotted as a function of the wind speed together with the maximum convertible power as given by the Betz limit.

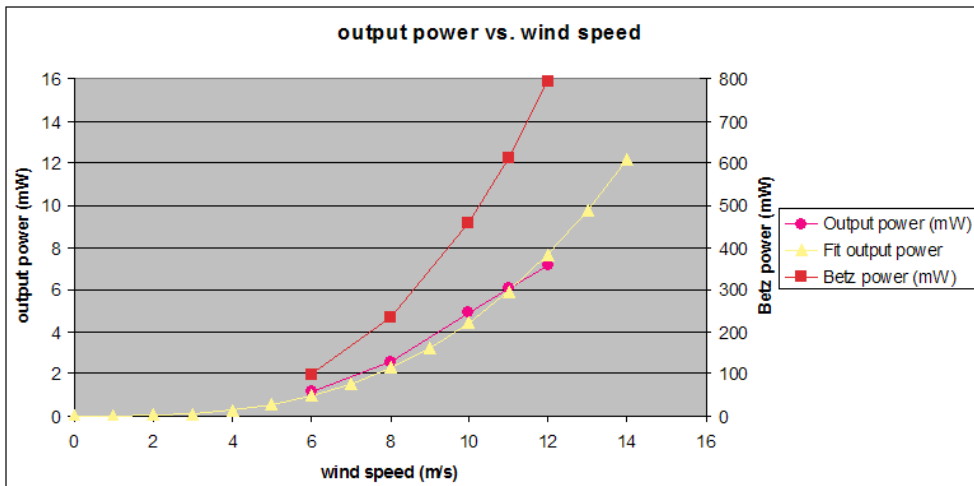


Figure 5.15. The output power as a function of the wind speed shown in pink, together with the fitted curve in yellow. The maximum convertible power from the wind as given by the Betz limit has also been plotted, shown in red.

It should be noted that the order of the Betz power is 100 times higher than the generated output power.

We can see that the output power rises with increasing wind speed. The data has been fitted with a cubic polynomial function in MATLAB, see appendix D, and this yielded the following expression for the output power:

$$P_{out}(v_w) = 4.437 \cdot 10^{-3} \cdot v_w^3 \quad (5-3)$$

which has also been included in Figure 5.15. In this fit, the other coefficients have been set to zero. We can conclude that the output power of the EWICON system relates to the 3rd power of the wind speed. It has to be noted, though, that the EWICON system can convert the wind power to electrical power only if sufficient charged droplet are available to be moved by the wind.

5.5.6 Efficiencies of the spraying systems, EPI

In section 2.3, the efficiency, η , and the EWICON Performance Index, EPI were defined and, for all the systems discussed in Table 5.2, these have been calculated for as shown in Table 5.3. The wind surface area, A , has been determined by visual inspections of the sprayed droplets as they were sprayed away from the nozzles. Together with the wind speed, the maximum recoverable power, $P_{max, wind}$, could be calculated with (2-2).

The electrical power, $P_{electrical}$, for EHDA based spraying was estimated by observing that there was no measurable current ($< 0.05 \mu A$) flowing back from the electrodes to the DC source supplies. At any given time during these experiments, the sum of the potentials applied to each of these electrodes was never higher than 20 kV. Therefore, the upper limit of the required electrical power was estimated to be 0.1 mW.

The power required to pump the spraying liquid or the mechanical power, $P_{mechanical}$, has been calculated using (4-4) for a height of 2 metres.

Table 5.3. The efficiencies and the EWICON Performance Indices of all the discussed configurations listed in Table 5.2. The grey areas are the experiments that did not yield an output power.

#	P_{out} (mW)	$P_{max, wind}$ (mW)	$P_{electrical}$ (mW)	$P_{mechanical}$ (mW)	P_{in} (mW)	Q (l/h)	A (cm ²)	η (%)	EPI
EHDA systems									
1	0.2	33	0.1	0.109	33.209	0.02	4	0.6	2.2
2									
3	3.1	33	0.1	0.109	33.209	0.02	4	1.17	3.7
4	0.4	33	0.1	0.109	33.209	0.02	4	0.15	1.9
5									
6	3.3	265	0.1	0.872	265.972	0.16	32	0.27	1.2
7	10.5	794	0.1	2.616	796.716	0.48	96	0.29	0.8
8	12.5	199	0.1	0.654	199.754	0.12	24	0.79	2.5
9	6.4	199	0.1	0.654	199.754	0.12	24	0.40	2.0
10	3.3	199	0.1	0.654	199.754	0.12	24	0.21	1.4
11	2.9	199	0.1	0.654	199.754	0.12	24	0.18	1.3
12	2.7	99	0.1	0.327	99.427	0.06	12	0.34	2.1
13	0.43	99	0.1	0.327	99.427	0.06	12	0.05	0.5
14									
HPMS systems									
15	1.63	345	0.0	1.6	345.127	0.035	9	0.47	2.4
16	5.7	1034	0.0	5.1	1039.1	0.105	27	0.55	2.0

The first observation that can be made is that, with exception of configuration #1, all configurations, both EHDA and HPMS, yielded a higher output power than the required electrical and mechanical power. Secondly, if we look at P_{in} which is comprised of $P_{max,wind}$, $P_{electrical}$ and $P_{mechanical}$, then the main factor in P_{in} is the maximum recoverable power from the wind, $P_{max,wind}$, and thus the determining factor in the efficiencies.

With regard to spraying liquids for EHDA based spraying systems, the efficiencies are higher when water/ethanol mixtures are sprayed than tap or demineralised water. Also, if we look at the efficiencies of the EHDA based

spraying systems, then the rounded ring electrodes yield the highest efficiencies. Based on the *EPI*, configurations #3 and #8 are the best performers.

If we compare the *EPIs* of EHDA and HPMS, then it can be concluded that there is no significant difference between them. Therefore, at this point, it can be concluded that with respect to the EWICON system, both spraying methods are equally suitable.

5.6 Conclusions

Overall, we can conclude that the EWICON system can be charged up to a potential by allowing the wind to move charged droplets against an electric field. This was possible using both EHDA and HPMS as the spraying method. It was also possible to deliver output power to an electrical load.

In most cases, the output power of the EWICON system was higher than the required electrical and mechanical power. However, if the output power is compared to the maximum recoverable power in the wind, the conversion efficiency is very low and in most case less than a percent. This is due to two reasons. Firstly, the current associated with the droplet creation process per nozzle is lower than expected, which has been observed with both EHDA and HPMS. Secondly, for EHDA, this current does not scale proportionally with the number of nozzles.

5.7 Scaling up the EWICON

5.7.1 General considerations

In chapter 2, a few words were spent on the scaling up of the EWICON system. If 900 nozzles were positioned in one square metre, then an output power of 102 W could be achieved. Here, we assumed that we could spray 10 μm droplets with 70% of the maximum charge as given by the Rayleigh limit.

In such a scenario, a 100 kilowatt version of the EWICON system could be achieved by placing roughly 10^6 nozzles with 2 cm spacing in a frame sized 20 metres by 20 metres. The current sprayed by the nozzles would then be 1.7 ampere and the EWICON system operating potential would then be roughly 60 kV.

Concerning public safety, the following can be said. If such a structure is placed at a height of e.g. 30 metres, the electric field at ground level would already be lower than the 600 V/m, which is the electric field strength at which no harmful effects on humans have been observed, [42]. A current produced by the EWICON

system will produce a magnetic field and, since this current is a DC current, the magnetic field will be static. According to [43], even high static magnetic fields have no proven harmful effects on humans, except in indirect cases.

5.7.2 Extrapolation based on the conducted experiments

Considering the results stated in Table 5.2 and Table 5.3, we can conclude that the considerations in the previous section are premature. If we take the best multi-nozzle system result, which is the 6 nozzles with the rounded ring electrodes configuration spraying the water/ethanol mixture, then the output power per nozzle is 2.1 mW.

A 1 kilowatt version using this configuration would require $4.8 \cdot 10^5$ spraying nozzles, roughly 700 by 700 nozzles or 14 metres by 14 metres if we assume 2 cm spacing. This means that spraying nozzles need to be more closely packed together before a kilowatt version will be feasible from an economical point of view.

For EHDA, achieving this with spraying needles will be a serious challenge and, therefore, the self-adjusting nozzles concept should be further investigated as an option for charged droplet generation. It was already possible to create 13 Taylor cones in the same area where normally only 6 to 8 spraying needles could be fitted.

For HPMS, even with the lower than expected charging efficiencies, the increase in produced current should be feasible. At this point in time, the devices are equipped with 34 pores. The current technology allows for hundreds of pores to be manufactured on the same area. This should increase the current density output and thus provide a good option for a scaled-up EWICON.

6

Conclusions and recommendations

“All truths are easy to understand once they are discovered; the point is to discover them.”

– Galileo Galilei

In this thesis, the EWICON concept has been introduced as an interesting future alternative to the conventional wind turbine generator. In the first few chapters, the theoretical foundation was provided on which, in the subsequent chapters, the practical aspects could be built, such as droplet creation and charging methods or the choice of spraying liquids.

Firstly, in section 6.1, we will recap the conclusions for each chapter, after which a number of general conclusions will be drawn with regard to the practical feasibility of the EWICON concept.

Lastly, in section 6.2, we will give some recommendations on future work and steps that need to be undertaken in order to solve crucial scientific obstacles and thus increase the commercial viability of an industrial implementation of the EWICON concept.

6.1 Conclusions

6.1.1 Conclusions per chapter

In chapter 1, we concluded that the Type B implementation of the EWICON concept, i.e. the implementation with a charging system isolated from earth without a collector unit, is best suited for commercial exploitation. The fact that no separate collector unit is needed means that product costs are lower. Also, the wind only has to move the charged droplets to earth instead of towards a certain fixed point. Otherwise, this would require a relatively large unit to take in all the droplets or wind-direction following system.

In chapter 2, we concluded, from a theoretical point of view using an analytical model with a small number of charged droplets, that it is possible to

transport these droplets by the wind against the electric field. We also concluded that the increase of electrostatic energy is sufficiently high to make use of the potential energy contained in the wind, provided that a high density of droplet creation units could be achieved.

Using this theoretical approach, parameters, like e.g. the minimum required wind speed as a function of droplet diameter, charge and the existing electric field have been determined. If the electric field is not higher than 10^4 V/m, then the minimum wind speed for droplets diameters varying from 0.1 to 100 μm is less than 3.3 m/s (2 on the scale of Beaufort). These droplets are assumed to be highly charged, which, in this case, is 70% of the maximum charge allowed on a droplet.

In chapter 3, we concluded that out of a number of droplet creation and charging methods, at this moment, two viable methods exist, each having their own merits and drawbacks.

The first method is electrohydrodynamic atomisation (EHDA) and two important factors have been found for successful operation. Firstly, the surface tension of the liquid should preferably be low, in the order of $40 \cdot 10^{-3}$ N/m. Secondly, the electric field, responsible for the creation and charging should be focussed on the liquid exiting the nozzle.

The main advantage of EHDA is that it requires little input power compared to the other methods available. However, while the results of using water as the spraying liquid have improved significantly during the course of this thesis work, it still has not been possible to make full use of the other main advantage of EHDA, namely the production of highly charged monodisperse droplets.

The second method is high pressure monodisperse spraying (HPMS). The main advantage of HPMS is that it is possible to use (saline) water as the spraying liquid, which is positive with respect to availability and environmental issues. The second advantage is the fact that the droplets produced by HPMS are monodisperse, which facilitates the optimisation of the EWICON system. However, the required power is higher compared to the EHDA method, because a high pressure is needed to create the droplets.

In chapter 4, we concluded that it was possible to design the EWICON system in such a way, that the charged droplets were actually removed by the wind, thus creating a charging current. Using both EHDA and HPMS methods, several multiple-nozzle spraying systems were constructed and tested, both showing varying degrees of linearity with respect to the output current.

In chapter 5, we concluded that the transportation of the charged droplets by the wind resulted in an output current that could charge the EWICON system up to a potential, depending on the wind speed and the charging current. It was possible to connect the EWICON to an electrical load which resulted in an output power. As expected, this output power increased with the wind speed. With both

spraying methods, it was possible to achieve a positive conversion efficiency, even though this efficiency was a few percent.

Based on these results, the output power per wind surface area needs to be increased by a factor of 50 in order to make an EWICON system comparable to a conventional wind turbine, thus making a large scale EWICON feasible.

6.1.2 Overall conclusions on the EWICON concept

In general, the EWICON concept has been proven to be able to achieve a net gain in terms of output power depending on the used methods and more importantly, the used spraying liquid. Using mixtures of water and ethanol in combination with the EHDA method proved that it was possible to generate high droplet currents which resulted in positive conversion efficiencies. However, using tap, salt or demineralised water, yielded lower conversion efficiencies, even when considerable amount of effort was put into the design of the charging system. Therefore, the EHDA method needs to be optimised to spray water with high currents, in order to develop a commercially viable wind energy converter based on the EWICON concept.

With respect to the HPMS method, also a positive gain was achieved. However, at this point in time, the spraying devices that were available did not allow for a high number of nozzles with respect to the wind surface area. Also, the charging process was found to be insufficient as the charge on the droplets was 3-4% of the maximum as given by the Rayleigh limit. Therefore, while again the EWICON concept equipped with HPMS proves to be successful in the laboratory environment, the charging process needs to be upgraded in order for a commercially viable product to be produced.

Looking at the considerations made on the subject of up scaling, we can conclude, that it is reasonably feasible to increase the current production per wind surface area with both methods, which means that a commercially viable product is still a realistic goal.

The EHDA spraying method still has several unexplored implementations, like the optimisation of the cylindrical water spraying electrodes or the self-adjusting multi-nozzles set-up. Both concepts have the potential to increase the output current by optimising the spraying process or by either increasing the rate of charged droplets.

The HPMS devices can be designed in such a way that a significantly higher number of pores can be applied than the 34 pores currently present on the device. New experiments will have to prove that the output current scales linearly with the increase of pores. Moreover, earlier testing has already proved that increasing the number of spraying devices results in a linear increase of the output current.

6.2 Recommendations

The main cause of the lower output power of the EWICON system with EHDA is the fact that the total produced current is lower than what is expected based on the proportionality of the spraying nozzles. Therefore, research should be focussed on the processes that take place on a fundamental level when multiple spraying nozzles are electrically connected. The effect of the different materials at the liquid/nozzle interface on the mobility of the charged carriers should be investigated.

Preferably, these experiments should be conducted in a wind tunnel that has sufficiently large dimensions, so that a high number of nozzles can be placed together. In this way, any fringe effects by the outer nozzles will have a negligible impact on the total output current.

With respect to the EHDA spraying method, the use of water should be thoroughly investigated. In the field of electrospray, the spraying of water does not have a high priority compared to the spraying of medicine or coating material. However, in order for the EWICON system to be commercially successful and environmentally acceptable, the electrospraying of tap and salt water is a prerequisite. The cylindrical nozzles described in chapter 3 can act as a base point for further research in which also the high conductivity of tap and salt water has to be taken into account.

With respect to the HPMS method, spraying devices with a higher concentration of pores should be developed. Also, keeping in mind that, because of the affinity for saline water, HPMS devices are a candidate for an EWICON at sea, filtering techniques should be developed as to prevent the clogging of the pores.

On the matter of alternative methods for liquid supply to a certain height, condensation of water in greenhouses is an interesting phenomenon. A greenhouse area of 10000 m², which is a prevalent size in the Netherlands, could potentially produce 2000 litres per hour of water. In this way, the spraying liquid could be transported to the EWICON operating height without the use of pumps.

A substantial part of the losses in the EWICON system are due to the inability of the charged droplets to reach earth. Calculations have shown that the electric field generated by the whole EWICON system should not be higher than 10⁴-10⁵ V/m anywhere along the trajectory of the charged droplets. Any new charging system should be modelled in a simulation software package to ascertain that this is the case.

Appendices

Appendix A. Betz' law

In this appendix, we will derive the maximum recoverable power from the wind in a manner analogous to the derivation done by Betz [16] and Lanchester [17].

First of all, we will define the parameters. The wind velocity far upstream of the converter is v_1 (v_w in chapter 2), the wind velocity at the converter is v and the wind velocity far downstream of the converter is v_2 . This has been illustrated in Figure A.1.



Figure A.1. Illustration of the Betz limit.

At these points, the wind flows through surface areas A_1 , A and A_2 . If we look at the mass of air, m , that passes through an area A in a time dt , then

$$m = \rho \cdot A \cdot dx \quad (\text{A-1})$$

in which ρ is the density of air and dx is the distance travelled by the wind with velocity, thus

$$dx = v \cdot dt \quad (\text{A-2})$$

The kinetic energy associated with this flow of air is

$$E_k = \frac{1}{2} \cdot m \cdot v^2 \quad (\text{A-3})$$

which with equation (A-1) can be written as

$$E_k = \frac{1}{2} \cdot \rho \cdot A \cdot v^3 \cdot dt \quad (\text{A-4})$$

which means that the power associated with the wind is

$$P = \frac{1}{2} \cdot \rho \cdot A \cdot v^3 \quad (\text{A-5})$$

which is equation (2.1).

In order to get to equation (2.2), we first need to determine the wind velocity, v , at the converter as a function of the wind velocity up and downstream of the converter, v_1 and v_2 respectively. We do this by considering the continuity equation

$$\rho_1 \cdot A_1 \cdot v_1 = \rho \cdot A \cdot v = \rho_2 \cdot A_2 \cdot v_2 \quad (\text{A-6})$$

which means that the mass flow rate is constant. The momentum flow rate is the mass flow rate times the velocity or $\rho \cdot A \cdot v^2$. The change in the momentum flow rate flowing from A_1 to A_2 is equal to the force, F , acting on the converter. The power, P , is then $F \cdot v$, so that we can write for the power extracted from the wind

$$P_{\text{extracted}} = (\rho \cdot A_1 \cdot v_1^2 - \rho \cdot A_2 \cdot v_2^2) \cdot v \quad (\text{A-7})$$

We can also write for the extracted power, the change in power associated with the wind as it passes through the converter

$$P_{\text{extracted}} = \frac{1}{2} \cdot \rho_1 \cdot A_1 \cdot v_1^3 - \frac{1}{2} \cdot \rho_2 \cdot A_2 \cdot v_2^3 \quad (\text{A-8})$$

If we equate (A-7) and (A-8), we find by using the continuity equation (6) that the wind velocity at the converter, v , is the average of v_1 and v_2

$$v = \frac{1}{2} \cdot (v_1 + v_2) \quad (\text{A-9})$$

If we use this result in (A-7) with the continuity equation (A-6), then we find that the power extracted by the wind is

$$P_{\text{extracted}} = \frac{1}{4} \cdot \rho \cdot A \cdot (v_1^3 - v_2^3 + v_1^2 v_2 - v_1 v_2^2) \quad (\text{A-10})$$

The maximum of this function can be found by

$$\frac{dP_{\text{max}}}{dv_2} = 0 \quad (\text{A-11})$$

which gives us

$$v_2 = \frac{1}{3} \cdot v_1 \quad (\text{A-12})$$

If we insert this in equation (A-10), then we find for the maximum recoverable power from the wind that

$$P_{\text{max}} = \frac{8}{27} \cdot \rho \cdot A \cdot v_1^3 \quad (\text{A-13})$$

which is equation (2.2) where v_w is v_I .

Appendix B. Evaporation and relaxation times of droplets

In this appendix, based on [18], we will give the rate of evaporation, which is the rate of change of the droplet diameter, and the droplet lifetime, which is the time required for a droplet to evaporate completely. We will briefly indicate in what way the wind speed and the relative humidity, also called the saturation ratio S_R , influence the droplet lifetime, t . We will also discuss how to determine the relaxation times of droplets.

The rate of evaporation for droplets with a droplet diameter $d_l > 0.1 \mu\text{m}$ is

$$\frac{d(d_d)}{dt} = \frac{4D_v M}{R\rho_d d_d} \left(\frac{p_\infty}{T_\infty} - \frac{p_d}{T_d} \right) \quad (\text{B-1})$$

in which d_d is the droplet diameter, D_v is the diffusion coefficient, M is the molar mass, R is the universal gas constant, ρ_d is the density of the liquid, p_∞ is the partial pressure surrounding the droplet, p_d is the partial pressure at the droplet surface, T_∞ is the temperature of the surrounding vapour and T_d is the temperature at the droplet surface.

By integrating (B-1) from d_l to 0 for d_d , we can determine the droplet lifetime t

$$t = \frac{R\rho_d d_l^2}{8D_v M \left(\frac{p_d}{T_d} - \frac{p_\infty}{T_\infty} \right)} \quad (\text{B-2})$$

which according to [18] is accurate for calculating the droplet lifetimes of droplets with a diameter from 10 to 50 μm , because these droplets are larger than 1.0 μm most of their lifetime. Above 1.0 μm , the droplet life time is proportional to the square of the droplet diameter. In a dry environment, the partial pressure of the surrounding vapour, p_∞ , is negligible.

For T_d , p_d and D_v empirical relations exist. The following relation exists between T_d and T_∞

$$T_d - T_\infty = \frac{(6.65 + 0.345 \cdot T_\infty + 0.0031 \cdot T_\infty^2)(S_R - 1)}{1 + (0.082 + 0.00782 \cdot T_\infty) \cdot S_R} \quad (\text{B-3})$$

which is valid for ambient temperatures, T_∞ , of 0–40 °C and saturation ratios, S_R , of 0–5. The following relation exists for p_d

$$p_d = \exp\left(16.7 - \frac{4060}{T_d - 37}\right) \quad (\text{B-4})$$

which is valid for ambient temperatures of 0–100 °C. The following relation exists for the diffusion coefficient of water vapour in air, D_v

$$D_v = 21.2 \cdot 10^{-6} (1 + 0.0071 \cdot T) \quad (\text{B-5})$$

which is valid for ambient temperatures of 0–45 °C. Using these equations, the evaporation times can be calculated for a water droplet in dry static air.

For example, a droplet with a diameter of 20 μm would take 0.31 seconds to fully evaporate in dry static air at 20 °C. In order to take into the account the effect of wind, we have to calculate the relaxation time, τ , of the droplet. This is the time that a droplet needs to adjust to a new set of conditions of forces, which according to [18] can be calculated as follows

$$\tau = \frac{\rho_d d_d^2}{18\eta} \quad (\text{B-6})$$

in which η is the viscosity of air. If we calculate the relaxation times and compare them to the evaporation times of the droplets, then, in general, we see that the relaxation time is lower than 0.5% of the evaporation time. In other words, on the scale of the evaporation time, the droplet almost immediately acquires the prevailing wind speed and, therefore, expression (B-2) can be used to estimate the evaporation time.

Another issue concerning the evaporation of droplets is the relative humidity or saturation ratio. The evaporation times have been calculated for a single droplet in dry air where p_∞ is assumed to be zero. However, in the case of the EWICON, the droplets are sprayed at a rate of 10^6 per second in a small volume. Therefore, we can assume that the relative humidity in this mist of droplets is between 80% and 100%.

In Figure B.1, taken out of [18], (B-2) has been calculated for several relative humidities. We can see that at a relative humidity of 100%, the droplet lifetime is in the order of 10 seconds for droplets larger than $5 \mu\text{m}$.

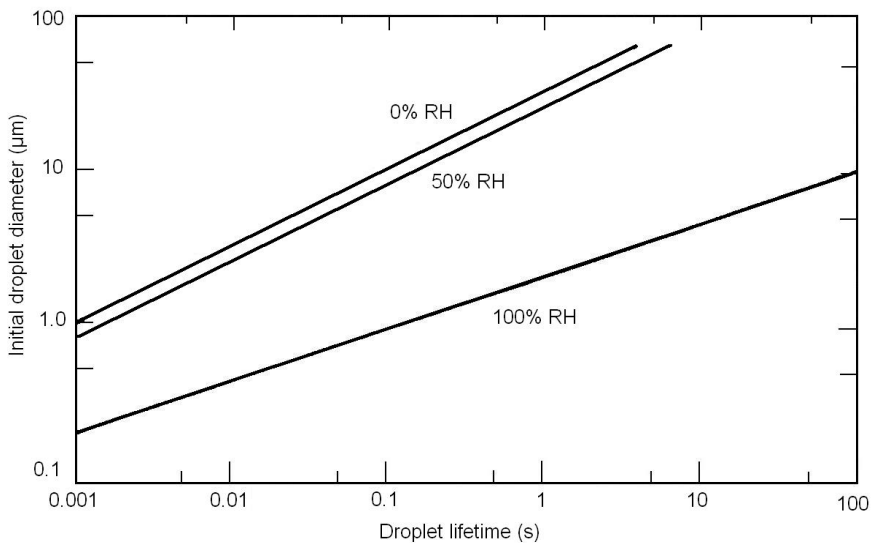


Figure B.1. The droplet lifetimes as a function of the droplet diameter at relative humidities of 0%, 50% and 100%. We can see that at a relative humidity of 100%, the droplet lifetime is in the order of 10 seconds for droplets larger than $5 \mu\text{m}$.

Appendix C. Numerical modelling in MATLAB

In this appendix, the listing of the MATLAB program used in chapter 2 will be given. The numerical method used to calculate the positions, velocities and accelerations of the charged droplets is Velocity-Verlet.

```
% M-File: TenDroplets
%
% This programs will simulate 10 charged droplets in an electric field
% under the influence of wind and gravity
%
% D.Djairam 04/04/2008
%
% Variables
% eo                free space permittivity (F/m)
% g                gravity acceleration (m/s^2)
% rho_droplet      density of liquid (kg/m^3)
% rho_air          density of air (kg/m^3)
% gamma           surface tension liquid (N/m)
% eta             dynamic viscosity
% dl..d10         droplet diameter (m)
% rayl1.. rayl10  charge on droplet in terms of the Rayleigh limit
% vw             wind speed (m/s)
% Eex            external electric field (V/m)
% totaltime      total simulation time (s)
% dt            time step (s)
% dtsq          time step squared (s)
% qml..qml0     maximum charge on the droplets (C)
% ql..ql0       charge on the droplets (C)
% x,v 1..10     position and velocity for all ten droplets
% ml..ml0       mass of the droplets (kg)
% Fg            gravity force (N)
% Fb            buoyancy (N)
% Fw            wind force due to drag
% Fex           electric force due to external field
% Fqq          electric forces due to other charged droplets

% Initialize variables
eo=8.854e-12;
g=-9.81;
K=1/(4*pi*eo);
rho_droplet=0.998e3;
rho_air=1.225;
gamma=7.28e-2;
eta=17.8e-6;
d1=10e-6;d2=10e-6;d3=10e-6;d4=10e-6;d5=10e-6;
d6=10e-6;d7=10e-6;d8=10e-6;d9=10e-6;d10=10e-6;
rayl1=0.7;rayl2=0.7;rayl3=0.7;rayl4=0.7;rayl5=0.7;
rayl6=0.7;rayl7=0.7;rayl8=0.7;rayl9=0.7;rayl10=0.7;
vw=[10 0 0];
Eex=-80000;
totaltime=1;
dt=0.00001;
dtsq=dt*dt;
N=int32(totaltime/dt); % number of calculations
```

The Electrostatic Wind Energy Converter

```
% Preallocate time and positions matrices for end result storage
time=zeros(N+1,1);
x1pos=zeros(N+1,3);x2pos=zeros(N+1,3);x3pos=zeros(N+1,3);x4pos=zeros(N+1,3);
x5pos=zeros(N+1,3);x6pos=zeros(N+1,3);x7pos=zeros(N+1,3);x8pos=zeros(N+1,3);
x9pos=zeros(N+1,3);x10pos=zeros(N+1,3);

% Calculate the charges on the droplets
qm1=8*pi*sqrt(eo*gamma*(d1/2)^3);q1=rayl1*qm1;
qm2=8*pi*sqrt(eo*gamma*(d2/2)^3);q2=rayl2*qm2;
qm3=8*pi*sqrt(eo*gamma*(d3/2)^3);q3=rayl3*qm3;
qm4=8*pi*sqrt(eo*gamma*(d4/2)^3);q4=rayl4*qm4;
qm5=8*pi*sqrt(eo*gamma*(d5/2)^3);q5=rayl5*qm5;
qm6=8*pi*sqrt(eo*gamma*(d6/2)^3);q6=rayl6*qm6;
qm7=8*pi*sqrt(eo*gamma*(d7/2)^3);q7=rayl7*qm7;
qm8=8*pi*sqrt(eo*gamma*(d8/2)^3);q8=rayl8*qm8;
qm9=8*pi*sqrt(eo*gamma*(d9/2)^3);q9=rayl9*qm9;
qm10=8*pi*sqrt(eo*gamma*(d10/2)^3);q10=rayl10*qm10;

% Calculate the mass of the droplets
volumel=(4/3)*pi*(d1/2)^3;m1=volume1*rho_droplet;
volume2=(4/3)*pi*(d2/2)^3;m2=volume2*rho_droplet;
volume3=(4/3)*pi*(d3/2)^3;m3=volume3*rho_droplet;
volume4=(4/3)*pi*(d4/2)^3;m4=volume4*rho_droplet;
volume5=(4/3)*pi*(d5/2)^3;m5=volume5*rho_droplet;
volume6=(4/3)*pi*(d6/2)^3;m6=volume6*rho_droplet;
volume7=(4/3)*pi*(d7/2)^3;m7=volume7*rho_droplet;
volume8=(4/3)*pi*(d8/2)^3;m8=volume8*rho_droplet;
volume9=(4/3)*pi*(d9/2)^3;m9=volume9*rho_droplet;
volume10=(4/3)*pi*(d10/2)^3;m10=volume10*rho_droplet;

% Assigning starting position and velocity of the droplets
x1=[1 5.99 4.99];v1=[0 0 0];
x2=[1 6.00 4.99];v2=[0 0 0];
x3=[1 6.01 4.99];v3=[0 0 0];

x4=[1 5.99 5.01];v4=[0 0 0];
x5=[1 6.00 5.01];v5=[0 0 0];
x6=[1 6.01 5.01];v6=[0 0 0];

x7=[1 5.99 5]; v7 =[0 0 0];
x8=[1 5.995 5];v8 =[0 0 0];
x9=[1 6.005 5];v9 =[0 0 0];
x10=[1 6.01 5];v10=[0 0 0];

time(1,1)=0;

x1pos(1,1:3)=x1;x2pos(1,1:3)=x2;x3pos(1,1:3)=x3;x4pos(1,1:3)=x4;x5pos(1,1:3)=x5;
x6pos(1,1:3)=x6;x7pos(1,1:3)=x7;x8pos(1,1:3)=x8;x9pos(1,1:3)=x9;x10pos(1,1:3)=x10;

% Start with work done on droplet set to zero
W1=0;W2=0;W3=0;W4=0;W5=0;W6=0;W7=0;W8=0;W9=0;W10=0;

% Start calculation
% from 1 until N
for i = 1:N

% -----
% Calculation distances and unit vectors
r12=magvector(x1-x2);u12=unitvector(x1-x2);r13=magvector(x1-x3);u13=unitvector(x1-x3);
r14=magvector(x1-x4);u14=unitvector(x1-x4);r15=magvector(x1-x5);u15=unitvector(x1-x5);
r16=magvector(x1-x6);u16=unitvector(x1-x6);r17=magvector(x1-x7);u17=unitvector(x1-x7);
r18=magvector(x1-x8);u18=unitvector(x1-x8);r19=magvector(x1-x9);u19=unitvector(x1-x9);
r110=magvector(x1-x10);u110=unitvector(x1-x10);

r21=magvector(x2-x1);u21=unitvector(x2-x1);r23=magvector(x2-x3);u23=unitvector(x2-x3);
r24=magvector(x2-x4);u24=unitvector(x2-x4);r25=magvector(x2-x5);u25=unitvector(x2-x5);
r26=magvector(x2-x6);u26=unitvector(x2-x6);r27=magvector(x2-x7);u27=unitvector(x2-x7);
r28=magvector(x2-x8);u28=unitvector(x2-x8);r29=magvector(x2-x9);u29=unitvector(x2-x9);
r210=magvector(x2-x10);u210=unitvector(x2-x10);
```

```

r31=magvector(x3-x1);u31=unitvector(x3-x1);r32=magvector(x3-x2);u32=unitvector(x3-x2);
r34=magvector(x3-x4);u34=unitvector(x3-x4);r35=magvector(x3-x5);u35=unitvector(x3-x5);
r36=magvector(x3-x6);u36=unitvector(x3-x6);r37=magvector(x3-x7);u37=unitvector(x3-x7);
r38=magvector(x3-x8);u38=unitvector(x3-x8);r39=magvector(x3-x9);u39=unitvector(x3-x9);
r310=magvector(x3-x10);u310=unitvector(x3-x10);

r41=magvector(x4-x1);u41=unitvector(x4-x1);r42=magvector(x4-x2);u42=unitvector(x4-x2);
r43=magvector(x4-x3);u43=unitvector(x4-x3);r45=magvector(x4-x5);u45=unitvector(x4-x5);
r46=magvector(x4-x6);u46=unitvector(x4-x6);r47=magvector(x4-x7);u47=unitvector(x4-x7);
r48=magvector(x4-x8);u48=unitvector(x4-x8);r49=magvector(x4-x9);u49=unitvector(x4-x9);
r410=magvector(x4-x10);u410=unitvector(x4-x10);

r51=magvector(x5-x1);u51=unitvector(x5-x1);r52=magvector(x5-x2);u52=unitvector(x5-x2);
r53=magvector(x5-x3);u53=unitvector(x5-x3);r54=magvector(x5-x4);u54=unitvector(x5-x4);
r56=magvector(x5-x6);u56=unitvector(x5-x6);r57=magvector(x5-x7);u57=unitvector(x5-x7);
r58=magvector(x5-x8);u58=unitvector(x5-x8);r59=magvector(x5-x9);u59=unitvector(x5-x9);
r510=magvector(x5-x10);u510=unitvector(x5-x10);

r61=magvector(x6-x1);u61=unitvector(x6-x1);r62=magvector(x6-x2);u62=unitvector(x6-x2);
r63=magvector(x6-x3);u63=unitvector(x6-x3);r64=magvector(x6-x4);u64=unitvector(x6-x4);
r65=magvector(x6-x5);u65=unitvector(x6-x5);r67=magvector(x6-x7);u67=unitvector(x6-x7);
r68=magvector(x6-x8);u68=unitvector(x6-x8);r69=magvector(x6-x9);u69=unitvector(x6-x9);
r610=magvector(x6-x10);u610=unitvector(x6-x10);

r71=magvector(x7-x1);u71=unitvector(x7-x1);r72=magvector(x7-x2);u72=unitvector(x7-x2);
r73=magvector(x7-x3);u73=unitvector(x7-x3);r74=magvector(x7-x4);u74=unitvector(x7-x4);
r75=magvector(x7-x5);u75=unitvector(x7-x5);r76=magvector(x7-x6);u76=unitvector(x7-x6);
r78=magvector(x7-x8);u78=unitvector(x7-x8);r79=magvector(x7-x9);u79=unitvector(x7-x9);
r710=magvector(x7-x10);u710=unitvector(x7-x10);

r81=magvector(x8-x1);u81=unitvector(x8-x1);r82=magvector(x8-x2);u82=unitvector(x8-x2);
r83=magvector(x8-x3);u83=unitvector(x8-x3);r84=magvector(x8-x4);u84=unitvector(x8-x4);
r85=magvector(x8-x5);u85=unitvector(x8-x5);r86=magvector(x8-x6);u86=unitvector(x8-x6);
r87=magvector(x8-x7);u87=unitvector(x8-x7);r89=magvector(x8-x9);u89=unitvector(x8-x9);
r810=magvector(x8-x10);u810=unitvector(x8-x10);

r91=magvector(x9-x1);u91=unitvector(x9-x1);r92=magvector(x9-x2);u92=unitvector(x9-x2);
r93=magvector(x9-x3);u93=unitvector(x9-x3);r94=magvector(x9-x4);u94=unitvector(x9-x4);
r95=magvector(x9-x5);u95=unitvector(x9-x5);r96=magvector(x9-x6);u96=unitvector(x9-x6);
r97=magvector(x9-x7);u97=unitvector(x9-x7);r98=magvector(x9-x8);u98=unitvector(x9-x8);
r910=magvector(x9-x10);u910=unitvector(x9-x10);

r101=magvector(x10-x1);u101=unitvector(x10-x1);
r102=magvector(x10-x2);u102=unitvector(x10-x2);
r103=magvector(x10-x3);u103=unitvector(x10-x3);
r104=magvector(x10-x4);u104=unitvector(x10-x4);
r105=magvector(x10-x5);u105=unitvector(x10-x5);
r106=magvector(x10-x6);u106=unitvector(x10-x6);
r107=magvector(x10-x7);u107=unitvector(x10-x7);
r108=magvector(x10-x8);u108=unitvector(x10-x8);
r109=magvector(x10-x9);u109=unitvector(x10-x9);

% Calculation forces on droplets: Stokes' force, electric force from
% external field, electric force from other charged droplets and gravity
% Stokes' force
Fw1=[6*pi*eta*(vw(1)-v1(1))*(d1/2) 6*pi*eta*(vw(2)-v1(2))*(d1/2) 6*pi*eta*(vw(3)-
v1(3))*(d1/2) ];
Fw2=[6*pi*eta*(vw(1)-v2(1))*(d2/2) 6*pi*eta*(vw(2)-v2(2))*(d2/2) 6*pi*eta*(vw(3)-
v2(3))*(d2/2) ];
Fw3=[6*pi*eta*(vw(1)-v3(1))*(d3/2) 6*pi*eta*(vw(2)-v3(2))*(d3/2) 6*pi*eta*(vw(3)-
v3(3))*(d3/2) ];
Fw4=[6*pi*eta*(vw(1)-v4(1))*(d4/2) 6*pi*eta*(vw(2)-v4(2))*(d4/2) 6*pi*eta*(vw(3)-
v4(3))*(d4/2) ];
Fw5=[6*pi*eta*(vw(1)-v5(1))*(d5/2) 6*pi*eta*(vw(2)-v5(2))*(d5/2) 6*pi*eta*(vw(3)-
v5(3))*(d5/2) ];
Fw6=[6*pi*eta*(vw(1)-v6(1))*(d6/2) 6*pi*eta*(vw(2)-v6(2))*(d6/2) 6*pi*eta*(vw(3)-
v6(3))*(d6/2) ];

```

The Electrostatic Wind Energy Converter

```

Fw7=[6*pi*eta*(vw(1)-v7(1))*(d7/2) 6*pi*eta*(vw(2)-v7(2))*(d7/2) 6*pi*eta*(vw(3)-
v7(3))*(d7/2) ];
Fw8=[6*pi*eta*(vw(1)-v8(1))*(d8/2) 6*pi*eta*(vw(2)-v8(2))*(d8/2) 6*pi*eta*(vw(3)-
v8(3))*(d8/2) ];
Fw9=[6*pi*eta*(vw(1)-v9(1))*(d9/2) 6*pi*eta*(vw(2)-v9(2))*(d9/2) 6*pi*eta*(vw(3)-
v9(3))*(d9/2) ];
Fw10=[6*pi*eta*(vw(1)-v10(1))*(d10/2) 6*pi*eta*(vw(2)-v10(2))*(d10/2) 6*pi*eta*(vw(3)-
v10(3))*(d10/2) ];

% The electric force from external E-field.
% We assume that the E-field drops off
% with the square of the x-distance and that the source of the E-field is
% at the plane x=0
Fex1=[q1*sign(x1(1))*Eex/x1(1)^2 0 0];Fex2=[q2*sign(x2(1))*Eex/x2(1)^2 0 0];
Fex3=[q3*sign(x3(1))*Eex/x3(1)^2 0 0];Fex4=[q4*sign(x4(1))*Eex/x4(1)^2 0 0];
Fex5=[q5*sign(x5(1))*Eex/x5(1)^2 0 0];Fex6=[q6*sign(x6(1))*Eex/x6(1)^2 0 0];
Fex7=[q7*sign(x7(1))*Eex/x7(1)^2 0 0];Fex8=[q8*sign(x8(1))*Eex/x8(1)^2 0 0];
Fex9=[q9*sign(x9(1))*Eex/x9(1)^2 0 0];Fex10=[q10*sign(x10(1))*Eex/x10(1)^2 0 0];
% mutual electric forces from charged droplets
Fq1q2=K*q1*q2/r12^2*u12;Fq1q3=K*q1*q3/r13^2*u13;
Fq1q4=K*q1*q4/r14^2*u14;Fq1q5=K*q1*q5/r15^2*u15;
Fq1q6=K*q1*q6/r16^2*u16;Fq1q7=K*q1*q7/r17^2*u17;
Fq1q8=K*q1*q8/r18^2*u18;Fq1q9=K*q1*q9/r19^2*u19;
Fq1q10=K*q1*q10/r110^2*u110;

Fq2q1=K*q2*q1/r21^2*u21;Fq2q3=K*q2*q3/r23^2*u23;
Fq2q4=K*q2*q4/r24^2*u24;Fq2q5=K*q2*q5/r25^2*u25;
Fq2q6=K*q2*q6/r26^2*u26;Fq2q7=K*q2*q7/r27^2*u27;
Fq2q8=K*q2*q8/r28^2*u28;Fq2q9=K*q2*q9/r29^2*u29;
Fq2q10=K*q2*q10/r210^2*u210;

Fq3q1=K*q3*q1/r31^2*u31;Fq3q2=K*q3*q2/r32^2*u32;
Fq3q4=K*q3*q4/r34^2*u34;Fq3q5=K*q3*q5/r35^2*u35;
Fq3q6=K*q3*q6/r36^2*u36;Fq3q7=K*q3*q7/r37^2*u37;
Fq3q8=K*q3*q8/r38^2*u38;Fq3q9=K*q3*q9/r39^2*u39;
Fq3q10=K*q3*q10/r310^2*u310;

Fq4q1=K*q4*q1/r41^2*u41;Fq4q2=K*q4*q2/r42^2*u42;
Fq4q3=K*q4*q3/r43^2*u43;Fq4q5=K*q4*q5/r45^2*u45;
Fq4q6=K*q4*q6/r46^2*u46;Fq4q7=K*q4*q7/r47^2*u47;
Fq4q8=K*q4*q8/r48^2*u48;Fq4q9=K*q4*q9/r49^2*u49;
Fq4q10=K*q4*q10/r410^2*u410;

Fq5q1=K*q5*q1/r51^2*u51;Fq5q2=K*q5*q2/r52^2*u52;
Fq5q3=K*q5*q3/r53^2*u53;Fq5q4=K*q5*q4/r54^2*u54;
Fq5q6=K*q5*q6/r56^2*u56;Fq5q7=K*q5*q7/r57^2*u57;
Fq5q8=K*q5*q8/r58^2*u58;Fq5q9=K*q5*q9/r59^2*u59;
Fq5q10=K*q5*q10/r510^2*u510;

Fq6q1=K*q6*q1/r61^2*u61;Fq6q2=K*q6*q2/r62^2*u62;
Fq6q3=K*q6*q3/r63^2*u63;Fq6q4=K*q6*q4/r64^2*u64;
Fq6q5=K*q6*q5/r65^2*u65;Fq6q7=K*q6*q7/r67^2*u67;
Fq6q8=K*q6*q8/r68^2*u68;Fq6q9=K*q6*q9/r69^2*u69;
Fq6q10=K*q6*q10/r610^2*u610;

Fq7q1=K*q7*q1/r71^2*u71;Fq7q2=K*q7*q2/r72^2*u72;
Fq7q3=K*q7*q3/r73^2*u73;Fq7q4=K*q7*q4/r74^2*u74;
Fq7q5=K*q7*q5/r75^2*u75;Fq7q6=K*q7*q6/r76^2*u76;
Fq7q8=K*q7*q8/r78^2*u78;Fq7q9=K*q7*q9/r79^2*u79;
Fq7q10=K*q7*q10/r710^2*u710;

Fq8q1=K*q8*q1/r81^2*u81;Fq8q2=K*q8*q2/r82^2*u82;
Fq8q3=K*q8*q3/r83^2*u83;Fq8q4=K*q8*q4/r84^2*u84;
Fq8q5=K*q8*q5/r85^2*u85;Fq8q6=K*q8*q6/r86^2*u86;
Fq8q7=K*q8*q7/r87^2*u87;Fq8q9=K*q8*q9/r89^2*u89;
Fq8q10=K*q8*q10/r810^2*u810;

Fq9q1=K*q9*q1/r91^2*u91;Fq9q2=K*q9*q2/r92^2*u92;

```

```

Fq9q3=K*q9*q3/r93^2*u93;Fq9q4=K*q9*q4/r94^2*u94;
Fq9q5=K*q9*q5/r95^2*u95;Fq9q6=K*q9*q6/r96^2*u96;
Fq9q7=K*q9*q7/r97^2*u97;Fq9q8=K*q9*q8/r98^2*u98;
Fq9q10=K*q9*q10/r910^2*u910;
Fq10q1=K*q10*q1/r101^2*u101;Fq10q2=K*q10*q2/r102^2*u102;
Fq10q3=K*q10*q3/r103^2*u103;Fq10q4=K*q10*q4/r104^2*u104;
Fq10q5=K*q10*q5/r105^2*u105;Fq10q6=K*q10*q6/r106^2*u106;
Fq10q7=K*q10*q7/r107^2*u107;Fq10q8=K*q10*q8/r108^2*u108;
Fq10q9=K*q10*q9/r109^2*u109;

% gravity forces
Fg1=[0 0 m1*g];Fg2=[0 0 m2*g];Fg3=[0 0 m3*g];Fg4=[0 0 m4*g];
Fg5=[0 0 m5*g];Fg6=[0 0 m6*g];Fg7=[0 0 m7*g];Fg8=[0 0 m8*g];
Fg9=[0 0 m9*g];Fg10=[0 0 m10*g];

% buoyancy
Fb1=[0 0 -volume1*rho_air*g];Fb2=[0 0 -volume2*rho_air*g];Fb3=[0 0 -volume3*rho_air*g];
Fb4=[0 0 -volume4*rho_air*g];Fb5=[0 0 -volume5*rho_air*g];Fb6=[0 0 -volume6*rho_air*g];
Fb7=[0 0 -volume7*rho_air*g];Fb8=[0 0 -volume8*rho_air*g];Fb9=[0 0 -volume9*rho_air*g];
Fb10=[0 0 -volume10*rho_air*g];

% sum of all forces on droplets
SF1=Fw1+Fex1+Fq1q2+Fq1q3+Fq1q4+Fq1q5+Fq1q6+Fq1q7+Fq1q8+Fq1q9+Fq1q10+Fg1+Fb1;
SF2=Fw2+Fex2+Fq2q1+Fq2q3+Fq2q4+Fq2q5+Fq2q6+Fq2q7+Fq2q8+Fq2q9+Fq2q10+Fg2+Fb2;
SF3=Fw3+Fex3+Fq3q1+Fq3q2+Fq3q4+Fq3q5+Fq3q6+Fq3q7+Fq3q8+Fq3q9+Fq3q10+Fg3+Fb3;
SF4=Fw4+Fex4+Fq4q1+Fq4q2+Fq4q3+Fq4q5+Fq4q6+Fq4q7+Fq4q8+Fq4q9+Fq4q10+Fg4+Fb4;
SF5=Fw5+Fex5+Fq5q1+Fq5q2+Fq5q3+Fq5q4+Fq5q6+Fq5q7+Fq5q8+Fq5q9+Fq5q10+Fg5+Fb5;
SF6=Fw6+Fex6+Fq6q1+Fq6q2+Fq6q3+Fq6q4+Fq6q5+Fq6q7+Fq6q8+Fq6q9+Fq6q10+Fg6+Fb6;
SF7=Fw7+Fex7+Fq7q1+Fq7q2+Fq7q3+Fq7q4+Fq7q5+Fq7q6+Fq7q8+Fq7q9+Fq7q10+Fg7+Fb7;
SF8=Fw8+Fex8+Fq8q1+Fq8q2+Fq8q3+Fq8q4+Fq8q5+Fq8q6+Fq8q7+Fq8q9+Fq8q10+Fg8+Fb8;
SF9=Fw9+Fex9+Fq9q1+Fq9q2+Fq9q3+Fq9q4+Fq9q5+Fq9q6+Fq9q7+Fq9q8+Fq9q10+Fg9+Fb9;
SF10=Fw10+Fex10+Fq10q1+Fq10q2+Fq10q3+Fq10q4+Fq10q5+Fq10q6+Fq10q7+Fq10q8+Fq10q9+Fg10+Fb10;
% -----

% Velocity Verlet algorithm in four steps
% first: calculate new position at whole time step
x1=x1+dt*v1+dtsq/2*SF1/m1;
x2=x2+dt*v2+dtsq/2*SF2/m2;
x3=x3+dt*v3+dtsq/2*SF3/m3;
x4=x4+dt*v4+dtsq/2*SF4/m4;
x5=x5+dt*v5+dtsq/2*SF5/m5;
x6=x6+dt*v6+dtsq/2*SF6/m6;
x7=x7+dt*v7+dtsq/2*SF7/m7;
x8=x8+dt*v8+dtsq/2*SF8/m8;
x9=x9+dt*v9+dtsq/2*SF9/m9;
x10=x10+dt*v10+dtsq/2*SF10/m10;

% second: calculate new speed at half time step
v1=v1+dt/2*SF1/m1;
v2=v2+dt/2*SF2/m2;
v3=v3+dt/2*SF3/m3;
v4=v4+dt/2*SF4/m4;
v5=v5+dt/2*SF5/m5;
v6=v6+dt/2*SF6/m6;
v7=v7+dt/2*SF7/m7;
v8=v8+dt/2*SF8/m8;
v9=v9+dt/2*SF9/m9;
v10=v10+dt/2*SF10/m10;

%third: calculate forces with new position and half-step velocity
% -----
% Calculation distances and unit vectors 2
r12=magvector(x1-x2);u12=unitvector(x1-x2);r13=magvector(x1-x3);u13=unitvector(x1-x3);
r14=magvector(x1-x4);u14=unitvector(x1-x4);r15=magvector(x1-x5);u15=unitvector(x1-x5);
r16=magvector(x1-x6);u16=unitvector(x1-x6);r17=magvector(x1-x7);u17=unitvector(x1-x7);
r18=magvector(x1-x8);u18=unitvector(x1-x8);r19=magvector(x1-x9);u19=unitvector(x1-x9);
r110=magvector(x1-x10);u110=unitvector(x1-x10);

```

The Electrostatic Wind Energy Converter

```
r21=magvector (x2-x1);u21=unitvector (x2-x1);r23=magvector (x2-x3);u23=unitvector (x2-x3);
r24=magvector (x2-x4);u24=unitvector (x2-x4);r25=magvector (x2-x5);u25=unitvector (x2-x5);
r26=magvector (x2-x6);u26=unitvector (x2-x6);r27=magvector (x2-x7);u27=unitvector (x2-x7);
r28=magvector (x2-x8);u28=unitvector (x2-x8);r29=magvector (x2-x9);u29=unitvector (x2-x9);
r210=magvector (x2-x10);u210=unitvector (x2-x10);

r31=magvector (x3-x1);u31=unitvector (x3-x1);r32=magvector (x3-x2);u32=unitvector (x3-x2);
r34=magvector (x3-x4);u34=unitvector (x3-x4);r35=magvector (x3-x5);u35=unitvector (x3-x5);
r36=magvector (x3-x6);u36=unitvector (x3-x6);r37=magvector (x3-x7);u37=unitvector (x3-x7);
r38=magvector (x3-x8);u38=unitvector (x3-x8);r39=magvector (x3-x9);u39=unitvector (x3-x9);
r310=magvector (x3-x10);u310=unitvector (x3-x10);

r41=magvector (x4-x1);u41=unitvector (x4-x1);r42=magvector (x4-x2);u42=unitvector (x4-x2);
r43=magvector (x4-x3);u43=unitvector (x4-x3);r45=magvector (x4-x5);u45=unitvector (x4-x5);
r46=magvector (x4-x6);u46=unitvector (x4-x6);r47=magvector (x4-x7);u47=unitvector (x4-x7);
r48=magvector (x4-x8);u48=unitvector (x4-x8);r49=magvector (x4-x9);u49=unitvector (x4-x9);
r410=magvector (x4-x10);u410=unitvector (x4-x10);

r51=magvector (x5-x1);u51=unitvector (x5-x1);r52=magvector (x5-x2);u52=unitvector (x5-x2);
r53=magvector (x5-x3);u53=unitvector (x5-x3);r54=magvector (x5-x4);u54=unitvector (x5-x4);
r56=magvector (x5-x6);u56=unitvector (x5-x6);r57=magvector (x5-x7);u57=unitvector (x5-x7);
r58=magvector (x5-x8);u58=unitvector (x5-x8);r59=magvector (x5-x9);u59=unitvector (x5-x9);
r510=magvector (x5-x10);u510=unitvector (x5-x10);

r61=magvector (x6-x1);u61=unitvector (x6-x1);r62=magvector (x6-x2);u62=unitvector (x6-x2);
r63=magvector (x6-x3);u63=unitvector (x6-x3);r64=magvector (x6-x4);u64=unitvector (x6-x4);
r65=magvector (x6-x5);u65=unitvector (x6-x5);r67=magvector (x6-x7);u67=unitvector (x6-x7);
r68=magvector (x6-x8);u68=unitvector (x6-x8);r69=magvector (x6-x9);u69=unitvector (x6-x9);
r610=magvector (x6-x10);u610=unitvector (x6-x10);

r71=magvector (x7-x1);u71=unitvector (x7-x1);r72=magvector (x7-x2);u72=unitvector (x7-x2);
r73=magvector (x7-x3);u73=unitvector (x7-x3);r74=magvector (x7-x4);u74=unitvector (x7-x4);
r75=magvector (x7-x5);u75=unitvector (x7-x5);r76=magvector (x7-x6);u76=unitvector (x7-x6);
r78=magvector (x7-x8);u78=unitvector (x7-x8);r79=magvector (x7-x9);u79=unitvector (x7-x9);
r710=magvector (x7-x10);u710=unitvector (x7-x10);

r81=magvector (x8-x1);u81=unitvector (x8-x1);r82=magvector (x8-x2);u82=unitvector (x8-x2);
r83=magvector (x8-x3);u83=unitvector (x8-x3);r84=magvector (x8-x4);u84=unitvector (x8-x4);
r85=magvector (x8-x5);u85=unitvector (x8-x5);r86=magvector (x8-x6);u86=unitvector (x8-x6);
r87=magvector (x8-x7);u87=unitvector (x8-x7);r89=magvector (x8-x9);u89=unitvector (x8-x9);
r810=magvector (x8-x10);u810=unitvector (x8-x10);

r91=magvector (x9-x1);u91=unitvector (x9-x1);r92=magvector (x9-x2);u92=unitvector (x9-x2);
r93=magvector (x9-x3);u93=unitvector (x9-x3);r94=magvector (x9-x4);u94=unitvector (x9-x4);
r95=magvector (x9-x5);u95=unitvector (x9-x5);r96=magvector (x9-x6);u96=unitvector (x9-x6);
r97=magvector (x9-x7);u97=unitvector (x9-x7);r98=magvector (x9-x8);u98=unitvector (x9-x8);
r910=magvector (x9-x10);u910=unitvector (x9-x10);

r101=magvector (x10-x1);u101=unitvector (x10-x1);
r102=magvector (x10-x2);u102=unitvector (x10-x2);
r103=magvector (x10-x3);u103=unitvector (x10-x3);
r104=magvector (x10-x4);u104=unitvector (x10-x4);
r105=magvector (x10-x5);u105=unitvector (x10-x5);
r106=magvector (x10-x6);u106=unitvector (x10-x6);
r107=magvector (x10-x7);u107=unitvector (x10-x7);
r108=magvector (x10-x8);u108=unitvector (x10-x8);
r109=magvector (x10-x9);u109=unitvector (x10-x9);
% Calculation forces on droplets: Stokes' force, electric force from
% external field, electric force from other charged droplets and gravity
% Stokes' force 2
Fw1=[6*pi*eta*(vw(1)-v1(1))*(d1/2) 6*pi*eta*(vw(2)-v1(2))*(d1/2) 6*pi*eta*(vw(3)-
v1(3))*(d1/2) ];
Fw2=[6*pi*eta*(vw(1)-v2(1))*(d2/2) 6*pi*eta*(vw(2)-v2(2))*(d2/2) 6*pi*eta*(vw(3)-
v2(3))*(d2/2) ];
Fw3=[6*pi*eta*(vw(1)-v3(1))*(d3/2) 6*pi*eta*(vw(2)-v3(2))*(d3/2) 6*pi*eta*(vw(3)-
v3(3))*(d3/2) ];
Fw4=[6*pi*eta*(vw(1)-v4(1))*(d4/2) 6*pi*eta*(vw(2)-v4(2))*(d4/2) 6*pi*eta*(vw(3)-
v4(3))*(d4/2) ];
```



```

Fw5=[6*pi*eta*(vw(1)-v5(1))*(d5/2) 6*pi*eta*(vw(2)-v5(2))*(d5/2) 6*pi*eta*(vw(3)-
v5(3))*(d5/2) ];
Fw6=[6*pi*eta*(vw(1)-v6(1))*(d6/2) 6*pi*eta*(vw(2)-v6(2))*(d6/2) 6*pi*eta*(vw(3)-
v6(3))*(d6/2) ];
Fw7=[6*pi*eta*(vw(1)-v7(1))*(d7/2) 6*pi*eta*(vw(2)-v7(2))*(d7/2) 6*pi*eta*(vw(3)-
v7(3))*(d7/2) ];
Fw8=[6*pi*eta*(vw(1)-v8(1))*(d8/2) 6*pi*eta*(vw(2)-v8(2))*(d8/2) 6*pi*eta*(vw(3)-
v8(3))*(d8/2) ];
Fw9=[6*pi*eta*(vw(1)-v9(1))*(d9/2) 6*pi*eta*(vw(2)-v9(2))*(d9/2) 6*pi*eta*(vw(3)-
v9(3))*(d9/2) ];
Fw10=[6*pi*eta*(vw(1)-v10(1))*(d10/2) 6*pi*eta*(vw(2)-v10(2))*(d10/2) 6*pi*eta*(vw(3)-
v10(3))*(d10/2) ];
% The electric force from external E-field 2.
% We assume that the E-field drops off
% with the square of the x-distance and that the source of the E-field is
% at the plane x=0
Fex1=[q1*sign(x1(1))*Eex/x1(1)^2 0 0];Fex2=[q2*sign(x2(1))*Eex/x2(1)^2 0 0];
Fex3=[q3*sign(x3(1))*Eex/x3(1)^2 0 0];Fex4=[q4*sign(x4(1))*Eex/x4(1)^2 0 0];
Fex5=[q5*sign(x5(1))*Eex/x5(1)^2 0 0];Fex6=[q6*sign(x6(1))*Eex/x6(1)^2 0 0];
Fex7=[q7*sign(x7(1))*Eex/x7(1)^2 0 0];Fex8=[q8*sign(x8(1))*Eex/x8(1)^2 0 0];
Fex9=[q9*sign(x9(1))*Eex/x9(1)^2 0 0];Fex10=[q10*sign(x10(1))*Eex/x10(1)^2 0 0];
% mutual electric forces from charged droplets 2
Fq1q2=K*q1*q2/r12^2*u12;Fq1q3=K*q1*q3/r13^2*u13;
Fq1q4=K*q1*q4/r14^2*u14;Fq1q5=K*q1*q5/r15^2*u15;
Fq1q6=K*q1*q6/r16^2*u16;Fq1q7=K*q1*q7/r17^2*u17;
Fq1q8=K*q1*q8/r18^2*u18;Fq1q9=K*q1*q9/r19^2*u19;
Fq1q10=K*q1*q10/r110^2*u110;

Fq2q1=K*q2*q1/r21^2*u21;Fq2q3=K*q2*q3/r23^2*u23;
Fq2q4=K*q2*q4/r24^2*u24;Fq2q5=K*q2*q5/r25^2*u25;
Fq2q6=K*q2*q6/r26^2*u26;Fq2q7=K*q2*q7/r27^2*u27;
Fq2q8=K*q2*q8/r28^2*u28;Fq2q9=K*q2*q9/r29^2*u29;
Fq2q10=K*q2*q10/r210^2*u210;

Fq3q1=K*q3*q1/r31^2*u31;Fq3q2=K*q3*q2/r32^2*u32;
Fq3q4=K*q3*q4/r34^2*u34;Fq3q5=K*q3*q5/r35^2*u35;
Fq3q6=K*q3*q6/r36^2*u36;Fq3q7=K*q3*q7/r37^2*u37;
Fq3q8=K*q3*q8/r38^2*u38;Fq3q9=K*q3*q9/r39^2*u39;
Fq3q10=K*q3*q10/r310^2*u310;

Fq4q1=K*q4*q1/r41^2*u41;Fq4q2=K*q4*q2/r42^2*u42;
Fq4q3=K*q4*q3/r43^2*u43;Fq4q5=K*q4*q5/r45^2*u45;
Fq4q6=K*q4*q6/r46^2*u46;Fq4q7=K*q4*q7/r47^2*u47;
Fq4q8=K*q4*q8/r48^2*u48;Fq4q9=K*q4*q9/r49^2*u49;
Fq4q10=K*q4*q10/r410^2*u410;

Fq5q1=K*q5*q1/r51^2*u51;Fq5q2=K*q5*q2/r52^2*u52;
Fq5q3=K*q5*q3/r53^2*u53;Fq5q4=K*q5*q4/r54^2*u54;
Fq5q6=K*q5*q6/r56^2*u56;Fq5q7=K*q5*q7/r57^2*u57;
Fq5q8=K*q5*q8/r58^2*u58;Fq5q9=K*q5*q9/r59^2*u59;
Fq5q10=K*q5*q10/r510^2*u510;

Fq6q1=K*q6*q1/r61^2*u61;Fq6q2=K*q6*q2/r62^2*u62;
Fq6q3=K*q6*q3/r63^2*u63;Fq6q4=K*q6*q4/r64^2*u64;
Fq6q5=K*q6*q5/r65^2*u65;Fq6q7=K*q6*q7/r67^2*u67;
Fq6q8=K*q6*q8/r68^2*u68;Fq6q9=K*q6*q9/r69^2*u69;
Fq6q10=K*q6*q10/r610^2*u610;

Fq7q1=K*q7*q1/r71^2*u71;Fq7q2=K*q7*q2/r72^2*u72;
Fq7q3=K*q7*q3/r73^2*u73;Fq7q4=K*q7*q4/r74^2*u74;
Fq7q5=K*q7*q5/r75^2*u75;Fq7q6=K*q7*q6/r76^2*u76;
Fq7q8=K*q7*q8/r78^2*u78;Fq7q9=K*q7*q9/r79^2*u79;
Fq7q10=K*q7*q10/r710^2*u710;

Fq8q1=K*q8*q1/r81^2*u81;Fq8q2=K*q8*q2/r82^2*u82;
Fq8q3=K*q8*q3/r83^2*u83;Fq8q4=K*q8*q4/r84^2*u84;
Fq8q5=K*q8*q5/r85^2*u85;Fq8q6=K*q8*q6/r86^2*u86;
Fq8q7=K*q8*q7/r87^2*u87;Fq8q9=K*q8*q9/r89^2*u89;
Fq8q10=K*q8*q10/r810^2*u810;

```

The Electrostatic Wind Energy Converter

```

Fq9q1=K*q9*q1/r91^2*u91;Fq9q2=K*q9*q2/r92^2*u92;
Fq9q3=K*q9*q3/r93^2*u93;Fq9q4=K*q9*q4/r94^2*u94;
Fq9q5=K*q9*q5/r95^2*u95;Fq9q6=K*q9*q6/r96^2*u96;
Fq9q7=K*q9*q7/r97^2*u97;Fq9q8=K*q9*q8/r98^2*u98;
Fq9q10=K*q9*q10/r910^2*u910;

Fq10q1=K*q10*q1/r101^2*u101;Fq10q2=K*q10*q2/r102^2*u102;
Fq10q3=K*q10*q3/r103^2*u103;Fq10q4=K*q10*q4/r104^2*u104;
Fq10q5=K*q10*q5/r105^2*u105;Fq10q6=K*q10*q6/r106^2*u106;
Fq10q7=K*q10*q7/r107^2*u107;Fq10q8=K*q10*q8/r108^2*u108;
Fq10q9=K*q10*q9/r109^2*u109;

% gravity forces 2
Fg1=[0 0 m1*g];Fg2=[0 0 m2*g];Fg3=[0 0 m3*g];Fg4=[0 0 m4*g];
Fg5=[0 0 m5*g];Fg6=[0 0 m6*g];Fg7=[0 0 m7*g];Fg8=[0 0 m8*g];
Fg9=[0 0 m9*g];Fg10=[0 0 m10*g];
% buoyancy 2
Fb1=[0 0 -volume1*rho_air*g];Fb2=[0 0 -volume2*rho_air*g];Fb3=[0 0 -volume3*rho_air*g];
Fb4=[0 0 -volume4*rho_air*g];Fb5=[0 0 -volume5*rho_air*g];Fb6=[0 0 -volume6*rho_air*g];
Fb7=[0 0 -volume7*rho_air*g];Fb8=[0 0 -volume8*rho_air*g];Fb9=[0 0 -volume9*rho_air*g];
Fb10=[0 0 -volume10*rho_air*g];
% sum of all forces on droplets 2
SF1=Fw1+Fex1+Fq1q2+Fq1q3+Fq1q4+Fq1q5+Fq1q6+Fq1q7+Fq1q8+Fq1q9+Fq1q10+Fg1+Fb1;
SF2=Fw2+Fex2+Fq2q1+Fq2q3+Fq2q4+Fq2q5+Fq2q6+Fq2q7+Fq2q8+Fq2q9+Fq2q10+Fg2+Fb2;
SF3=Fw3+Fex3+Fq3q1+Fq3q2+Fq3q4+Fq3q5+Fq3q6+Fq3q7+Fq3q8+Fq3q9+Fq3q10+Fg3+Fb3;
SF4=Fw4+Fex4+Fq4q1+Fq4q2+Fq4q3+Fq4q5+Fq4q6+Fq4q7+Fq4q8+Fq4q9+Fq4q10+Fg4+Fb4;
SF5=Fw5+Fex5+Fq5q1+Fq5q2+Fq5q3+Fq5q4+Fq5q6+Fq5q7+Fq5q8+Fq5q9+Fq5q10+Fg5+Fb5;
SF6=Fw6+Fex6+Fq6q1+Fq6q2+Fq6q3+Fq6q4+Fq6q5+Fq6q7+Fq6q8+Fq6q9+Fq6q10+Fg6+Fb6;
SF7=Fw7+Fex7+Fq7q1+Fq7q2+Fq7q3+Fq7q4+Fq7q5+Fq7q6+Fq7q8+Fq7q9+Fq7q10+Fg7+Fb7;
SF8=Fw8+Fex8+Fq8q1+Fq8q2+Fq8q3+Fq8q4+Fq8q5+Fq8q6+Fq8q7+Fq8q9+Fq8q10+Fg8+Fb8;
SF9=Fw9+Fex9+Fq9q1+Fq9q2+Fq9q3+Fq9q4+Fq9q5+Fq9q6+Fq9q7+Fq9q8+Fq9q10+Fg9+Fb9;
SF10=Fw10+Fex10+Fq10q1+Fq10q2+Fq10q3+Fq10q4+Fq10q5+Fq10q6+Fq10q7+Fq10q8+Fq10q9+Fg10+Fb10;

SA1=SF1-Fw1;SA2=SF2-Fw2;SA3=SF3-Fw3;SA4=SF4-Fw4;SA5=SF5-Fw5;
SA6=SF6-Fw6;SA7=SF7-Fw7;SA8=SF8-Fw8;SA9=SF9-Fw9;SA10=SF10-Fw10;
% -----
% fourth: calculate new speed at whole time step
v1=v1+(dt/2)*(SF1/m1);v2=v2+(dt/2)*(SF2/m2);v3=v3+(dt/2)*(SF3/m3);
v4=v4+(dt/2)*(SF4/m4);v5=v5+(dt/2)*(SF5/m5);v6=v6+(dt/2)*(SF6/m6);
v7=v7+(dt/2)*(SF7/m7);v8=v8+(dt/2)*(SF8/m8);v9=v9+(dt/2)*(SF9/m9);
v10=v10+(dt/2)*(SF10/m10);

% write position and time to file or visualizer
time(i+1,1)=i*dt;
x1pos(i+1,1:3)=x1;x2pos(i+1,1:3)=x2;x3pos(i+1,1:3)=x3;x4pos(i+1,1:3)=x4;
x5pos(i+1,1:3)=x5;x6pos(i+1,1:3)=x6;x7pos(i+1,1:3)=x7;x8pos(i+1,1:3)=x8;
x9pos(i+1,1:3)=x9;x10pos(i+1,1:3)=x10;

% calculate the work dW = F.dl using the SF per droplet
W1=W1+SA1(1)*(x1pos(i+1,1)-x1pos(i,1))+SA1(2)*(x1pos(i+1,2)-x1pos(i,2))+SA1(3)*(x1pos(i+1,3)-x1pos(i,3));
W2=W2+SA2(1)*(x2pos(i+1,1)-x2pos(i,1))+SA2(2)*(x2pos(i+1,2)-x2pos(i,2))+SA2(3)*(x2pos(i+1,3)-x2pos(i,3));
W3=W3+SA3(1)*(x3pos(i+1,1)-x3pos(i,1))+SA3(2)*(x3pos(i+1,2)-x3pos(i,2))+SA3(3)*(x3pos(i+1,3)-x3pos(i,3));
W4=W4+SA4(1)*(x4pos(i+1,1)-x4pos(i,1))+SA4(2)*(x4pos(i+1,2)-x4pos(i,2))+SA4(3)*(x4pos(i+1,3)-x4pos(i,3));
W5=W5+SA5(1)*(x5pos(i+1,1)-x5pos(i,1))+SA5(2)*(x5pos(i+1,2)-x5pos(i,2))+SA5(3)*(x5pos(i+1,3)-x5pos(i,3));
W6=W6+SA6(1)*(x6pos(i+1,1)-x6pos(i,1))+SA6(2)*(x6pos(i+1,2)-x6pos(i,2))+SA6(3)*(x6pos(i+1,3)-x6pos(i,3));
W7=W7+SA7(1)*(x7pos(i+1,1)-x7pos(i,1))+SA7(2)*(x7pos(i+1,2)-x7pos(i,2))+SA7(3)*(x7pos(i+1,3)-x7pos(i,3));

```

```

W8=W8+SA8(1)*(x8pos(i+1,1)-x8pos(i,1))+SA8(2)*(x8pos(i+1,2)-
x8pos(i,2))+SA8(3)*(x8pos(i+1,3)-x8pos(i,3));
W9=W9+SA9(1)*(x9pos(i+1,1)-x9pos(i,1))+SA9(2)*(x9pos(i+1,2)-
x9pos(i,2))+SA9(3)*(x9pos(i+1,3)-x9pos(i,3));
W10=W10+SA10(1)*(x10pos(i+1,1)-x10pos(i,1))+SA10(2)*(x10pos(i+1,2)-
x10pos(i,2))+SA10(3)*(x10pos(i+1,3)-x10pos(i,3));

% repeat N times
end

% plot the trajectories
t = 1:1000:N;
plot3(x1pos(t,1),x1pos(t,2),x1pos(t,3))
hold on
plot3(x2pos(t,1),x2pos(t,2),x2pos(t,3))
plot3(x3pos(t,1),x3pos(t,2),x3pos(t,3))
plot3(x4pos(t,1),x4pos(t,2),x4pos(t,3))
plot3(x5pos(t,1),x5pos(t,2),x5pos(t,3))
plot3(x6pos(t,1),x6pos(t,2),x6pos(t,3))
plot3(x7pos(t,1),x7pos(t,2),x7pos(t,3))
plot3(x8pos(t,1),x8pos(t,2),x8pos(t,3))
plot3(x9pos(t,1),x9pos(t,2),x9pos(t,3))
plot3(x10pos(t,1),x10pos(t,2),x10pos(t,3))

xlabel('X Axis')
ylabel('Y Axis')
zlabel('Z Axis')
grid on
hold off

```


Appendix D. Statistical analysis in MATLAB

In this appendix, the results of the statistical analysis that provided the fitting of the experimental data discussed in chapter 5 will be given. This will concern the single and six nozzle versions of the rounded ring electrode charging system.

Also, the results of the fitting of the output power as function of the wind speed will be provided.

D.1 Rounded ring electrode – single nozzle

Firstly, the results of the measurements of a single nozzle version were fitted with a decreasing exponential curve of which the result can be seen in Figure D.1 together with the 95% confidence bounds. The exponential curve is given by

$$I_c(U_{EWICON}) = 0.501 \cdot 10^{-6} \exp(-62.31 \cdot 10^{-6} \cdot U_{EWICON}) \quad (D-1)$$

in which I_c is the charging current and U_{EWICON} is the EWICON system potential.

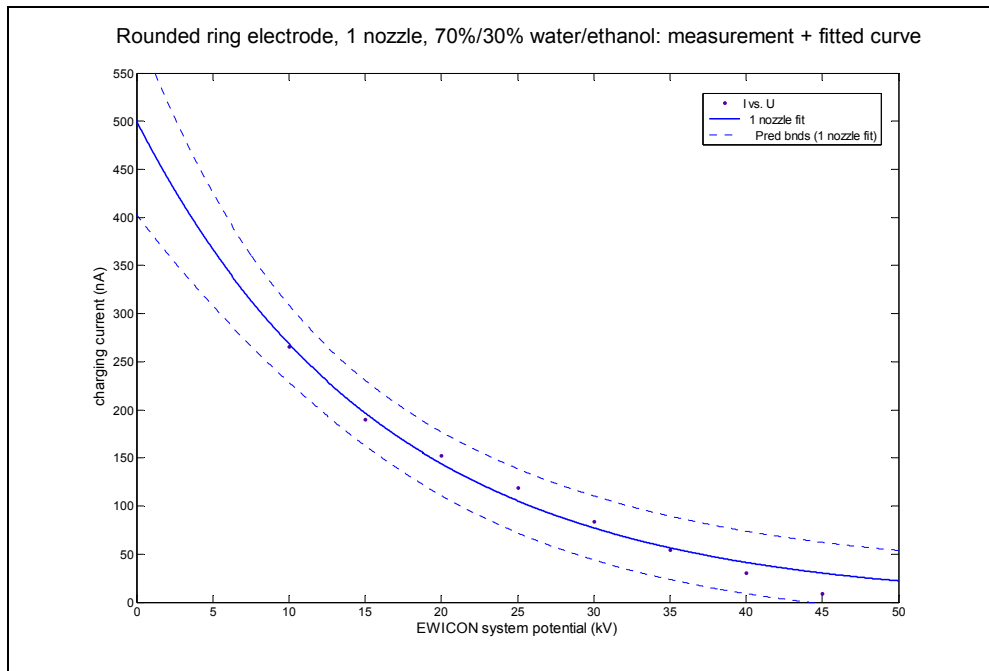


Figure D.1. The measurement of a single nozzle version together with the fitted curve and the 95% confidence bounds.

In this case, the coefficient of determination, R^2 , was found to be 0.9824.

D.2 Rounded ring electrodes – six nozzles

Secondly, the results of the measurements of a six nozzle version were fitted with a decreasing exponential curve of which the result can be seen in Figure D.2 together with the 95% confidence bounds. The exponential curve is given by

$$I_c(U_{EWICON}) = 1.581 \cdot 10^{-6} \exp(-58.85 \cdot 10^{-6} \cdot U_{EWICON}) \quad (D-2)$$

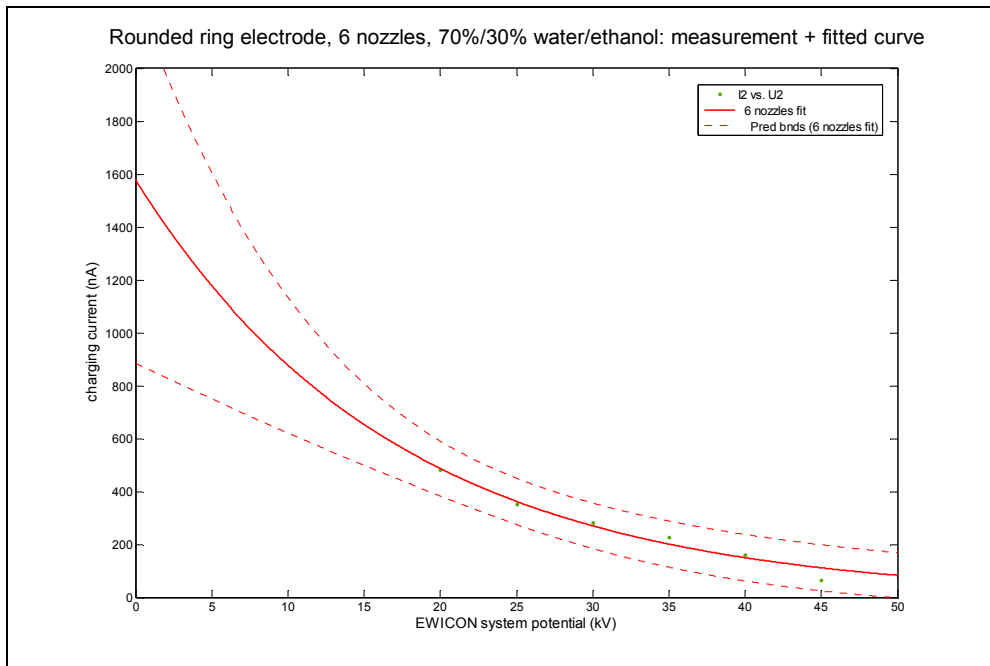


Figure D.2. The measurement of a six nozzle version together with the fitted curve and the 95% confidence bounds.

In this case, the coefficient of determination, R^2 , was found to be 0.9706.

D.3 Output power vs. wind speed

Finally, the output power, P_{out} , has been measured as a function of the wind speed, v_w , and the results have been fitted with a cubic polynomial curve

$$y(x) = c_0x^3 + c_1x^2 + c_2x + c_3 \quad (D-3)$$

where all the coefficients except c_0 have been set to zero. This resulted in an expression for the output power P_{out}

$$P_{out}(v_w) = 4.437 \cdot 10^{-3} \cdot v_w^3 \quad (D-4)$$

The result of the fitting can be seen in Figure D.3.

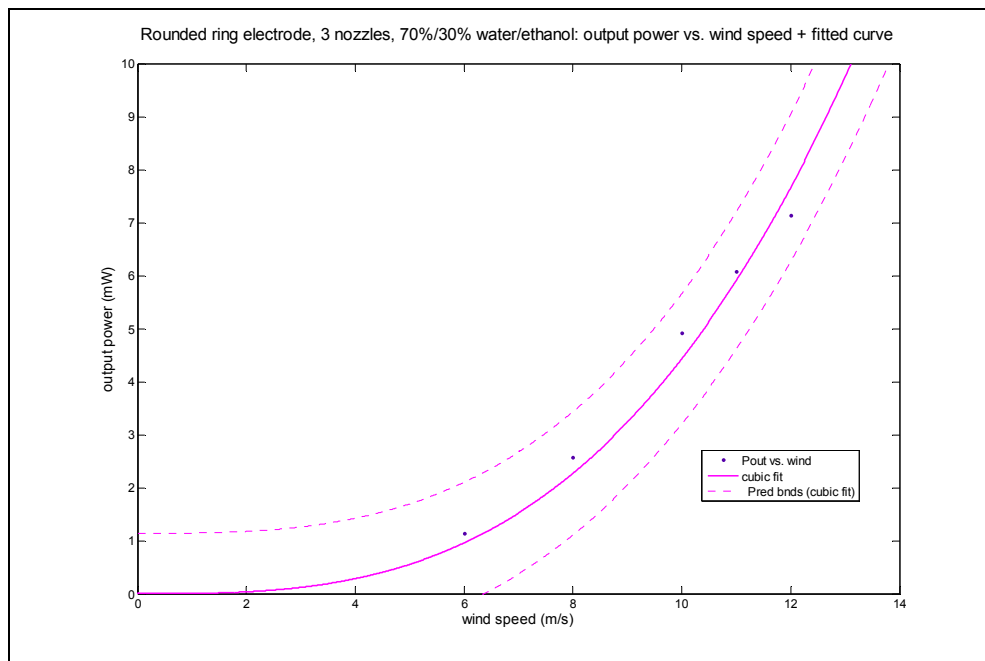


Figure D.3. The output power measurement of a three nozzle EWICON system as a function of the wind speed together with the fitted curve and the 95% confidence bounds

In this case, the coefficient of determination, R^2 , was found to be 0.9726.

Appendix E. LORENTZ

LORENTZ is a computer aided engineering (CAE) software by Integrated Engineering Software that has been used in this research to model and analyse the EWICON system.

In addition to calculating the electric fields generated by the electrodes present in the EWICON system, LORENTZ is also able to compute the trajectories of charged particles in the presence of electric and/or magnetic fields. During the calculation of the trajectories of the charged particles, LORENTZ also takes into account mechanical forces such as gravity and/or wind forces.

The numerical computational method that is employed by LORENTZ to solve the electric field is the boundary element method (BEM). The main advantage of this method over finite element method (FEM) is that only a mesh of the surfaces of the electrodes is required in order to provide a complete solution. This simplifies the modelling effort and it can reduce the calculation times when the volume to surface ratio of the electrodes is large. One disadvantage of BEM is that it is only applicable to certain linear problems, whereas FEM can handle nonlinear problems well.

Most electrostatic problems discussed in this thesis, however, are assumed to be linear and have been solved using BEM. The problems in which the trajectories of charged particles are involved the solution are obtained by using a hybrid technique of boundary and volume meshes.

The reader is referred to the website of Integrated Engineering Software, www.integratedsoft.com, for more detail on LORENTZ and the numerical techniques that are employed for solving models.

List of symbols and abbreviations

symbol	unit		description
A	m^2	–	Wind surface area
$C_{droplet}$	F	–	Capacitance between droplet and charging electrode
C_c	-	–	Cunningham slip correction factor
C_D	-	–	Drag coefficient
d_d	m	–	Droplet diameter
E	$V \cdot m^{-1}$	–	Electric field
ϵ_0	$C^2 \cdot s^2 \cdot kg^{-1} \cdot m^{-3}$	–	Permittivity of vacuum
ϵ_r	-	–	Liquid permittivity
F	N	–	Force
γ	$N \cdot m^{-1}$	–	Surface tension
h	m	–	Height of the EWICON system
η_{EWICON}	-	–	EWICON efficiency
η_a	Pa·s	–	Dynamic/Absolute viscosity
I	A	–	Current
K	$S \cdot m^{-1}$	–	Conductivity
μ	Pa·s	–	Dynamic/Absolute viscosity
μ_e	$m^2 \cdot V^{-1} \cdot s^{-1}$	–	Electrical mobility
μ_m	$s \cdot kg^{-1}$	–	Mechanical mobility
μ_g	-	–	Geometric mean
P_{in}	W	–	Input power
P_{max}	W	–	Maximum recoverable wind
P_{out}	W	–	EWICON output power
P_w	W	–	Power associated with the wind
Q	$m^3 \cdot s^{-1}$	–	Liquid flow rate
q	C	–	Charge
q_{max}	C	–	Maximum charge on a droplet
Re	-	–	Reynolds number
ρ	$kg \cdot m^{-3}$	–	Density
ρ_a	$kg \cdot m^{-3}$	–	Density of air
σ	-	–	Standard deviation
σ_g	-	–	Geometric standard deviation
v_d	$m \cdot s^{-1}$	–	Droplet velocity

v_T	$\text{m}\cdot\text{s}^{-1}$	–	Terminal electrostatic velocity
v_w	$\text{m}\cdot\text{s}^{-1}$	–	Wind velocity
V	V	–	Voltage
V_d	m^3	–	Droplet volume
VN	-	–	Viscosity number

abbreviation		description
CMR	–	Charge to Mass Ratio
CE	–	Charging Electrode
EHDA	–	Electrohydrodynamic Atomisation
ELPI	–	Electrical Low Pressure Impactor
EPI	–	EWICON Performance Index
EWICON	–	Electrostatic Wind Energy Converter
GSD	–	Geometric Standard Deviation
HPMS	–	High Pressure Monodisperse Spraying
HVDC	–	High Voltage Direct Current
LPDA	–	Laser Phase-Doppler Analyser
SE	–	Steering Electrode

List of references

- [1] International Energy Agency, World Energy Outlook 2006, pp.66-67, 2006
- [2] International Energy Agency, World Energy Outlook 2006, pp.72-73, 2006
- [3] International Energy Agency, World Energy Outlook 2006, pp.378-382, 2006
- [4] Federal Ministry for the Environment, Nature Conservation and Nuclear Safety, “Environmental Policy – Nuclear Safety – Report under the Convention on Nuclear Safety by the Government of the Federal Republic of Germany”, Public Relations Division, pp.1-5, September 2001
- [5] International Energy Agency, World Energy Outlook 2006, pp.265, 2006
- [6] International Energy Agency, Renewables in Global Energy Supply, An IEA Fact Sheet, 2007
- [7] Renewable Energy Policy Network for the 21st Century (REN21), Renewables 2007 Global Status Report, Paris: REN21 Secretariat and Washington, DC: Worldwatch Institute, Deutsche Gesellschaft für Technische Zusammenarbeit (GTZ) GmbH, 2008
- [8] Ministerie van VROM, brochure “Het kabinet zet in op windenergie”, juni 2008
- [9] Koninklijk Instituut van Ingenieurs, “Windenergie is een politieke keuze: Technisch haalbaar maar niet rendabel”, Persbericht referentienummer: An963049.P20, 2002
- [10] Williams, P., Lansdorp, B., and Ockels, W., “Flexible Tethered Kite with Moveable Attachment Points, Part II: State and Wind Estimation,” AIAA Atmospheric Flight Mechanics Conference, 2007
- [11] Keith, D.W., DeCarolis, J.F., Denkenberger, D.C., Lenschow, D.H., Malyshev, S.L., Pascala, S., Rasch, P.J., “The influence of large-scale wind power on global climate”, PNAS, volume 101, no. 46, 2006
- [12] Marks, A.M., US Patent No. 4.206.396 and 4.433.248

- [13] Visschedijk, B, Graduate thesis “Electrostatic Generators”, NanoStructured Materials Group, Faculty of Applied Sciences, Delft University of Technology, 2005
- [14] Sato, M., Nakayama, Y., Pan, R., Ueta, K., Shimada, Y., “Study on EHD Wind Power Generation Utilizing Charged Water Droplets due to Contact to Electrode”, International Symposium on Electrohydrodynamics, pp.33-36, Argentina, 2006
- [15] Young, A., Young, M., Scott, B., “High Voltage”, AC/DC, Australia, 1975
- [16] Betz, A., “Das Maximum der theoretisch möglichen Ausnützung des Windes durch Windmotoren”, Zeitschrift für das gesamte Turbinenwesen, vol. 26, pp.307-309, 1920
- [17] Lanchester, F.W., “A contribution to the theory of propulsion and the screw propeller”, Transactions of the Institution of Naval Architects, vol. 57, pp.98-116, 1915
- [18] Hinds, W.C., *Aerosol Technology: Properties, Behavior and Measurement of Airborne Particles*, Second Edition, New York, 1999
- [19] Cloupeau, M. “Research on Wind Conversion by Electrofluid Dynamic Processes”, Arch. Mech., vol. 5, no. 6, pp.529-538, 1986
- [20] Lawson, M.O., von Ohain, H., Wattendorf, F., “Performance potentialities of direct energy conversion processes between electrostatic and fluid dynamic energy”, Aviation Research Laboratory, vol. 178, 1961
- [21] Fuchs, N.A., Sutugin, A.G., “Generation and use of monodisperse aerosols.” in Davies, C.N., ed. "Aerosol Science", Academic Press, pp.1-30, New York, 1966
- [22] Bodega, R., Sonneveld, P.J., Morshuis, P.H.F., van Rooij, R., van Eldijk, L.G.M., ”Conversion of wind into electrical energy without the need for moving parts”, 8th International Symposium on High Voltage Engineering, Millpress, Rotterdam, 2003
- [23] Peskin, R.L., Raco, R.J., “Ultrasonic Atomization of Liquids”, Journal of Acoustical. Society of America, vol. 35, pp.1378, 1963

- [24] Teunou, E., Poncelet, D., “Rotary disc atomisation for microencapsulation applications—prediction of the particle trajectories”, *Journal of Food Engineering*, vol. 71, pp.345-353, 2006
- [25] Kreuger, F.H., “Industrial High Voltage”, Delft University Press, 1991
- [26] Kazkaz, G., “Electric field and space charge of spherical electrode at high voltage concentric with a spherical ground conductive target”, *IEEE Transactions of Industry Applications*, vol. 34, no. 4, 1998
- [27] Grace, J.M., Marijnissen, J.C.M., “A review of liquid atomization by electrical means”, *Journal of Aerosol Sciences*, vol. 30, no. 7, pp.1005-1019
- [28] Hartman, R.P., “Electrohydrodynamic atomization in the cone-jet mode. From physical modelling to powder production”, PhD thesis, Delft University of Technology, 1998
- [29] Borra, J.-P., Hartman, R., Marijnissen, J., Scarlett, B., “Destabilisation of sprays in the cone-jet mode by electrical discharges on the jet”, *Journal of Aerosol Sciences*, Suppl. 1, pp.203-204
- [30] Cloupeau, M., Prunet-Foch, B., “Electrohydrodynamic Spraying Functioning Modes: A Critical Review”, *Journal of Aerosol Sciences*, vol. 25, no. 6, pp.1021-1036, 1994
- [31] Gañán-Calvo, A.M., Davilla, J., Barrero A., “Current and droplet size in the electrospraying of liquids. Scaling laws”, *Journal of Aerosol Sciences*, vol. 28, pp.249-275
- [32] Keskinen, J., Pietarinen, K. and Lehtimäki, “Electrical Low Pressure Impactor”, *Journal of Aerosol Sciences*, vol. 23, pp.353-360, 1992
- [33] Lubetkin, S.D., Akhtar, M., “The variation of surface tension and contact angle under applied pressure of dissolved gases and the effects of these changes on the rate of bubble nucleation”, *Journal of Colloid and Interface Science*, volume 180, number 1, pp. 43-60, June 1996
- [34] Lastow, O., Balachandran, W., “Numerical and experimental study of electrohydrodynamic atomization (EHDA) of conducting of conducting liquids in the cone jet mode”, *International Symposium on Electrohydrodynamics*, pp.265-268, Argentina, 2006

- [35] Crowley, J.M., "Simple expressions for Force and Capacitance for a Conductive Sphere near a Conductive Wall", Paper D1, Proceedings of the Electrostatics Society of America 2008 Annual Meeting on Electrostatics, 2008
- [36] Nilsson, J., Palm, L., "Charging current measurements and charging synchronization in continuous jet", Review of Scientific Instruments, vol. 72, no. 2, pp.1574-1579, 2001
- [37] Taylor, G., "Disintegration of water drops in an electric field", Proceedings of the Royal Society of London. Series A, Mathematical and Physical Sciences, vol. 280, no. 1382, pp.383-397, 1964
- [38] Djairam, D., Morshuis, P.H.F., Smit, J.J., "Optimising electrode design and positioning for EHDA produced particles in a EWICON", Conference on Electrical Insulation and Dielectric Phenomena 2007, Canada, pp.478-481, 2007
- [39] Djairam, D., de Wit, A.T., Morshuis, P.H.F., Smit, J.J., "Controlled and efficient electrohydrodynamic spraying of water in an EWICON", Conference on Electrical Insulation and Dielectric Phenomena 2008, Canada, pp.169-172, 2008
- [40] Theodore, A.D., EWICON report "Continued prototype design and testing of self-adjusting multi-nozzle electro-spray system using porous technique", NanoStructured Materials Group, Faculty of Applied Sciences, Delft University of Technology, 2006
- [41] Djairam, D., Nijdam, W., Balendonck, J., Morshuis, P.H.F., Smit, J.J. Smit, "Converting wind energy to electrical energy using charged droplets in an electric field", Proceedings Conference on Electric Insulation and Dielectric Phenomena 2007, Canada, pp.474-477, 2007
- [42] Wever, R., "The effects of electric fields on circadian rhythmicity in men", American Journal of Epidemiology, vol. 109, pp.273-284, 1970
- [43] Repacholi, M.H., Greenebaum, B., "Interaction of static and extremely low frequency electric and magnetic fields with living systems: health effects and research needs", Bioelectromagnetics, vol. 20, no. 3, pp.133-160, 1999

Acknowledgements

“It is by chance that we met, by choice that we became friends.”

Writing a PhD thesis is often considered a solitary activity, but this work could not have been even remotely possible, were it not for the help and support of numerous people. These people have contributed in different ways: some did by helping me with experiments, by participating in brain storm sessions and, on more than one occasion, by pointing me in the right direction. Others did by just being there while joking around over the occasional cup of coffee or glass of beer and, thus, keeping me sane. Between the two groups, there was plenty of overlap and to all of them I want say a few little words...

First of all, I am greatly thankful to my promotor, professor Johan Smit, for his trust and the opportunity he has given me to work on this great project. I value the many discussions we have had about the chapters of my thesis and I truly feel that they have made this thesis much better.

I'd like to thank my daily supervisor, dr.ir. Peter Morshuis, for looking after me all these years. Peter, not only did you help you me with the EWICON by thinking with me and asking me the right questions, you also made me feel at home at the group.

Edward, I still remember you asking during my job interview while you were looking through my M.Sc. thesis, “What have you done for science?” After an extra four years, I'm sure I can give a better answer now. Sander, besides being a fun person to be around with, thanks for giving me the opportunity to teach. For me, that was definitely one of the most rewarding aspects of doing a PhD. Maria, thanks for making my life so much easier and all the “gezelligheid”!

Simulations, reading papers and thinking can only get you so far and none of my experimental results would have been possible without the invaluable support from ing. Paul van Nes, Aad van der Graaf and Bertus Naagen. Paul, I appreciate your support and your efforts to instil some form of discipline in me. Aad, thanks for all your pieces of art, “Wonderen doen we direct, het onmogelijke duurt iets langer!” Bertus, thanks for all the practical help during my experiments and for occasionally saving my life when I was sprinting towards my set-up in great enthusiasm.

The EWICON project group consisted of many people with whom I enjoyed working together. Anna Hubacz, Wietze Nijdam, Jan Marijnissen, Jos Balendonck, Piet Sonneveld, Alex Theodore and Ruud van Rooij. Together, we made important steps!

To me, a working environment with good atmosphere is just as important as the job itself and the High Voltage Group provided that in abundance. Riccardo, thanks for helping me get started with the EWICON and for being my roommate for 3.5 years. My current roommates, Thomas and Roman, I'm glad we all like music! Roma, in de toekomst gaan we alleen Nederlands praten! Thomas, thanks for being the fellow geek/bassist/movie buff of the group. Arie, the graduation work you did for the EWICON was as impressive as it was valuable.

My former fellow PhD's who have always been open for spirited conversation, Ben, Tjerk, Robert, Belma and Harry. My current fellow PhD's, Tom, Gautam, Roy, Piotr, Muhannad and Qikai, keep the group alive and kicking!

Pantelis, we still have to do a reunion of the High Voltage Band and I hope to see you graduate after me! Rogier, my fellow Dutch guy, together we made sure that the farmer's accent was regularly heard. I can't thank you enough for all the help with my research and thesis.

Guys, I've had a great time with you all, drinking beers in the /pub, all the Bond nights, doing sports together and just hanging out in general!

I've been wandering around in Delft for almost 14 years now and, along the way, I was lucky enough to meet a lot of people who I am fortunate enough to call my friends. My first mention goes out to my first student house "de Blokkendoos", both the old and new members, where I am still always welcome to unwind, even though I left the house six years ago. Vincent, Eva, Vincent, Arjen, Sieb, Menno, Widy, Edwin, Eelco, Tomas, Kristian, Piet, Hans, Pieter, Robert, Sjoerd, Bastiaan, Melanie, Rosemarijn. Dinners, parties, holidays... those were and still are good times! Tomas, just like with my M.Sc. thesis, many many many thanks for all the graphics works you did!

Martial arts will always be an influential part of my life and so will Yoroshi and all the people I've met through that. Sensei Dick, thanks for almost ten years of guidance. Linda, Hadewig, Dedmer, Boi, Gerard, Mohammed, Jeroen, Michael, see you either on the tatami or the slopes!

Sebastiaan, Hanneke, Ronald, Saskia, here's to many more dinners... and maybe some jogging!

Mathijs, Alwin, Joël, movie night soon? I'll do the cooking!

Esmee, Arvid, Nathan, my Donner buddies. It seems like ages ago that we were thrown together in the bookstore and even though we worked for a brief time and are all very different, we still can't seem to shake each other!

Acknowledgements

Piet and Griet, we've know each other for over ten years now and during that time, you've given me the opportunity to explore Leiden and this exotic subculture of bearded archaeologists. I wish you all the best with Jasper!

Becky, thirteen years of flowery English, that's the reason why my skills progressed beyond high school levels.

Luke and Janneke, visiting New Zealand and seeing you guys get married was definitely one of the best moments of my life. Is Dilan already trying to outsmart you?

Anne, you will go wherever your saxophone will take you, but that has never stopped us from seeing each other and trying to cram as much as possible in the few moments we have.

Mascha, ever since you set foot on the Blokkendoos, we have been great friends and shared many things and that never changed, not even when you moved to Eindhoven! Good luck with the new house and of course, Philip's PhD defence.

Bas, we've been friends since we were thirteen, so what can I say... we're both from the northern parts, we're both men of few and many words, so when we've got something to say, we talk and otherwise we play guitar. That level of comfort is rare and priceless. Now, a new phase has started for you together with Micheline and Midas. Thanks for taking me along for the ride!

Marnix, physics buddy, guitar buddy, partner-in-crime, we shared our high points and low points in life, exams, graduation, break-ups, family matters, breath taking holidays, band practice and much more. The only thing I can do is return the compliment: you have been a wonderful friend! The fact that we will graduate at the same point in our lives is just plain freaky and way cool!

The last part is reserved for the most important people in my life, my family. My grandparents and my many aunts and uncles, cousins, nieces and nephews have all contributed in their little way with advice and encouragements.

The knowledge, that I would always have a home to back to no matter what would happen in life, has given me strength and courage to do whatever I wanted.

Rishi, bedankt voor het zijn van een goed broertje, van een jong opstandig pubertje tot een verstandig volwassen man. We lijken in niets op elkaar en toch sta je altijd voor me klaar... zoals de vele autotrips. Sangieta, bedankt voor het zijn een onwijs lief zusje, ook van een jong opstandig pubertje tot een verstandig volwassen mooie vrouw. Zo vaak als je voor mij gezorgd heb met alles zal ik nooit vergeten.

Lieve pa en ma, door jullie onvoorwaardelijke steun en liefde, door jullie aanmoediging om the leren, al van heel jongs af aan, heb ik dit kunnen bereiken.

Erg bedankt!

Curriculum Vitae



Dhiradj Djairam was born on May 19th, 1977 in Groningen, the Netherlands. He received his secondary school degree from the Praedinius Gymnasium in Groningen in 1995. He received his M.Sc. degree in Applied Physics from the Delft University of Technology in 2002, specialising in experimental and laser optics.

He started his Ph.D. research project in 2004, called “EWICON II – Electrostatic Wind Energy Converter”, in which he has investigated an alternative method of extracting energy from the wind. He conducted this research, which led to this thesis, at the High Voltage Technology and Management Group, Delft University of Technology.

Currently, he works as a post-doc on the SINERGIE Smart Grids project, also at the High Voltage Technology and Management group, Delft University of Technology.